



University
of Glasgow

<https://theses.gla.ac.uk/>

Theses Digitisation:

<https://www.gla.ac.uk/myglasgow/research/enlighten/theses/digitisation/>

This is a digitised version of the original print thesis.

Copyright and moral rights for this work are retained by the author

A copy can be downloaded for personal non-commercial research or study, without prior permission or charge

This work cannot be reproduced or quoted extensively from without first obtaining permission in writing from the author

The content must not be changed in any way or sold commercially in any format or medium without the formal permission of the author

When referring to this work, full bibliographic details including the author, title, awarding institution and date of the thesis must be given

Enlighten: Theses

<https://theses.gla.ac.uk/>
research-enlighten@glasgow.ac.uk

THE PHOTODISINTEGRATION OF
OXYGEN, NEON AND ARGON.

by

I.M.H. PRESTON.

PRESENTED TO THE UNIVERSITY OF GLASGOW AS
A THESIS FOR THE DEGREE OF DOCTOR OF
PHILOSOPHY.

January, 1959.

ProQuest Number: 10656220

All rights reserved

INFORMATION TO ALL USERS

The quality of this reproduction is dependent upon the quality of the copy submitted.

In the unlikely event that the author did not send a complete manuscript and there are missing pages, these will be noted. Also, if material had to be removed, a note will indicate the deletion.



ProQuest 10656220

Published by ProQuest LLC (2017). Copyright of the Dissertation is held by the Author.

All rights reserved.

This work is protected against unauthorized copying under Title 17, United States Code
Microform Edition © ProQuest LLC.

ProQuest LLC.
789 East Eisenhower Parkway
P.O. Box 1346
Ann Arbor, MI 48106 – 1346

CONTENTS

PREFACE	(i)
ACKNOWLEDGEMENTS	(iv)
CHAPTER I. INTRODUCTION	
1.1 General Introduction	1.
1.2 Experimental Techniques	3.
1.3 Experimental Results on the 'Giant Resonance'	8.
1.4 Discussion of the theories of photodisintegration	15.
1.5 Reactions involving Multiple Nucleon Emission	27.
CHAPTER II. EXPERIMENTAL TECHNIQUE	34.
CHAPTER III. THE ANALYSIS PROCEDURE	48.
CHAPTER IV. PHOTOPROTONS FROM NEON	
4.1 Introduction	58.
4.2 Specific Experimental Conditions	58.
4.3 Experimental Results	58.
4.4 Discussion of the Results	62.
CHAPTER V. LOW ENERGY PHOTOPROTONS FROM OXYGEN	
5.1 The Published Data on the $^{16}\text{O}(\gamma, p)^{15}\text{N}$ Reaction	65.

CHAPTER V (Contd.)

5.2 Introduction to the Present Investigation	71.
5.3 Specific Experimental Conditions	72.
5.4 The Classification of the Events	73.
5.5 The Experimental Energy Distributions	76.
5.6 Discussion of the Results on the Energy Distributions	78.
5.7 The Experimental Angular Distribution	82.

CHAPTER VI. THE EMISSION OF He^3 AND He^4 PARTICLES FROM OXYGEN AND ARGON

6.1 Introduction	84.
6.2 Equipment and Procedure	84.
6.3 Results	88.
6.4 Discussion	90.

APPENDIX I. THE DETERMINATION OF SOME OF THE PARAMETERS OF THE PHOTON AND ELECTRON BEAMS OF THE 340 Mev SYNCHROTRON	99.
---	-----

APPENDIX II. PHOTONUCLEAR REACTIONS IN NEON	108.
---	------

REFERENCES.

PREFACE

This thesis contains an account of the research carried out by the author at the University of Glasgow between October 1954 and October 1958.

The introductory chapter contains a survey of the published literature on the photodisintegration of nuclei with bremsstrahlung beams of relatively low peak energy; a critical review of the experimental techniques which can or have been applied to this field; a review of the theories of photonuclear processes, and a brief survey of the published data relating to reactions in which more than one nucleon is emitted.

The equipment used in the experiments reported in this thesis and the method applied to analyse the recorded information are described in Chapters II and III respectively. The author can only claim to have slightly modified the system which was originally devised by Messrs. I.F. Wright and D.R.O. Morrison.

The account of the study of the (γ, p) reaction in neon, which is described in Chapter IV, is based on results obtained by Dr. G.I. Crawford with the assistance of the author.

Chapter V contains the results of the investigation into the emission of low energy

photoprotons from oxygen which was carried out by the author with the assistance of Dr. G.I. Crawford. The presentation of the results and the discussion are entirely the author's work.

In Chapter VI the results of the experiments performed on the photo-emission of He^3 and He^4 particles from oxygen and argon are presented. The experimental work and the interpretation are entirely the work of the author. The equipment used in these studies was originally designed and built by Mr. R.W.P. McWhirter, Dr. E.H. Bellamy and Dr. P. Palit.

Before any experimental work could be undertaken in studies of photonuclear reactions, it was necessary to determine the parameters of the photon and electron beams of the 340 Mev synchrotron, and the results presented in the first appendix were derived by the author under the direction of Dr. W. McFarlane.

The second appendix contains the results obtained by Messrs. I.F. Wright, D.R.O. Morrison, G.I. Crawford and Mrs. M.B. Lambie in an investigation of photonuclear reactions in neon (with the exception of the work on the (γ, p) reaction reported in Chapter IV). The author's contribution to the work in this appendix was merely to check the calculations, which were involved

(iii)

and laborious, in order to acquire experience and to eliminate arithmetical errors. This appendix is only included in order to present a complete picture of the photodisintegration of neon.

ACKNOWLEDGEMENTS

I wish to thank Professor P.I. Dee for his interest and encouragement throughout the period of my research. I would also like to express my appreciation to Dr. W. McFarlane, Mr. J.R. Atkinson and Dr. E.H. Bellamy for their encouragement and helpful supervision during the investigations reported in this thesis.

I am indebted to Mr. R. Irvine and the staff of the workshop for their assistance in the modifications to the equipment and to Mr. J. Robertson, who serviced it.

I would also like to acknowledge the helpful co-operation of the staffs of both the Glasgow synchrotrons and, in particular, Dr. K.G. McNeill, Mr. D. Dixon and Dr. W. McFarlane.

During the first three years of this research, I was in receipt of a maintenance allowance from D.S.I.R., to whom I wish to record my gratitude and appreciation.

CHAPTER I.

INTRODUCTION.

1.1 General Introduction.

The first investigations into the mechanism of photodisintegration were carried out using the γ -rays from the naturally occurring radioactive elements. Chadwick and Goldhaber (1) in 1934 irradiated deuterium with the 2.62 Mev γ -rays from ThC" and detected the protons from the reaction $D(\gamma, p)n$ in an ionisation chamber. In the same year Szilard and Chalmers (2) observed the neutrons from the reaction $Be^9(\gamma, n)Be^8$, when Be^9 was irradiated with the γ -rays from radium. However, since deuterium and beryllium were the only two elements with photo-thresholds below 5 Mev, no further reactions were investigated until sources of more energetic photons became available.

High energy γ -rays were first utilised to study photo-reactions in 1937 when Bothe and Gentner (3) used the 17.6 Mev and 14.7 Mev γ -rays from the reaction $Li^7(p, \gamma)Be^8$ and, after the development of the betatron by Kerst (4) in 1941, high energy bremsstrahlung beams were available to further photonuclear investigations.

Today, both sources of γ -rays are extensively employed. Several (p, γ) reactions are now used to provide monochromatic γ -rays of energies less than

20 Mev (5), while the peak energies of the bremsstrahlung beams, available from the betatrons and synchrotrons, now extend up to 1 Bev.

The fluxes of photons available from the (p, γ) reactions are low and the quanta produced have energies below 20 Mev. Consequently, considerable use has been made of the bremsstrahlung beams with peak energies extending up to the region around 30 Mev. The use of bremsstrahlung beams introduces difficulties due to the continuous energy spectrum of the γ -rays and consequently special methods have had to be devised to yield detailed information about the reaction mechanisms. For example:-

(a) A measurement of the energies of all the reaction products yields an unambiguous determination of the photon energy, provided none of the products is left in an excited state.

(b) Considerable interest is centred on the difference method (6) where the activity A , induced in a sample by photon bombardment, is measured as a function of the peak photon energy E_0 , under conditions of constant electron current in the accelerator. The function dA/dE_0 , evaluated for an energy E , gives the cross-section at that photon energy.

(c) The 'monochromator' (7,8) is a device conceived to overcome the problems set by the continuous energy spectrum. In principle, it involves the detection of the electrons which have been scattered from the machine target after they have radiated. The energy of the electrons is specified by the magnetic field of the machine. If a reaction product is measured in coincidence with one of these electrons, the energy of the γ -ray responsible for the reaction is specified.

(d) Average values of the integrated cross-sections of photonuclear reactions and the effective energy of the photons responsible have also been obtained (9,10). In particular, Marshall (10) determined the Z-dependence of the absorption of the photons responsible for the reaction under investigation. She obtained the effective energy of the photons by equating the total absorption cross-section in her absorbers to the sum of the Compton cross-section and the pair production cross-section.

1.2 Experimental Techniques.

The following experimental techniques have been extensively employed in studies of photonuclear reactions:-

- (a) Nuclear emulsions
- (b) Cloud chambers
- (c) Activation methods
- (d) Counter systems

Each has a limited range of applicability and these are now briefly discussed.

(a) Nuclear emulsions.

These have been widely used to measure the energy and angular distributions of the charged particles emitted in photonuclear reactions. They have also been employed for neutron detection where the energy of the neutrons was deduced from measurements of the ranges and angles of the 'knock-on' protons. In general, the energy of the protons detected by this technique has a lower limit at about 2 Mev and consequently emulsions are unsuited for measurements of the proton energy spectrum resulting from photon absorption in the energy region immediately above the reaction threshold. This limitation is more evident when detecting doubly-charged particles, since they have shorter ranges than singly-charged particles of the same energy. At high energies the fast, charged particles pass through the emulsions and, as a result, a determination of their energy is rendered more difficult.

A further disadvantage of this method stems from the inability to discriminate between particles of the same charge but different mass.

However, emulsions are ideally suited to studies where the incident photon flux is low, and a more complete discussion of the applicability of emulsions to photo-nuclear studies is presented in the review article by Titterton (11).

(b) Cloud chambers.

Measurements have been made of the energy distributions of photoprotons using cloud chambers (12), operated at gas pressures between one and two atmospheres. These distributions only occupied a narrow energy interval because the effective range of the protons in such chambers was small. Since the time to cycle a standard expansion chamber could be as long as two minutes, this instrument made inefficient use of the available photon flux. In this respect the efficiency of a diffusion chamber was found to be comparable to that of the expansion chamber, since there was a delay between the passage of the beam and the re-establishment of the sensitive region. This delay could be considerable if the photon flux was high (13). The introduction of fast cycling expansion chambers will allow a more efficient use to be made of the available photon flux.

Where cloud chambers have been operated with a magnetic field it has been possible to separate out particles of the same charge but different mass by simultaneous measurements of range and curvature of track.

Both methods (a) and (b) have been criticised on the grounds that a considerable time was required to analyse the experimental data. The development of automatic scanners will no doubt overcome this difficulty, and in consequence the results obtained by these methods will benefit from better statistics than those obtained previously.

(c) Activation methods.

These have been extensively employed in studies of the cross-sections of photonuclear reactions. They are only applicable where the reactions under investigation yield radioactive residual nuclei, and in general they suffer from the following disadvantages:-

(i) Where the peak photon energy is in excess of the threshold for multiple nucleon emission, the targets must be monoisotopic in order to yield unambiguous results.

(ii) The experimentally determined activation curve has to be converted into a cross-section curve and

this process is liable to a degree of arbitrariness. Further, it is necessary to ensure precision monitoring in this procedure if consistent results are to be obtained.

By studying the characteristic decay of the isomeric states of some reaction products it has been possible to estimate the relative importance of the roles played by the ground state and these excited states in the decay of the excited nucleus.

(d) Counter Systems.

Counters for the detection of uncharged particles.

In the majority of experiments in which neutrons have been detected, these neutrons were first slowed down in a moderator and then detected by BF_3 counters or rhodium foils. More recently an increasing use has been made of 'threshold' detectors where the neutron must possess considerable kinetic energy in order to produce an (n,p) reaction in the detector, e.g., of the order of 4 Mev for an aluminium detector (14). The energies of fast neutrons have been inferred from the energies of the 'knock-on' protons produced by these neutrons in hydrogenous materials. Liquid and plastic scintillators have both been used in such high energy investigations (15). Unfortunately such

detectors have low efficiencies and in consequence their use complicates the experimental procedure.

Counters for the detection of charged particles.

These counters have been widely used despite the fact that there was not a type analogous to the thermal-neutron detectors. Many workers have used only one counter and, although they could measure the energy of the particle detected, they were unable to determine its character. Those who have used counter telescopes, on the other hand, have been able to determine the energy and character of the particles detected. Counter telescopes suffer from the disadvantage that they are only applicable to high energy investigations since the particles must be sufficiently energetic to penetrate through the first counter and still have enough energy to record in the second.

1.3 Experimental Results on the 'Giant Resonance'.

Although the primary interest in photo-disintegration centres round the elucidation of the process of photon absorption, it has been found necessary to approach this topic through investigations of individual partial reactions because nuclear absorption cross-sections are much smaller than electronic absorption cross-sections. As a result,

the data on photon absorption must be synthesised from the results obtained in studies of individual reactions. Unfortunately, for the majority of nuclei, only one partial reaction (usually the (γ, n)) has been investigated and consequently only a crude estimate can be made of the total absorption cross-section. Therefore, since it is not possible to compare the parameters of the total absorption cross-section curves throughout the periodic table, it is necessary to infer their probable characteristics from the corresponding quantities measured for one of the partial reactions. Wherever possible, the conclusions deduced from this procedure should be compared to the sum of all the partial cross-sections. The majority of the published data relating to 'giant resonances' in the cross-sections for the partial photoreactions has been obtained from studies of (γ, n) reactions. This data will provide a suitable example to illustrate the properties of the cross-section of a partial photoreaction.

Without doubt, the most outstanding feature of photonuclear reactions is the occurrence in the cross-section of the so-called 'giant resonance' and the theoretical approach to the subject has been primarily concerned with an explanation of this phenomenon.

The properties of the 'giant resonance' are normally specified in terms of the following parameters (see Figure 1):-

- (a) The energy at which the peak of the cross-section curve occurs (E_m).
- (b) The width of this resonance (Γ).
- (c) The height of this peak, i.e., the maximum cross-section (σ_m).
- (d) The integrated cross-section ($\sigma_{int.}$).

Each of the above quantities will now be considered in turn, with reference to the (γ, n) reaction:-

(a) Montalbetti, Katz and Goldemberg (16) have plotted the experimental values of the energy at which the maximum cross-sections occur, as a function of the mass number A . They find the variation of E_m with A to be of the form $E_m = A^n$. The thresholds for the reaction show a similar variation with A . The graph shown in Figure 2 illustrates in addition that the thresholds for the (γ, n) reaction in nuclei of odd N and even Z are lower than the general trend. Schuhl and Basile (17) have derived a formula for E_m of the form

$$E_m = 13 \sqrt{20.2A^{-2/3} + 0.85 (1 - 1.6A^{-1/3})} \text{ Mev}$$

and this is also shown in the figure. The wide variation of the experimental points precludes the observation of structure in this figure if, in fact, any exists.

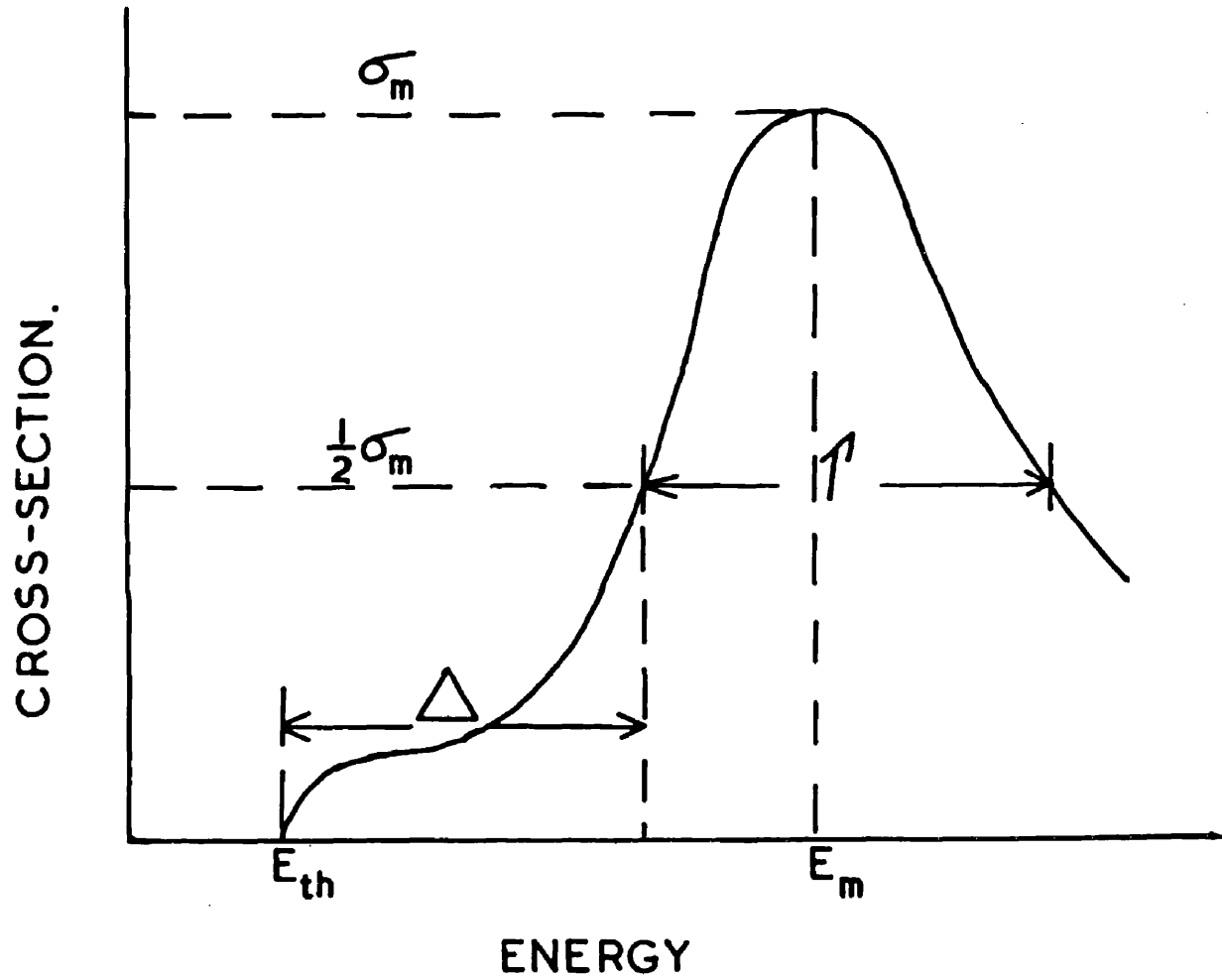


Figure 1.

The parameters of the 'giant resonance'.

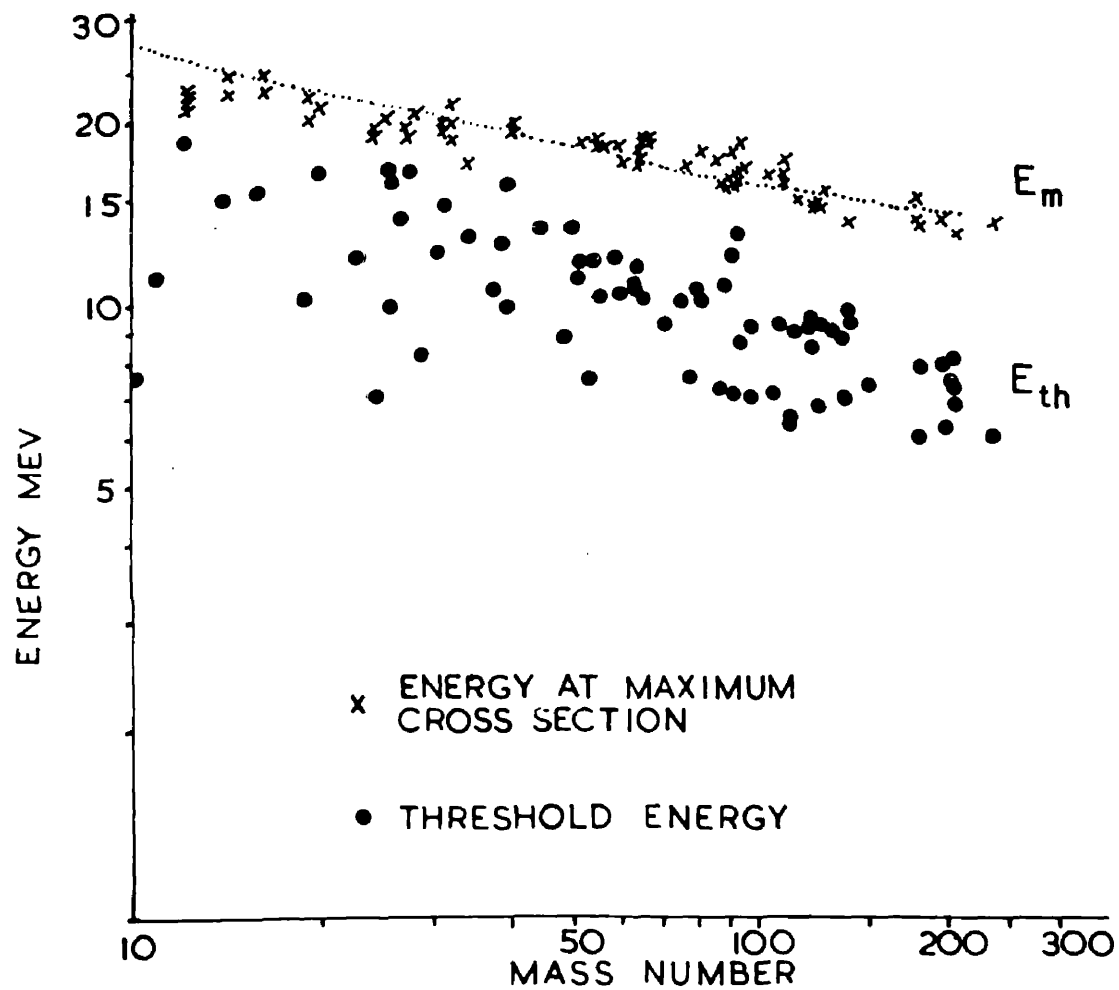


Figure 2.

The variation of E_m as a function of the mass number.

(b). A general survey of the published literature illustrated a considerable discrepancy between the results of different groups of workers with regard to the width of the resonance in the cross-section. The results of Nathans and Halpern (18) corresponded to a measurement of the total neutron yield and the values of the widths that they obtained were greater than those of Montalbetti et al. (16), who detected the residual activity produced by the reaction under investigation. It is interesting to note that the results quoted by Nathans and Halpern show a marked shell-structure effect, while those of Montalbetti et al. show none. The accompanying diagram (Figure 3) shows the results of Nathans and Halpern combined with those of Yergin and Fabricand (19). Here the widths are plotted as a function of the neutron number N and the figure illustrates that the widths decrease slowly as a function of N except at the magic neutron numbers where the widths are well below the general trend. Although the number of experimental points is limited, the structure is well displayed.

The widths quoted by Nathans and Halpern were open to the criticism that the measurements included contributions from other reactions in which a neutron was emitted. For this reason Goldemberg and Lopes (20)

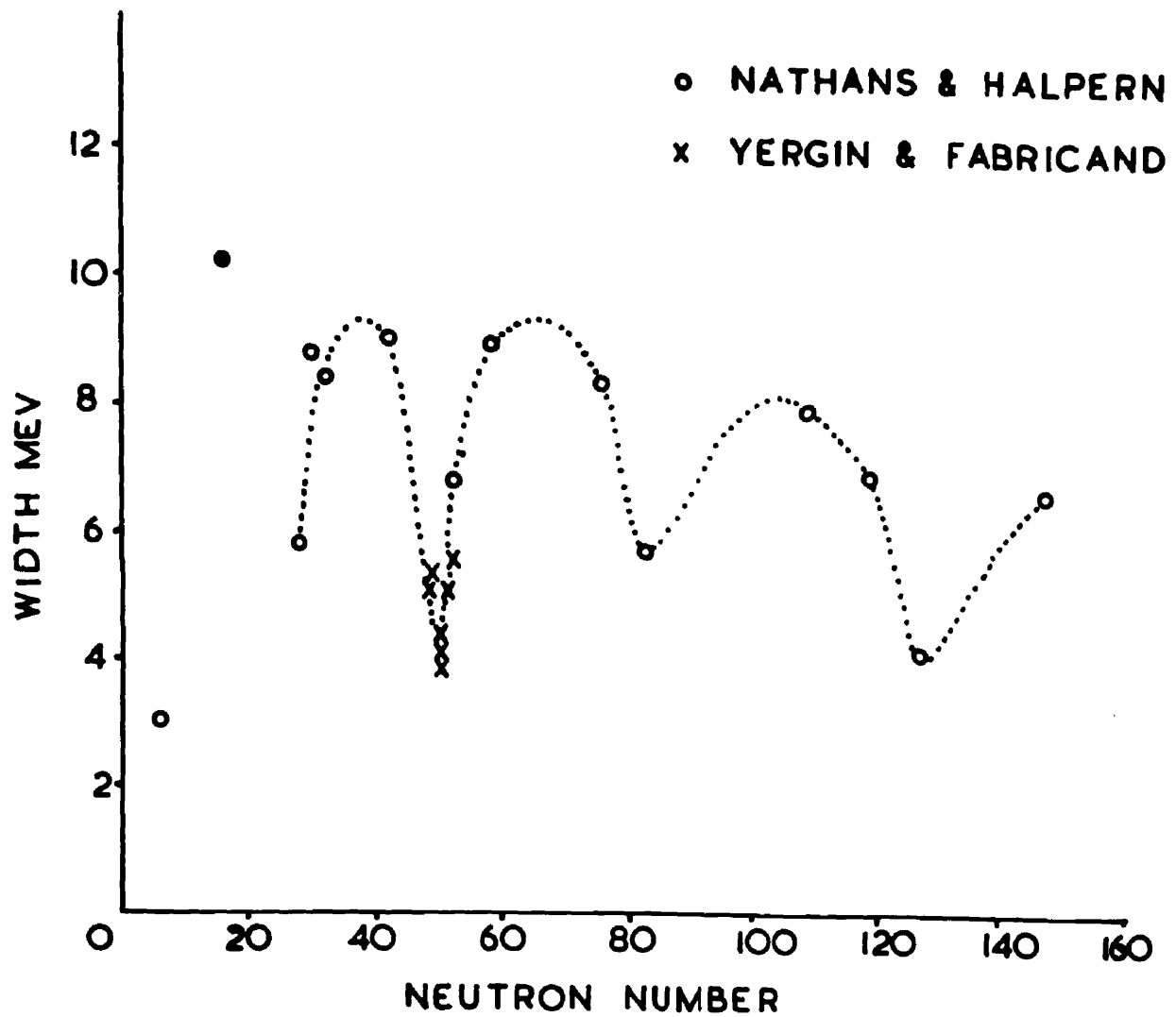


Figure 3.

Width of the 'giant resonance' plotted against the neutron number of the target nucleus.

introduced a new parameter which they justified as follows: They stated that the onset of reactions in which a neutron was emitted, other than the (γ, n) reaction, i.e., (γ, pn) and $(\gamma, 2n)$ would in general affect the width of the resonance, and further, that this effect would be confined to the high energy side of the resonance. They regarded the difference between the threshold energy and the energy corresponding to the half maximum on the front edge of the peak as a more significant parameter (Δ). They plotted Δ as a function of A and claimed peaks corresponding to the magic neutron numbers 20, 28, 50, 82 and 126. Here their data is plotted (Figure 4) as a function of the neutron number. In order to lessen the confusion only those nuclei with even N and odd Z are included. If, in fact, their assertion that the width was increased by interference from other reactions, then values of Δ calculated from $(E_m - E_{th} - \frac{1}{2})$ should lie below their curve. This is generally true, although there are a few exceptions. No mention was made in their paper of the justification for the selection of the experimental values shown in the figure. Consequently this detracts somewhat from the significance of their results. In conclusion it appears that there

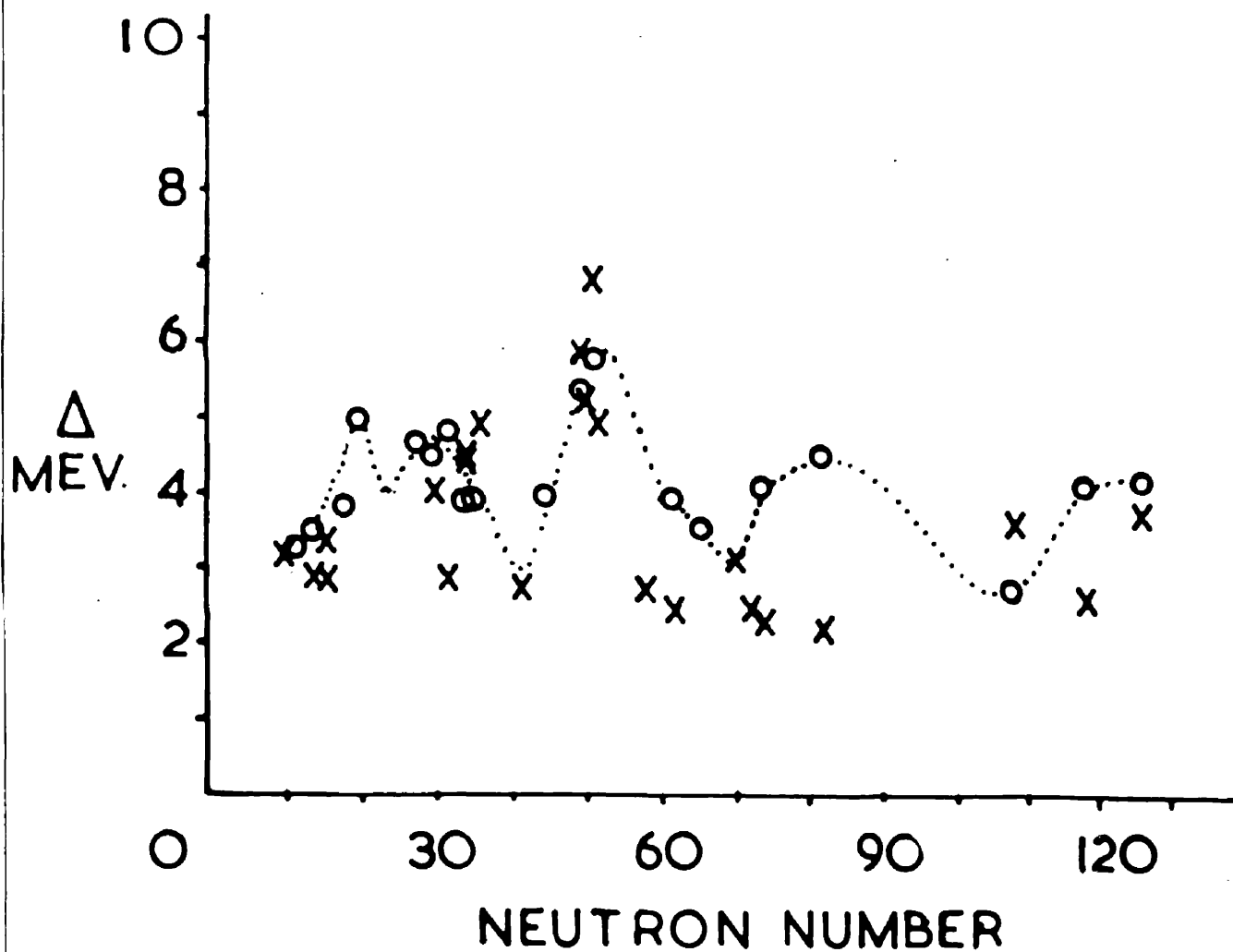


Figure 4.

Δ plotted against the neutron number for odd-even nuclei.

O - values derived from reference 20.

X - calculated values referred to in text.

is some evidence for the inclusion of shell model effects in the description of the nuclear photoeffect.

(c). The results of Yergin and Fabricand (19) on nuclei with neutron numbers of about 50 indicated that the maximum cross-section of the resonance increased sharply at the magic number and did not decrease thereafter. Bearing this in mind, an attempt has been made to continue this process throughout the periodic table. The trend of the experimental results can be described as a smoothly varying function of N , but a series of 'steps', as shown in Figure 5, would not be inconsistent with the data. It should be noted here that the values quoted by Montalbetti et al. in general lie above those of Nathans and Halpern. The work of Hartley, Stephens and Winhold (21) on the cross-sections of (γ, n) reactions in several nuclei confirmed that the Montalbetti values were too high and they quoted the error as being approximately 50%. They suggested that the standard value used by the Canadian group, i.e., that of the $\text{Cu}^{63}(\gamma, n)$ reaction, was in error.

(d) The integrated cross-sections reported in the literature fail to exhaust the dipole sum as calculated from the relationships of Levinger and Bethe (22) and Gell-Mann, Goldberger and Thirring (23), although for

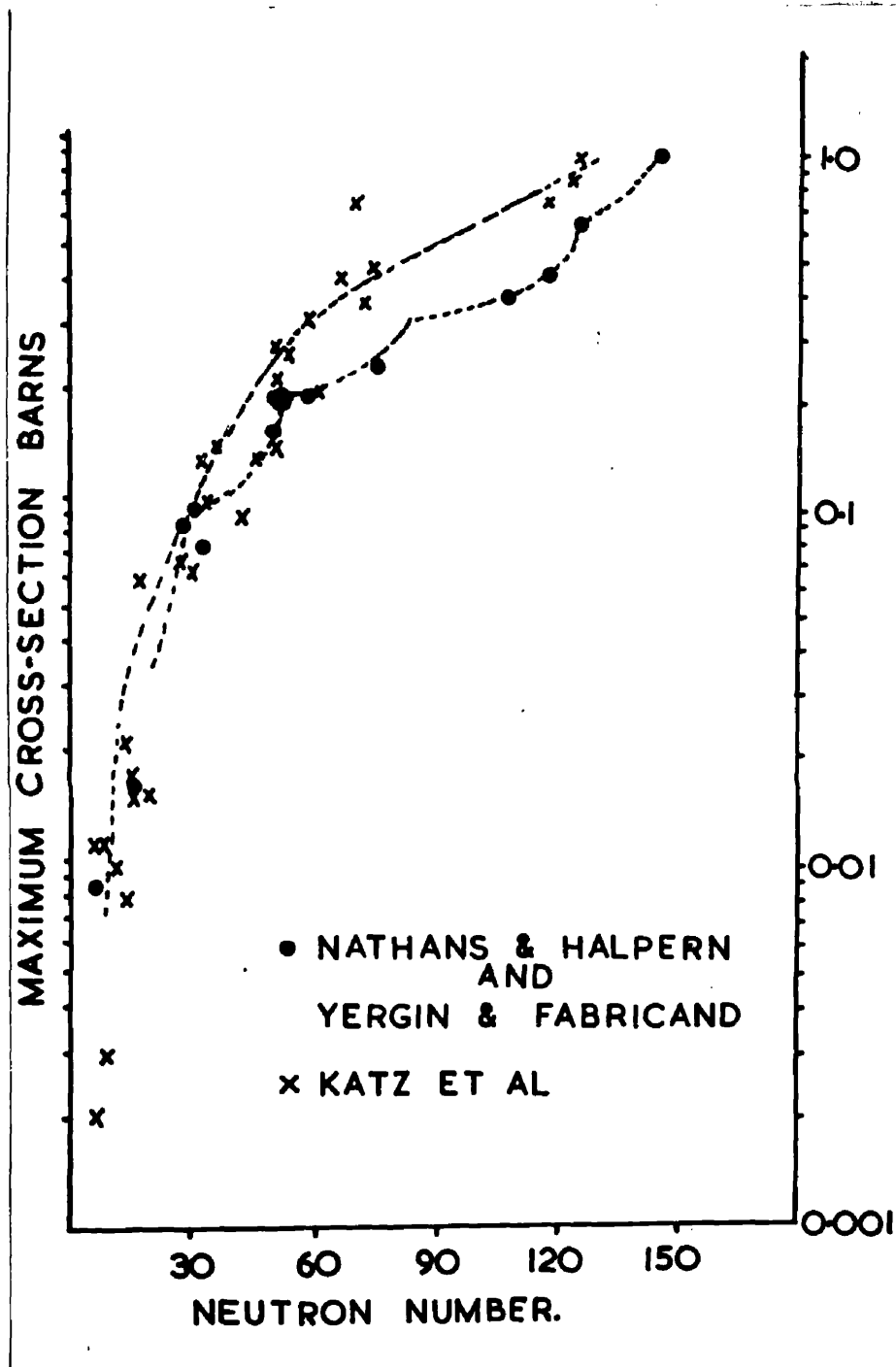


Figure 5.

Experimental values of the maximum
cross-section of the 'giant resonance'.
(ref.16,18,19)

high Z the (γ, n) integrated cross-sections nearly do so. The values obtained by the two main groups of workers appear to be in agreement here, as also are those calculated for several reactions using a known integrated cross-section as a standard. The experimental values are plotted in Figure 6 together with the theoretically predicted relationship.

Having illustrated the properties of the 'giant resonances' for the (γ, n) reaction it is now necessary to determine whether or not these resonances occur in the cross-section for photon absorption. This can be answered by an examination of the nuclear photoeffect in C^{12} . The possible reactions are listed with their respective properties in the following table(5):

TABLE 1

<u>Reaction</u>	<u>Threshold</u>	<u>Peak cross-section</u> (millibarns)	<u>Energy at maximum</u> (Mev)	<u>Integrated cross-section</u> (Mev-barns)
(γ, n)	18.73	8.3	22.5	56×10^{-3}
(γ, p)	15.9	34 ± 8	21.5	63×10^{-3}
$(\gamma, 2n)$	32.0	not measured		
(γ, pn)	27.4	not measured		
$(\gamma, 3\alpha)$		0.1	18 & 25 ⁴	
$(\gamma, n) +$				
$2(\gamma, pn) +$			21.5	
$2(\gamma, 2n)$				
(γ, γ')		not measured		

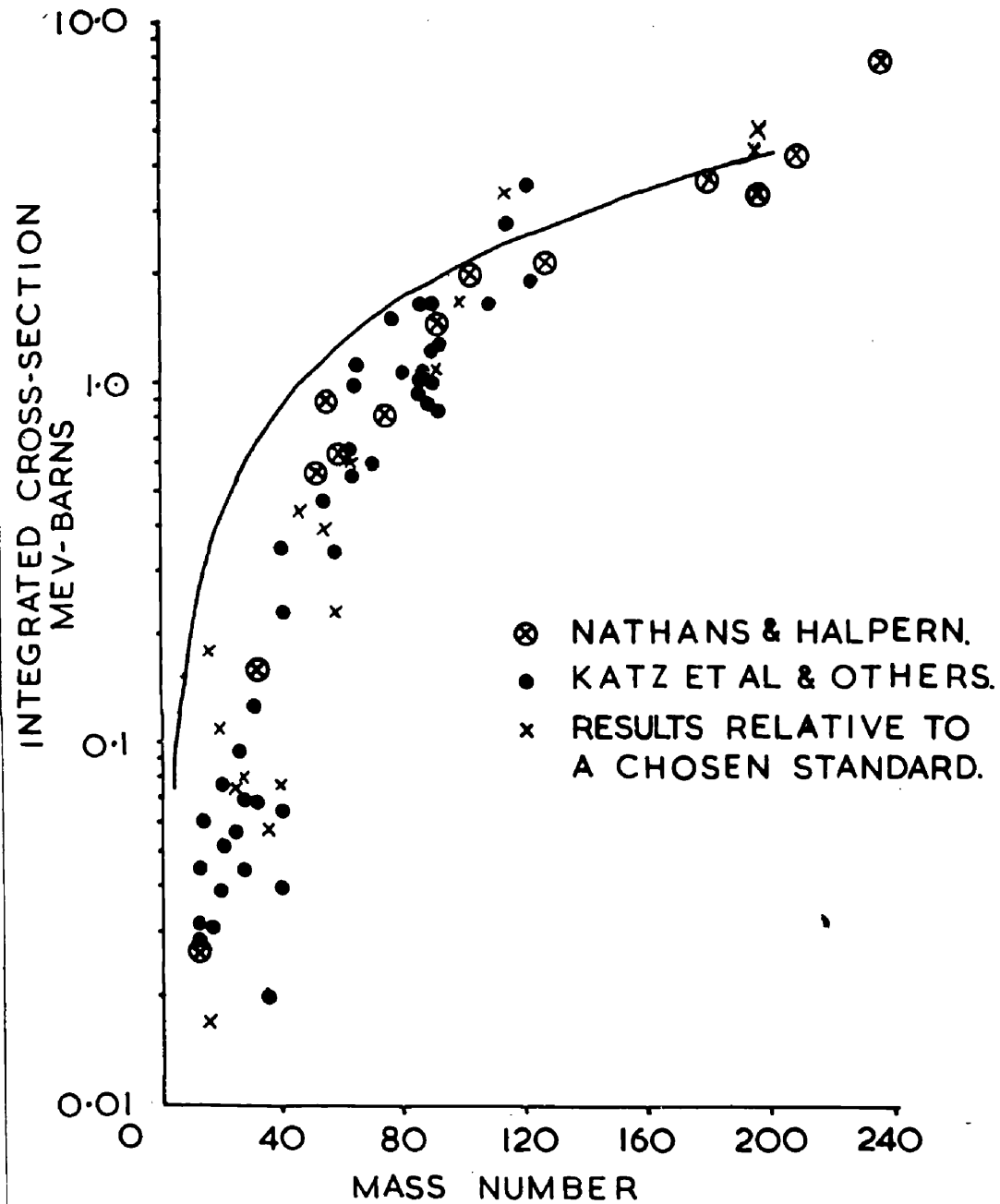


Figure 6.

Experimental values of the integrated cross-section (ref.16,18). The smooth curve was derived from the relationships quoted on page 16.

The main contributions to the total photon absorption came from the (γ, n) and (γ, p) reactions which both had peaks at about 22 Mev and this would lead one to expect the total absorption cross-section to be peaked here also. In another case, such as aluminium, the peak of the cross-section for the (γ, n) reaction was found to lie at 19.5 Mev, which was also the threshold for the (γ, pn) reaction. Could the fall-off of the cross-section have been due in any way to competition from the (γ, pn) or $(\gamma, 2n)$ reactions? A study of the cross-section curve for total neutron emission, irrespective of the reaction, showed that it was also peaked at the same energy and the decrease in the cross-section was therefore not due to competition from the other reactions. One therefore concludes that in fact the peak occurs in the absorption cross-section and that the effects of the other reactions are mainly confined to increasing the width of the resonance. One now feels more confident to discuss the features of the absorption process in terms of the general features noted in the survey of the (γ, n) reaction.

1.4 Discussion of the Theories of Photodisintegration.

Levinger and Bethe (22) have calculated the total integrated cross-section for electric dipole photon

absorption ($\int_0^\infty \sigma_t dE$) and obtained

$$\int_0^\infty \sigma_t dE = 0.060 \frac{NZ}{A} \text{ Mev-barns} \text{ ----- (1)}$$

Feenberg (24) and Siegert (25) showed that the sum rules were modified by exchange forces and Levinger and Bethe included the fraction of the neutron-proton exchange force x as a parameter in their calculations. They then obtained

$$\int_0^\infty \sigma_t dE = 0.060 \frac{NZ}{A} (1 + 0.8x) \text{ ----- (2)}$$

The inclusion of exchange forces necessitates that the calculations be performed on a specific model while relation (1) was a general result and independent of model. Result (2) could be increased further by the addition of correlation between the nucleons (5).

Gell-Mann et al. (23) have derived the sum rule for all multipolarities from a dispersion relation and obtained (μ = meson threshold)

$$\int_0^\mu \sigma_t dE = 0.060 \frac{NZ}{A} (1 + 0.1 \frac{A^2}{NZ}) \text{ ----- (3)}$$

Relationships (2) and (3) are plotted in Figure 6 together with the integrated cross-sections for (γ, n) reactions reported in the literature. In this figure the value of x in (2) was assumed to be $\frac{1}{2}$ (26) and with this choice the relationships are equal.

It should be noted that σ_t is in fact the sum over all the partial reactions, i.e.,

$$\sigma_t = \sigma(\gamma, \gamma') + \sigma(\gamma, n) + \sigma(\gamma, p) + \sigma(\gamma, 2n) + \sigma(\gamma, np) + \dots$$

For this reason, the values of the integrated cross-section obtained from measurements of the total neutron yield should approximate more closely to the $\int_0^\infty \sigma_t dE$ than the values of the integrated cross-section determined for the (γ, n) reaction alone. For high Z values, the charged particle emission is suppressed by the Coulomb barrier and the integrated cross-sections derived from measurements of the neutron yield will be close to $\int_0^\infty \sigma_t dE$.

Plots of the neutron yields as a function of the mass number A (27, 28, 29) showed that (a) for nuclei lighter than copper the yield was not a smooth function of the atomic number and that (b) above $Z = Z_{Cu}$ the yield varied smoothly as Z^2 and not as NZ/A . Halpern and Mann (30) showed that the proton yield was not a smooth function of Z for the light elements but that $(\sigma(\gamma, p) + \sigma(\gamma, n))$ varied as NZ/A within the experimental errors. This result accounts for (a) and the multiplicity of neutron emission might explain (b).

In conclusion it can be said that for heavy nuclei the experimental values agree reasonably well with expression (2) with $x = \frac{1}{2}$, but for the light elements even the sums of the (γ, p) and (γ, n)

contributions (up to 24 Mev) fall below the predicted values. One is therefore led to suspect that a considerable part of the integrated cross-section may be tied up in bound particle states (below any particle threshold) or in a high energy tail in the cross-section. Experimental evidence derived by Jones and Terwilliger (31) indicated that in fact the high energy photo-absorption cross-section did have such a high energy tail.

Two models have been devised to explain the process of photon absorption, namely the collective model and the independent particle model.

(A). The collective model.

Studies of the sum rules indicated that correlations between the nucleons were of considerable importance and should be included in the model for photon absorption. The first model was devised by Goldhaber and Teller (32), who assumed that all the protons were moving collectively in the opposite direction to that of all the neutrons. Different assumptions about the forces between the nucleons gave a variety of models, e.g., if the neutrons and protons were treated as compressible fluids constrained within the nucleus, then the variation of E_m was proportional

to $A^{-1/3}$; if, however, the neutrons and protons were considered as incompressible interpenetrating spheres, then the variation of E_m was proportional to $A^{-1/6}$. The experimental variation was illustrated in Figure 2.

The integrated cross-section gave the sum rule value for no exchange forces, as it should have, since they were not included in the model which included all the dipole vibrations.

The width of the resonance Γ was explained as being due to the coupling of the ordered vibrations to other modes of nuclear motion, i.e., similar to damping by friction.

This model automatically involved the formation of a compound nucleus since the energy of the incident quantum was shared among all the nucleons, and while this was a reasonable approximation for the heavy elements it was less applicable to the light elements where a considerable amount of direct photoeffect occurred (33,34). The model can be further criticised on the grounds that it includes complete internucleon correlation which cannot be reconciled with the satisfactory description of nuclear ground states in terms of the shell-model.

The compound nucleus so formed will decay

through the allowed channels in a manner independent of the mode of formation. Where there are a large number of states a statistical procedure can be used. Such a system was presented by Diven and Almy (35), who incorporated the work of Weisskopf and Ewing (36) in a derivation of their expression for the proton energy spectrum. It was noted that the proton spectra calculated by this method were in disagreement with the experimental results in that there appeared to be an excess of high energy protons and a deficiency of low energy ones. Similar results were obtained by Byerly and Stephens (37). The more recent work of the Italian group (14) showed that a similar discrepancy was present in the spectra of the neutrons emitted in (γ, n) reactions.

(B) The independent particle model.

This model has been used by Wilkinson (38) to explain the parameters of the 'giant resonance'. In general terms one starts with a nucleus in its ground state, which is fairly well described by the shell-model. Consider an electric dipole (E1) transition in which one nucleon changes orbit by one unit of angular momentum. Since the dipole sum is exhausted by the 'giant resonance', transitions involving the nucleons in the 'core' are considered as distinct from the valence nucleons. As a result of the interaction

between the excited nucleon and the rest of the nucleus, the upper state of these transitions is not a well defined single-particle state but in fact the absorption proceeds to many final states containing part of the ideal single-particle state in their shell-model description. However, the interest lies with the gross features of the 'giant resonance', and consequently the important quantity is the summed effect over these levels, which is that appropriate to the ideal single-particle state dissolved in them. One might then expect to find fine structure in the resonance, and such is the case (39,40,41).

Wilkinson showed that after he had inserted the experimental values for E_m in his formula for the integrated cross-section, he obtained a good account of the trend but, although the absolute magnitude was correct for the light elements, it was too low by a factor of two for the heavy nuclei.

When considering E_m , Wilkinson calculated that it was of the order of 9 Mev for the heavy nuclei and not 14 Mev as has been found experimentally. However, using a reduced mass of about a half of the normal mass and $R = 1.2 \times A^{1/3} \times 10^{-13}$ cm., the calculation was repeated and the experimental points were found to lie between the two theoretical calculations. This theory

can therefore give a qualitative explanation of the variation of E_m as a function of A .

The width Γ of the resonance can be due to several causes but none can be quantitatively evaluated, e.g., (1) separation in energy of the single-particle transitions; (2) wide-spread contributions of the valence nucleons and the effect of their coupling to the excited core. Qualitative evidence for this can be drawn from the earlier section on the widths of the resonances measured for (γ, n) reactions, where narrow widths were recorded for the 'magic' nuclei which have no valence nucleons.

When considering the energy distributions of the emitted particles, the following pictorial presentation describes the mechanism of emission following photon absorption.

As a result of the absorption of the incident photon, a nucleon is elevated to a higher single-particle state where it may interact with the rest of the nucleus to form a compound nucleus, which will then decay statistically, or be emitted directly without sharing its energy. The latter possibility would account for the fast nucleons found in several experiments, i.e., Toms and Stephens (42). Ferrero (43) also confirmed that the fast neutrons originated in the 'giant resonance'.

Where proton emission is concerned, the results of Hirzel and Wäffler (44) for heavy elements indicated that the experimental cross-section at 17.6 Mev was considerably higher than the value predicted by the statistical theory. A model of the above type, in which all the energy of the absorbed photon is centred on a single nucleon, provides a simple explanation of the above discrepancy. Since the statistical process in general involves protons of energy lower than the single-particle process, the Coulomb barrier has a considerably greater effect on the evaporated protons than on the 'resonance-direct' protons. This is well seen in the results of Toms and Stephens (42) for indium, cerium and bismuth. The energy distributions obtained for the photoprotons were fitted with the sum of the spectra calculated on the basis of a 'resonance-direct' process and the evaporation process. The fraction of the total spectrum contributed by the statistical process decreased as the atomic number increased. Similar results have been obtained by other workers and in particular Dawson (45) found that the percentage of direct emission varied from 0% for aluminium up to 50% for rhodium.

The independent particle model, as envisaged by

Wilkinson gains further support from a study of the angular distributions of the emitted nucleons. In particular, take the case of the angular distribution measured by Mann, Stephens and Wilkinson (33) for the reaction $C^{12} (\gamma, p) B^{11}$. They found that it was of the form $1 + 1.5 \sin^2 \theta$. Here the ground state of C^{12} is 0^+ and E1 absorption would lead to a 1^- excited state. If the compound nucleus were to decay to the ground state of B^{11} ($3/2^-$) or the first excited state ($1/2^-$), then the angular distribution would be isotropic since the s-wave emission would be favoured over d-wave emission.

Wilkinson's model predicts the form of the angular distribution to be

$$I(\theta) = 1 + 1/2 (1 + 2/1) \sin^2 \theta$$

and here $I(\theta)$ should be $1 + 1.5 \sin^2 \theta$, in agreement with experiment.

Consider also the earlier result of Halpern, Mann and Rothman (46) who obtained an angular distribution of the form $1 + (\sin \theta + 0.25 \sin \theta \cos \theta)^2$. Although the form is different, the anisotropic character of the angular distribution is confirmed.

Since B^{11} and C^{11} are mirror nuclei, one might expect the ground states and the first excited states to have the same spins and parities respectively.

The above argument could then be applied to the (γ, n) process as well. The results of Fabricand, Allison and Halpern (47) indicated an angular distribution of the form $1 + (1.35 \pm 0.88) \sin^2 \theta$ for the neutrons emitted from the $\text{Cl}^{35} (\gamma, n) \text{Cl}^{34}$ reaction. It seems therefore that the independent particle model is very successful in describing the angular distributions of the emitted nucleons from Cl^{35} .

More generally, it should be noted that similar angular distributions have been reported for the emitted protons from various nuclei throughout the periodic table (34,45,48).

The angular distributions of the photoprotons are in many cases not only anisotropic but also asymmetric. A forward peak is seen in the distribution and it is interpreted as the effect of interference between the dipole absorption and the quadrupole absorption. Mann, Halpern and Rothman (48) stated that provided there was no random redistribution of the energy and angular momentum of the absorbed photon, the interference between the p- and d-wave emission of the protons, represented by the asymmetric angular distribution, in fact represented interference between dipole and quadrupole absorption. Asymmetry was observed in the angular distributions of photoneutrons

by various workers (14,47) and Fabricand et al. (47) explained this by stating that the only effective charge in this case was that of the residual core.

Price (49) has measured the angular distributions of the neutrons emitted from (γ, n) reactions in several nuclei and on the assumption that they were of the form $A + B \sin^2 \theta$, he plotted the ratio B/A as a function of Z . This is reproduced in the accompanying Figure 7.

Leikin, Osokina and Ratner (50) demonstrated that the model envisaged by Wilkinson was not wholly satisfactory. They investigated photo-proton emission from nuclei with $Z = 28$ and 29 . In the Wilkinson model the effect of the valence nucleons is confined to increasing the width of the resonance and they do not contribute greatly to the total absorption. These Russian workers claimed that they did play an important part in the absorption process. They measured a quantity ($p\%$) which represented the fast proton fraction of the total proton yield. This quantity was plotted against the maximum energy of the bremsstrahlung beam and the resulting curves differed from one another in a marked fashion. The curve corresponding to the nucleus with $Z = 28$ was smoothly varying, while in that for copper ($Z = 29$), $p\%$ rose suddenly by a factor of 2.5 between $E_0 = 25$ Mev and $E_0 = 28$ Mev. The authors of this communication suggested that the difference in the

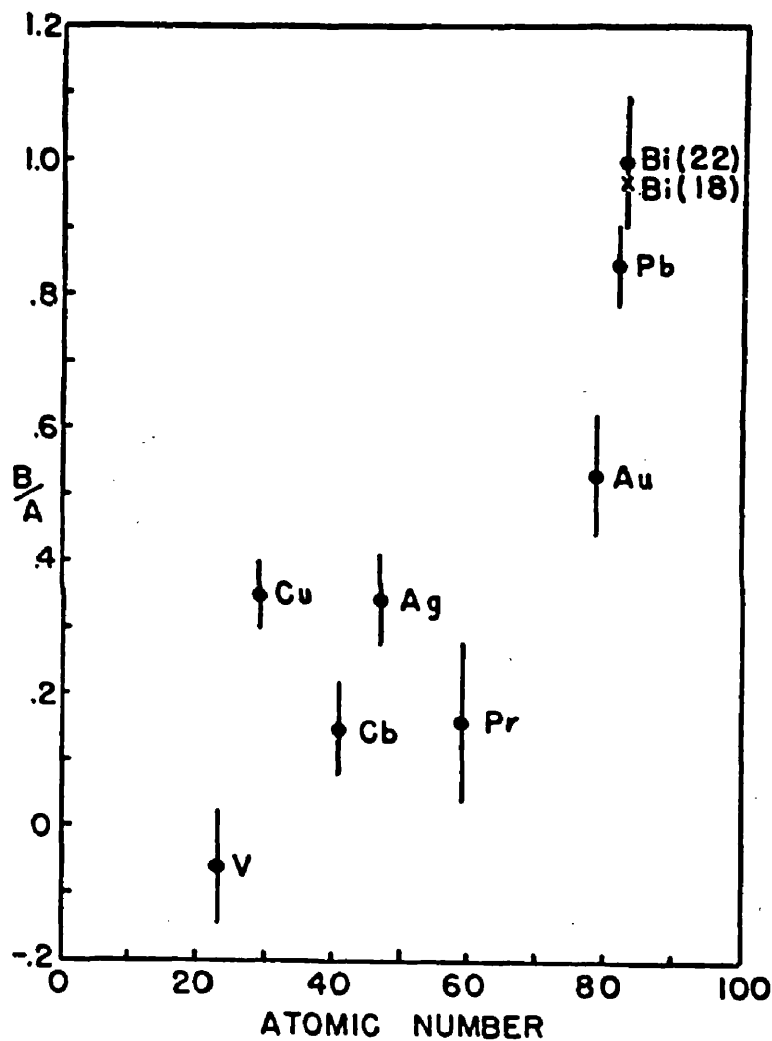


Figure 7.

The ratio B/A derived from photoneutron angular distributions of the form $A + B \sin^2 \theta$ as a function of Z .

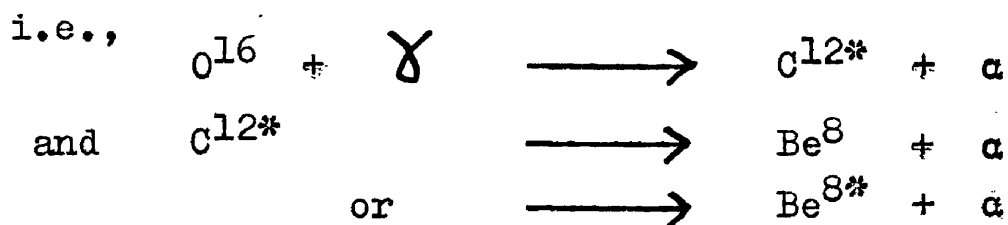
behaviour of $p\%$ for these nuclei could be related to the valence nucleons as $Z = 28$ represented a closed shell.

1.5 Reactions Involving Multiple Nucleon Emission.

In addition to the photonuclear reactions in which only one nucleon was emitted, preliminary investigations have been made into reactions in which several nucleons were emitted, individually or in small aggregates, i.e., deuterons, tritons, He^3 and He^4 particles. In general, these multiple reactions have high thresholds and have not been extensively studied, due in part to the limited number of machines of intermediate or high energy which were available for such experiments. These reactions also present considerable experimental difficulties if all the reaction products have to be detected. Although the scope of this field is too wide to be discussed in detail here, the results of several investigations are presented below and it is felt that they are representative of the published data on this topic.

(a). The $\text{Cl}^{35} (\gamma, 3\alpha)$ and $\text{O}^{16} (\gamma, 4\alpha)$ reactions have been studied by many workers (51,52,53) who irradiated photographic emulsions. In particular, considering the $\text{O}^{16} (\gamma, 4\alpha)$ reaction, Goward and Wilkins (51b) showed that for an oxygen nucleus, excited by photons of energy less than 25 Mev, the most probable mode of decay was by an

alpha-particle cascade via the excited states of C^{12}



They estimated that in 3% of the stars which they measured the data was consistent with an interpretation in which the process proceeded via two Be^8 nuclei in their ground states.

The cross-section for this reaction (51e) is shown in Figure 8 and it illustrates the presence of several resonances which have been correlated to levels or groups of levels in the nucleus. These were confirmed by Livesey and Smith (52) who also estimated that for $E_\gamma > 25$ Mev the cascade via C^{12*} was unlikely.

Millar and Cameron (54) obtained results which were in contrast to those above in that they estimated that 40% of the stars that involved Be^8 nuclei in their ground states were produced in an $O^{16} (\gamma, Be^8) 2\alpha$ reaction and 60% of the stars that involved Be^8 in excited states corresponded to the $O^{16} (\gamma, 4\alpha)$ reaction.

It would appear that the formation of a compound nucleus followed by a cascade decay is satisfactory in explaining the features of this reaction. In particular, when Hsiao and Telegdi (55) assumed that for $E_\gamma < 25$ Mev

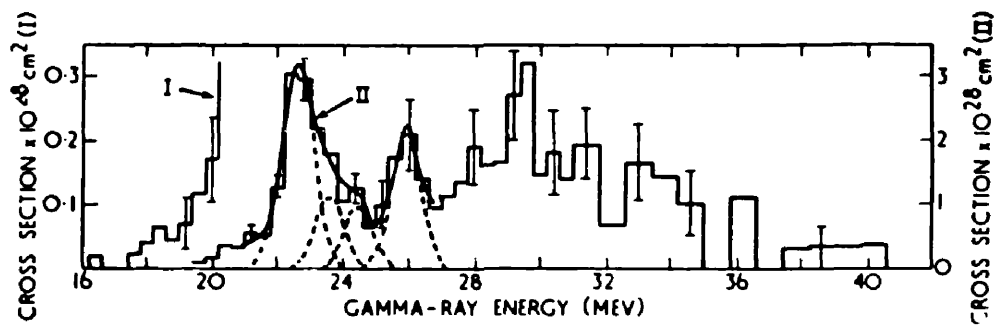


Figure 8.

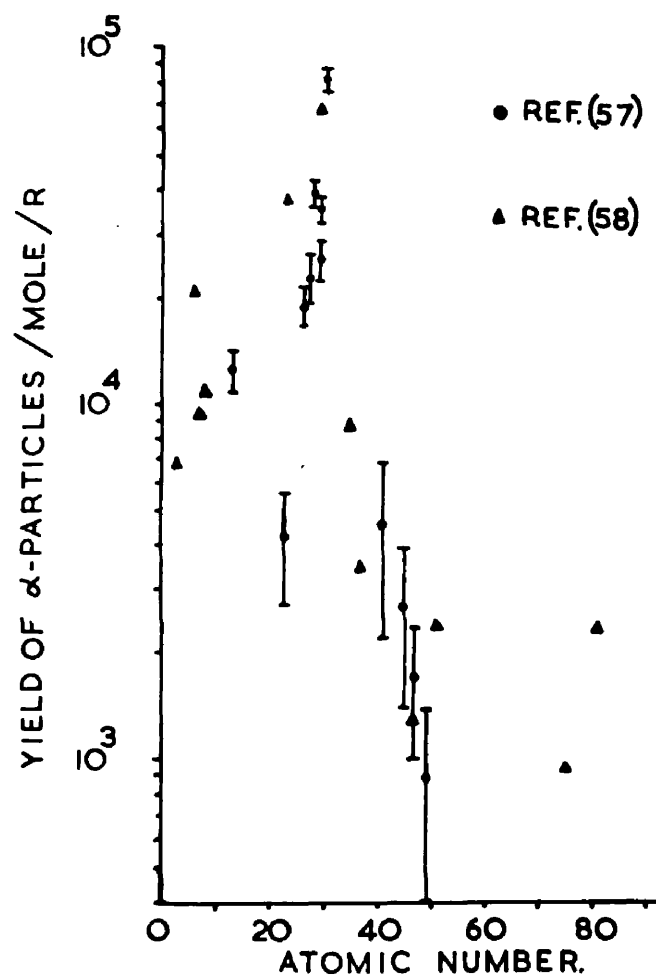
The cross-section for the $^{16}\text{O}(\gamma, 4\alpha)$ reaction quoted by Goward and Wilkins (51e).

the absorption was electric dipole in character, they found that their results bore out the predictions of Gell-Mann and Telegdi (56), who considered the oxygen data on the basis of the isotopic spin formalism.

(b). Although the cross-sections for the (γ, α) reactions have not been investigated thoroughly, two comprehensive sets of data on the yields of such reactions at low energies have been published. The first was obtained by Toms and McElhinney (57), who used a 21.5 Mev bremsstrahlung beam, and the second was reported by Erdos, Scherrer and Stoll (58), who irradiated their targets with a beam of peak energy 32 Mev. Both groups of results are illustrated in Figure 9. The yields increased with atomic number until $Z = 30$ and thereafter decreased because the inhibiting effect of the Coulomb barrier was stronger than the enhancing effect of the lower reaction threshold (57). Contrary to the previously held beliefs, Erdos, Scherrer and Stoll found that the (γ, α) and (γ, p) yields were approximately constant for $Z > 50$.

The cross-sections for (γ, α) reactions (58) show the familiar resonance behaviour and, as can be seen from Figure 10, the cross-sections have become very small by the time the energy of the absorbed photon has increased to about 40 Mev.

The energy distribution of the alpha-particles



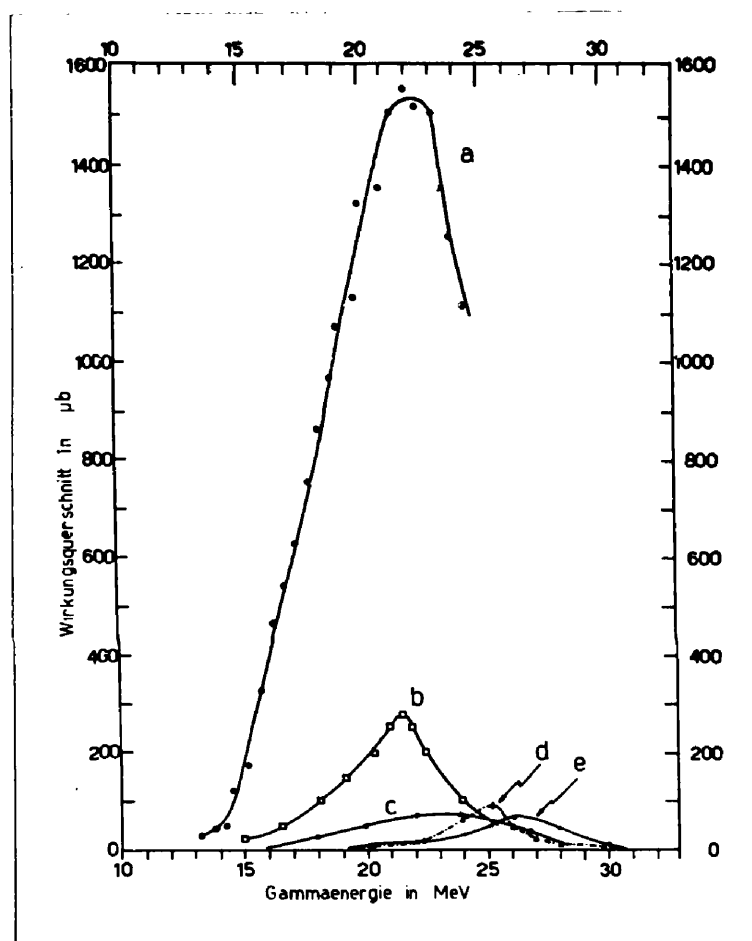


Figure 10.

Cross-sections for (γ, α) reactions.

- a. $\text{Cu}^{65}(\gamma, \alpha)\text{Co}^{61}$ (Haslam, R.N.H., Smith, J. & Taylor, J.G.V. Phys. Rev., 87, 633 (1952).
- b. $\text{Br}^{81}(\gamma, \alpha)\text{As}^{77}$ (Taylor, J.G.V. & Haslam, R.N.H. Phys. Rev., 87, 1138 (1952).
- c. $\text{Rb}^{87}(\gamma, \alpha)\text{Br}^{83}$ (Haslam, R.N.H. & Skarsgard, H.M. Phys. Rev., 81, 479 (1951).
- d. $\text{Sb}^{121}(\gamma, \alpha)\text{In}^{117\text{m}}$ (59)
- e. $\text{Tl}^{205}(\gamma, \alpha)\text{Au}^{201}$ (59)

emitted from copper was measured by Byerly and Stephens (37) at $E_0 = 24$ Mev and they concluded that these particles were emitted in an evaporation process.

(c). Two approaches have been made to illustrate the properties of those reactions in which very many nucleons are emitted. The first, namely the irradiation of photographic emulsions, was used by Kikuchi (59) who determined the yield of stars as a function of the peak photon energy. He found that, when the peak energy was raised from 150 Mev to 300 Mev, the major increase in yield came from three or more prong stars. The experimental results were not sufficiently conclusive to enable a definite estimate to be placed on the yield of two-prong stars and it is possible that they showed a comparable increase in yield. Little variation was found for the yield of single protons in this energy range. The second involved the measurement, after chemical separation, of the relative activities of the decay products from the irradiated nucleus. A typical example of this method was published by Debs. et al. (60) who irradiated arsenic, germanium, gallium, zinc and copper, and detected isotopes which differed from the target nucleus by as much as 20 nucleons.

The energy dependence of the yield of some reactions of this type was illustrated by Sugihara and Halpern (61)

who combined their results with those of Holtzman and Sugarman (62) to show that

(i) for the $\text{As}^{75} (\gamma, 2pn)$ reaction, the yield rose by a factor of approximately 4 when the peak energy was increased from 50 to 140 Mev, but only by a factor of 1.3 when the peak energy was further increased to 320 Mev. They concluded that for this reaction the energies of the absorbed photons were < 140 Mev.

(ii) in reactions leading to Ga^{73} , Ga^{68} , Ga^{66} , Cu^{67} , Cu^{61} and Ni^{66} they could assume that the photons had energies > 140 Mev. As can be seen from the published data, the main disadvantages of this method were that no estimate could be made of the probability of emission of nucleons in the form of composite particles and that, where non mono-isotopic targets were irradiated, the interpretation of the yields was complicated by the production of the same daughter nucleus from different target nuclei.

It appeared therefore that such reactions were produced by photon absorption in a wide energy range. Apart from the emission of a few fast particles immediately after the absorption of the photon, the remaining fragments were found to behave in a manner consistent with an evaporation process.

Measurements of the energy and angular distributions of high energy protons which were emitted from

photonuclear reactions have led to a general confirmation of the proposal formulated by Levinger (63) who suggested that, at high energies and in complex nuclei, the incident photon interacted directly with a two nucleon sub-structure. Barton and Smith (64) have detected coincident pairs of protons and neutrons from lithium and found that the angular distribution was consistent with the predictions of the quasi-deuteron theory. Similar results were obtained by Wattenberg et al. (65) for other nuclei. Further support for the quasi-deuteron model was derived from the photoproton measurements where breaks in the energy distributions and forward peaks in the angular distributions were interpreted as evidence of the interaction of the incident photon with a two nucleon sub-structure. At these energies it was accepted that electric dipole absorption was predominant and the very low yields of proton-proton pairs were interpreted as an indication that the contribution from quadrupole absorption was small.

Finally, it would appear that for reactions in which two or more nucleons are emitted, at low energies, the absorption is followed by the formation of a compound nucleus which then decays in a manner governed by statistical theory. On the other hand, at very high energies the primary interaction is between the incident

photon and a two nucleon sub-unit with the subsequent formation of a compound nucleus if both particles failed to emerge. The intermediate energy range has not been investigated in detail and consequently no estimate can yet be made of the relative contributions of these two mechanisms in this region. Similarly, one cannot neglect the possibility that there exists a primary interaction between the incident photons and alternative sub-units within complex nuclei, e.g., a quasi- α -particle sub-structure.

CHAPTER II.

EXPERIMENTAL TECHNIQUE.

A volume-defined Wilson cloud chamber, 12 inches in diameter, was used in studies of the photo-disintegration of neon and oxygen. The chamber was filled with the gas under investigation and consequently played the rôles of both target and detector. The bremsstrahlung beam passed through the chamber and the tracks of charged particles, emitted in photon-induced reactions in the target gas, were recorded photographically.

The annotated diagram, Figure 11, illustrates the component parts of this chamber. The target gas was contained in a volume which was defined by the cylinder, top-plate and the flexible diaphragm located beneath the chamber base-plate. The top was of Triplex glass, 30 cms. in diameter and 2 cms. thick, and the base was a brass plate perforated with a large number of small holes to allow uniform gas flow between the volumes which lay above and below. The volume was made gas tight by fitting neoprene gaskets at the top and the bottom of the cylinder.

Before the top-plate was clamped to the Perspex cylinder, a few c.c.'s of a dilute solution of acetylsalicylic acid in water were sprinkled on the velvet which covered the chamber base. This was necessary as it had been found in the past that the presence of a small quantity of this solution prevented the growth of mould on

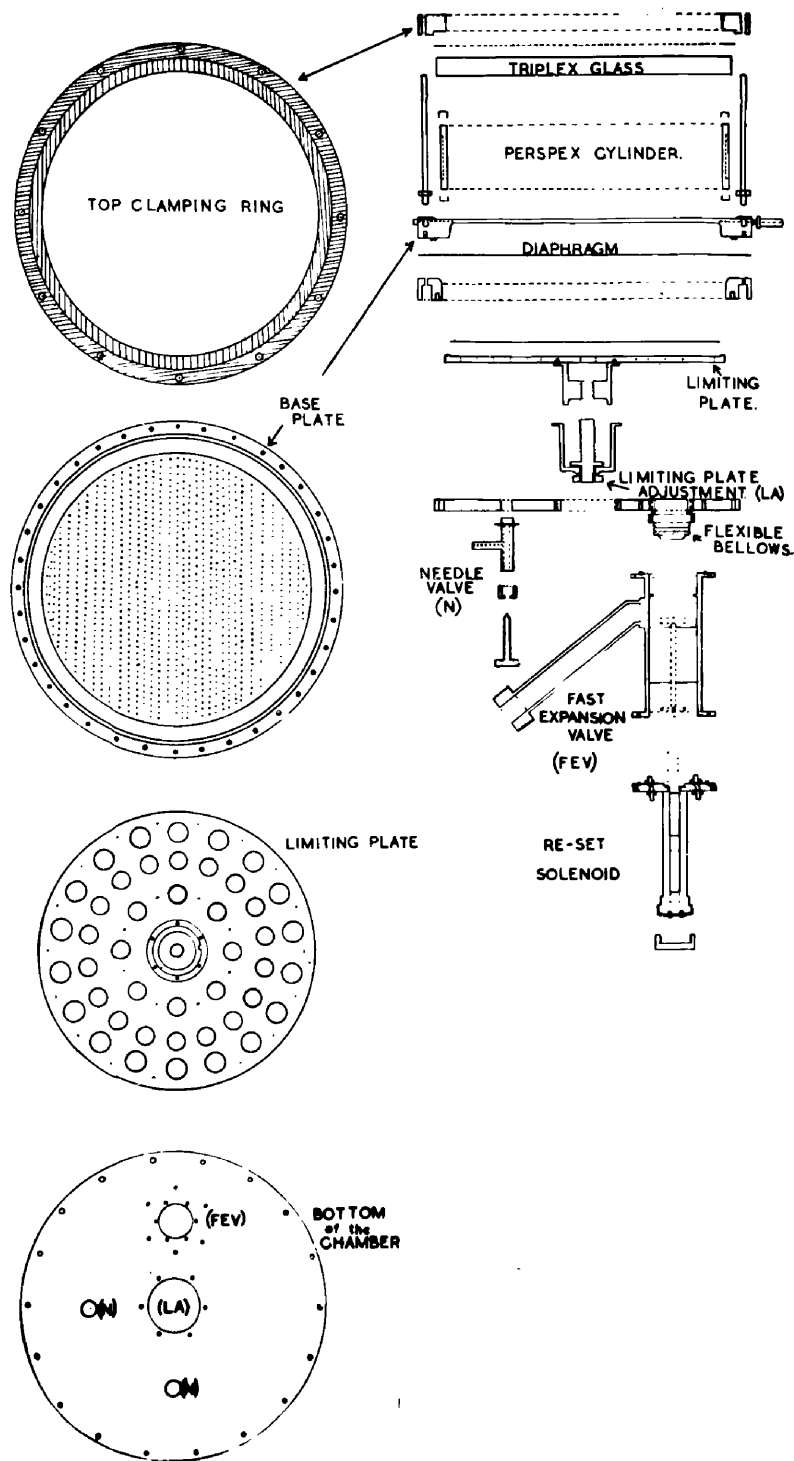


Figure 11.

Component parts of the cloud chamber.

the velvet. If only water were added to the chamber, the mould appeared after the chamber had been sealed for a period of a few weeks. As a precaution against the phenomena associated with vapour depletion, a relatively large quantity of water was added in the above procedure because a considerable amount of water vapour was later removed during the vacuum tests, etc.

The chamber was first evacuated and then filled with the appropriate gas, saturated with water vapour, through a port in the base-plate, and, when filled to the required pressure, this port was sealed.

The cylinder was made of quarter-inch thick Perspex 11.5 inches internal diameter and 2.5 inches high. A significant reduction in the number of electron tracks was achieved by reducing the thickness of the chamber walls to 0.09 inches over two diametrically opposite areas of approximately 1.5 inches x 3.75 inches, which provided entry and exit 'windows' for the beam.

For the investigations reported in Chapters IV and V, diaphragms of neoprene and 1/16-inch para-rubber respectively were used. The position of the diaphragm could be varied by altering the pressure difference across it. The upwards travel was limited by the bottom of the base-plate while the extent of the downwards motion was governed by a limiting plate. The position of this plate

could be altered by turning the threaded screw at the bottom of the chamber assembly. To move the diaphragm upwards, compressed air was fed into the volume below the diaphragm from a reservoir tank, the pressure in which was controlled by a reducing valve. The compressed air flowed through a solenoid-operated valve and a needle valve into the chamber. In the case of a 'fast' expansion this air was released to the atmosphere through the one-inch diameter exit arm of the 'fast' valve, while for a 'slow' expansion the gas passed to the atmosphere through a second solenoid valve.

When the piston of the 'fast' expansion valve was in its uppermost position it pressed against the smooth rim of a flexible brass bellows, thereby sealing the lower section of the chamber from the atmosphere. The shaft of this piston was made of steel and it was held in place by the action of a D.C. solenoid through which passed the cathode current of a pair of 6L6 output tetrodes connected in parallel. This current was of the order of 80 milliamps. When a large negative pulse was applied to the control grids of these valves, the current was cut off and the pressure acting on the upper face drove the piston downwards and allowed the gas to pass out through the side orifice. After the expansion a second solenoid, situated below the first, was energised by closing a relay which connected the

coil to a 24-volt D.C. supply. The half-steel, half-brass armature within this coil was driven upwards and forced the 'fast' valve piston into its original position where it was held by the field of the first solenoid.

An electric field was applied between the top and bottom of the chamber in order to remove unwanted charged ions. The brass base of the chamber was earthed and a clearing field of 400 volts D.C. was connected to a thin conducting ring on the under-side of the top-plate. This ring was painted directly on to the glass using a colloidal suspension of graphite in water (Aquadag). At one point on the circumference of the top-plate the ring was extended on to a wide area of the side to which the field supply was fed through thin copper straps held firmly against the graphite. This field was switched off before the 'fast' expansion took place.

To provide a satisfactory matt surface against which to photograph, black velvet was stretched over the upper surface of the perforated base-plate. Thin nickel wires were stretched across the chamber to form a grid which rested on the surface of the velvet. Since the longitudinal wires (parallel to the beam direction) were also parallel to the light sources, they reflected more light than the transverse ones and consequently were made as thin as practicable - in fact, 0.002 inches. The

transverse wires were 0.005 inches. The nett result was a grid of the form shown in Figure 12, which was later used in the analysis of the recorded events.

As any single 'run' was likely to last a period of at least four hours, it was necessary to stabilise the gas temperature. This was achieved by fitting an aluminium shield round the chamber to which were attached water-cooling pipes. This shield served a dual purpose in that it also screened the chamber from any unwanted light. The inside surface was covered with a black, matt-finish paper to prevent unwanted light reflections. Five rectangular 'windows' were cut in the wall of the cylinder to provide three ports through which to illuminate the chamber and two which acted as entry and exit ports for the photon beam. The gas temperature was monitored by a thermistor whose resistance could be measured on a bridge of which it constituted one arm.

A weak polonium source was mounted on the inside surface of the Perspex cylinder. Initially the operating conditions were adjusted until the alpha-particles from this source provided sharp tracks in the chamber.

The chamber was illuminated by two flash lamps situated on either side of the chamber. Each lamp consisted of a Mullard LSD16 xenon-filled discharge tube enclosed in an ebonite box with an inset plano-convex cylindrical lens

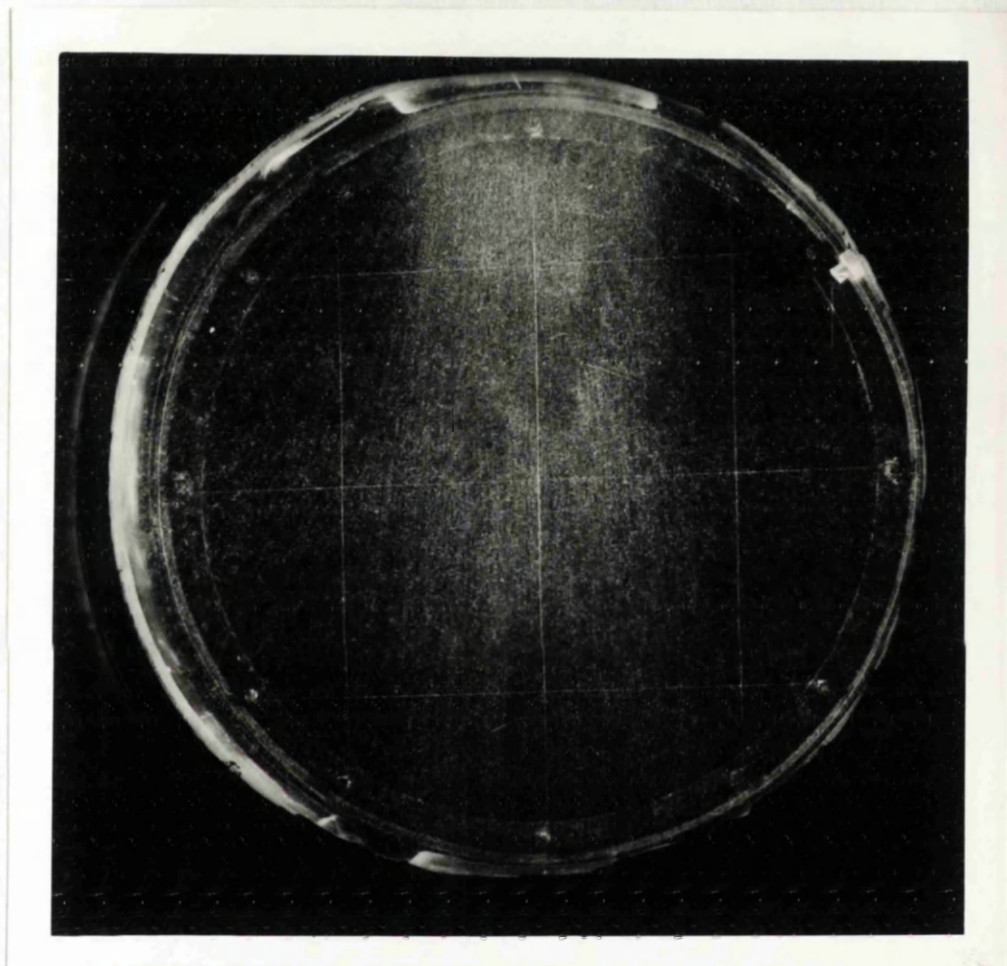


Figure 12.

Typical cloud chamber photograph which illustrates the grid and the background of electron tracks. The track of an α -particle from the polonium source can be seen top-right, while a proton track is visible within the beam.

10.5 inches long and 1 inch broad. The discharge tube approximated to a line source and was positioned along the focus of the cylindrical lens. The lamp boxes were 4.3 inches from the Perspex cylinder and lay parallel to the central grid wire. They were mounted in such a manner that they could be adjusted individually. Each of the discharge tubes was connected across a bank of condensers, of capacity 300 μF , which could be charged to a maximum of 2.5 kv. The energy stored in the condensers was discharged through the lamps when the gas discharge was triggered by a high voltage pulse supplied by the secondary of an automobile ignition coil. This pulse was fed on to a wire spiral wound round the discharge tube. The duration of the flash was lengthened to about 0.5 millise. by including a choke in the discharge circuit. A 'steady' lamp (consisting of a 6 volt, 24 watt bulb behind a cylindrical lens) was used when the tracks were being examined visually, as the flash was too brief and intense. The light from the lamps formed a parallel beam which passed horizontally through the chamber. The cameras, situated above the chamber, recorded the light which was scattered upwards by tracks in the sensitive volume.

The type of camera used in the experiments reported in Chapters IV and V is shown in Figure 13 and the features of this camera are discussed overleaf.

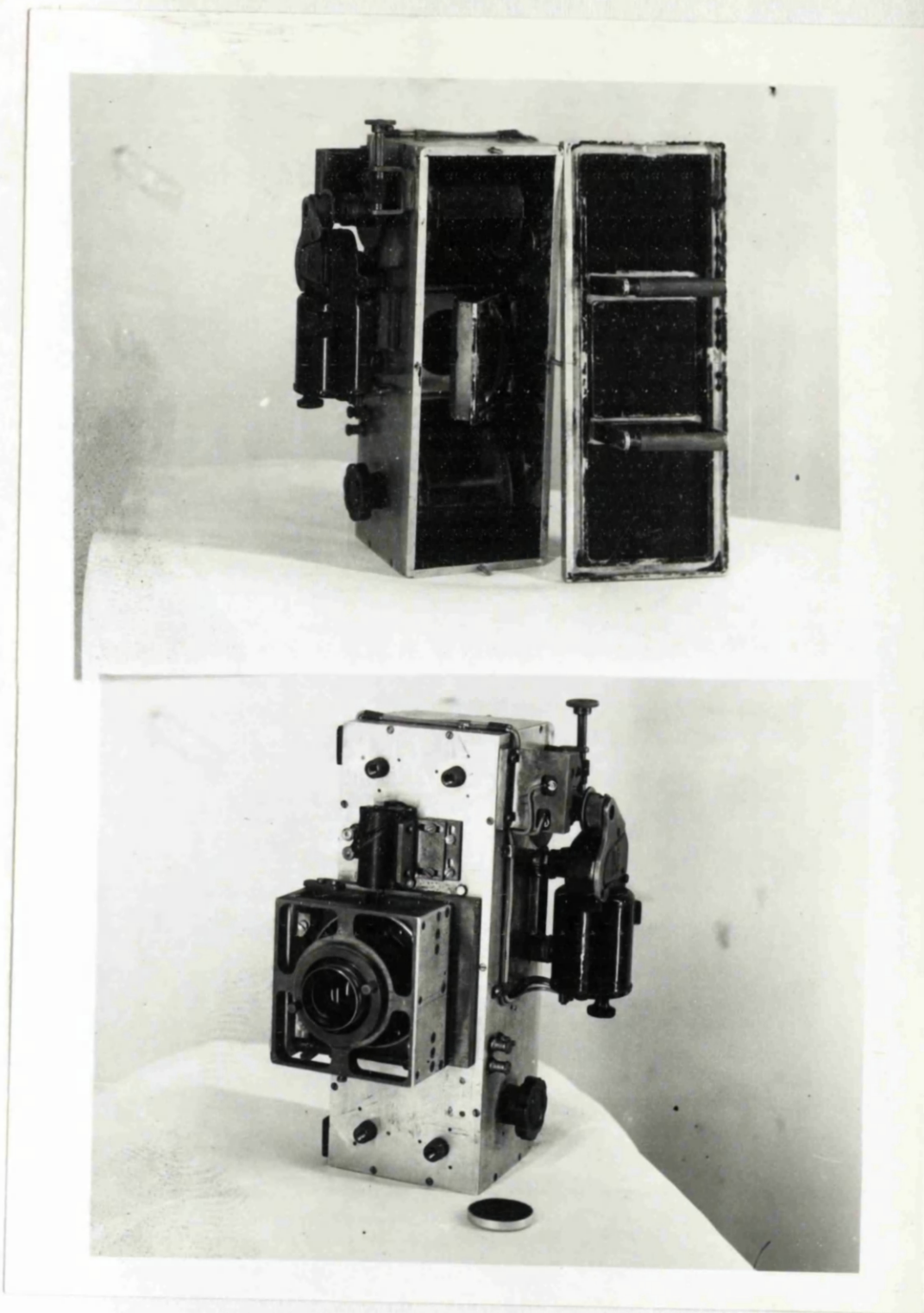


Figure 13.

One of the cameras.

Ental 80 mm. f/4.5 enlarging lenses were mounted in a manner that permitted the alteration of the focus and, in the cameras labelled S2 and S3, the whole lens assembly was displaced laterally to enable a full view of the chamber to be recorded on each film. Solenoid-operated shutters, which were inserted behind the lenses, were opened for a period of from one to two seconds by energising the solenoid, but the exposure time was in fact determined by the duration of the lamp flash. Under normal conditions the photographs were taken with the beam room in total darkness.

5G91 Ilford recording film, 60 mm. wide, was used in 25-foot rolls and approximately 120 exposures were recorded on each. The film was drawn through the 'gate' by a 24 volt D.C. motor which rotated the 'take-up' spool. The 'gate' consisted of an aluminium base with a glass pressure plate above and lateral definition of the film position was provided by a spring-loaded guide on one side of the 'gate'. A fine adjustment was also provided on the shaft of the 'take-up' spool but this was only used where the normal reprojection procedure was in operation.

The 'take-up' drum rotated through 120° between successive exposures and the extent of the rotation was determined by a micro-switch which pressed against the shaft. The diameter of the drum was so chosen that the

length of film that passed through the 'gate' during each of these rotations slightly exceeded the diameter of the images.

Four asymmetric studs located each camera on a 'Tufnol' board which was supported, 62.7 cm. above the top-plate of the chamber by the camera stand whose base consisted of a circular ring which was bolted to the twelve supporting pillars of the chamber when the stand was in position. The stand was orientated in such a manner that the films ran at right angles to the central grid wire.

In order to facilitate the analysis, the magnifications of the cameras were made exactly equal. Each was determined from microscope measurements made on test photographs of a grid.

Further test photographs were taken in order to estimate the quality of the chamber illumination. The effects produced by poor collimation of the light beam were immediately obvious on examination of these exposures. The peak voltage of the condenser bank was varied and an exposure taken at each value in order to determine the optimum operating voltage.

The condensation nuclei which remained after a 'fast' expansion had to be removed before the next expansion if the cloud chamber was to be used successfully. In order to achieve this, 'slow' or 'clearing' expansions were made between successive 'fast' expansions, in the manner

described previously. Over as lengthy a period as 120 complete cycles it was of the utmost importance to ensure uniformity of track quality and to this end the 'slow' expansions were made fully automatic.

A uniselector mechanism was the basic component of the unit built to carry out this procedure. In principle this consisted of a switch with eight banks, each with 25 contacts. These were selected in turn by eight wiper arms which were moved to successive positions by energising the control solenoid. The coil was situated in the cathode of a thyatron whose grid was at a fixed negative potential. The anode was connected to the positive terminal of a 30 μF condenser which was charged up through one of several resistances from a stabilised high tension supply. When the voltage on the anode of the thyatron exceeded the critical value, the valve conducted and the condenser discharged through it, thus energising the uniselector solenoid. The interval of time between successive discharges was determined by the time constant of the condenser and the resistance appropriate to the position occupied by the wiper arm before each discharge took place. Hence by using one bank of contacts to select the appropriate resistances, it was possible for the uniselector to control the timing of its own cycle.

The solenoid valves, which controlled the 'slow' expansions and compressions, were energised when a wiper arm made contact with the appropriate contacts on one bank. The other banks were used to control the auxiliary operations associated with the cycling of the cloud chamber. These included

- (a) opening and closing the shutters;
- (b) energising the reset solenoid;
- (c) winding the films forward after each exposure;
- (d) the inclusion of a delay after the last 'slow' expansion to ensure that the working gas had returned to a stable condition. (This was necessary, because turbulence distorted the tracks).
- (e) switching off the clearing field before the 'fast' expansion. If this were not done, the ions were dragged out of the tracks, with the result that they became less well defined.

Five seconds were required to complete each 'slow' expansion and the variable delay, which followed the last of these, was greater than 35 seconds. The number of 'slow' expansions which were required to clear the chamber was dependent on the intensity of ionisation which was present, and it was found that a minimum of three was required. In the construction of this unit provision was made for a maximum of five 'slow' expansions.

Before the cloud chamber was moved into the synchrotron beam room, the photon beam had to be collimated. The position of maximum intensity of the uncollimated beam was determined by irradiating an array of thin copper rods and counting the induced beta-activity of each in a standard geometry. A block of lead with a rectangular aperture cut in it was positioned so that the centre of the aperture coincided with the position of maximum beam intensity. The near face of this block was 36.8 cms. from the synchrotron target. The aperture measured 3.9 cms. by 0.95 cms. at the face nearest the synchrotron and 5.5 cms. by 1.4 cms. on the other. The collimator was mounted in position and the intensity distribution of the beam that emerged from it was recorded on an X-ray film located on the beam room side of the collimator. Two lead plates were mounted, one on each side of the collimator, each with a row of three pin-holes drilled in it, the middle one being located at the centre of the collimator aperture. The line joining the three holes in the one plate was at 45 degrees to the corresponding line in the other. When an X-ray plate was irradiated beyond the lead plates, the pattern of spots that was observed indicated the orientation of the collimator with respect to the beam direction. When correctly aligned, i.e., when the axis of the collimator

passed through the synchrotron target, the spots corresponding to the two central holes were superimposed. Finally the intensity distribution of the beam that emerged from the correctly orientated collimator was determined by irradiating another array of copper rods. The chamber was then positioned in front of the collimator and its height adjusted until the beam passed centrally through the sensitive region.

In a study of photonuclear reactions, it is essential that good track quality be obtained in order to be able to differentiate between singly- and doubly-charged reaction products. In order to achieve this, the output of the synchrotron was reduced to single, short bursts of γ -rays. Once the value of the expansion ratio had been fixed, the track quality depended on the time delay between the 'fast' expansion and the passage of the photon beam. When the synchrotron was operated under 'single-shot' conditions, the magnet was permanently energised and the bursts of γ -rays were obtained when the synchrotron gun was pulsed via a push button. When this button was pressed, a pulse, derived from a peaker coil within the magnet, was passed to a flip-flop circuit in the cloud chamber control unit which produced the negative pulse that triggered the 'fast' expansion. After the cloud chamber pulse there was a finite delay before the pulse was passed

to the synchrotron gun. This delay could be altered in steps of 5 milliseconds between 30 and 70 milliseconds and the shortest delay consistent with good track quality was used in the experiments. This optimum value was approximately 40 milliseconds. Too short a delay produced diffuse tracks; too long a delay increased the background intensity. After a further delay, a pulse was fed from the chamber control unit to the primary of the ignition coil whose secondary provided the pulse that triggered the lamps. This delay was continuously variable with an optimum value of approximately 120 milliseconds. This was the minimum delay selected so that although sufficient condensation had occurred on the heavy charged-particle tracks, the electron background intensity was not at its maximum nor had the tracks of interest become diffuse.

To monitor the beam an ionisation chamber was mounted on the wall of the synchrotron beam room behind the cloud chamber and the pulses from it were amplified by a conventional amplifier before being displayed on a Cossor oscilloscope. The height of each pulse was measured on the screen of the cathode-ray oscilloscope and the total irradiation dose for each experiment was obtained by summing these pulse heights. The monitoring system was calibrated by comparing the pulse heights noted during an irradiation of a standard copper sheet to the activity

induced in the sheet. This activity was counted in a standard geometry and use was then made of the calibration derived by I.F. Wright (66), who compared the activity induced in the copper sheet with the response of a Victoreen thimble mounted at the centre of a Perspex block.

Under conditions of constant magnet current, the peak energy of the bremsstrahlung beam was determined by displaying the r-f envelope and a pulse from a peaking coil on the two traces of a twin-beam oscilloscope and arranging that the 'back edge' of the r-f envelope coincided in time with the pre-set position of the pulse from the peaker coil. The value of the bias current, which determined at what time the peaker pulse appeared in the magnet cycle, provided a measure of the maximum energy of the circulating electron beam. Before each run the bias current was set at the required value (obtained from the machine calibration) and the 'back edge' of the r-f envelope was brought into coincidence with the peaker pulse on a time scale. No adjustments were made to the r-f envelope without subsequently repeating the above procedure. It was estimated that the peak energy of the circulating electron beam was stable to within ± 0.5 Mev.

CHAPTER III.

THE ANALYSIS PROCEDURE.

In earlier experiments the chamber was photographed with three cameras, with tilted lenses, inclined to one another and the photographs of the recorded events were analysed by a standard reprojection method. In this method the films were replaced in the appropriate cameras and light was shone down through the cameras from above. The images of the events recorded on the films were cast on a pivoted table below. The table was moved until the three images were superimposed. In this condition the coincident images corresponded exactly, in orientation and magnitude, to the original track.

In cloud chamber studies of photonuclear reactions it is sometimes necessary to measure the ranges of the recoiling residual nuclei. Such nuclei normally yield tracks of less than 1 cm. and the reprojection technique was intrinsically incapable of measuring such short tracks to any reasonable degree of accuracy. One solution to this problem was proposed by I.F. Wright (12) who measured, directly on the films, the lengths of these short tracks using a binocular microscope of low magnification ($\times 25$).

In this technique the true length of the track could be calculated from the measurements using the known geometry of the camera system. Such calculations could be complicated and laborious and consequently liable to arithmetic error but could be greatly simplified by

choosing a suitable camera geometry. In the system chosen, the three cameras were mounted on a horizontal board with the lenses at the vertices of an isosceles triangle (Figure 14). The origin of the co-ordinate system associated with the cameras was defined by the intersection of the vertical projection through the centre of the lens of the T_1 camera and the plane of the chamber grid. The X-axis was defined to be the beam direction, which was also the direction of the central grid wire, while the Y and Z axes completed the orthogonal set. The calculations thereafter assumed that the film from the T_1 camera was used together with one other. Where there were three cameras in use, the second film was chosen to be that from the camera nearest to the particular event under examination, thereby reducing lens distortion to a minimum.

When the cameras were mounted in the reprojection stand shown in Figure 15, the vertical separation of the camera board and the moveable table, in its lowest position, was made equal to the previously measured distance between the board and the chamber grid. The origin of the reprojection frame of reference was defined by a plumb line suspended from the centre of the lens of the T_1 camera. By replacing the films in the appropriate cameras and aligning the reprojected images, it was possible to define the direction of the central grid wire and hence the X-axis.

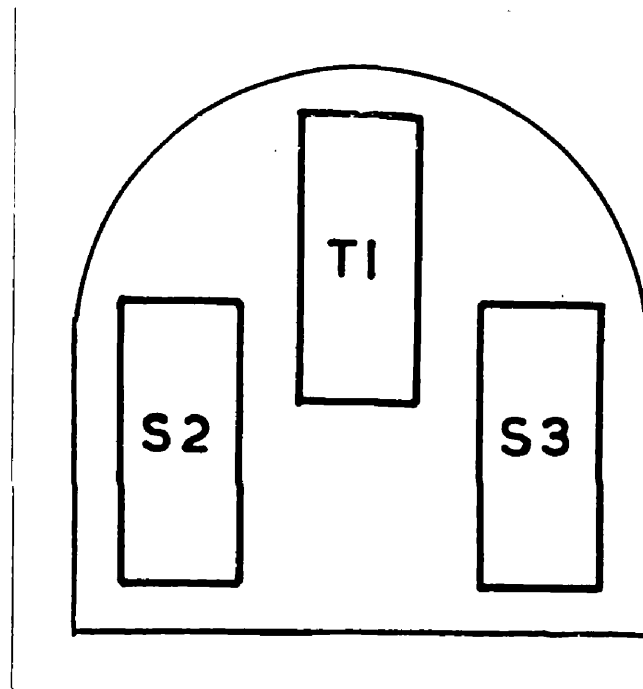


Figure 14.

The relative positions of the
cameras.

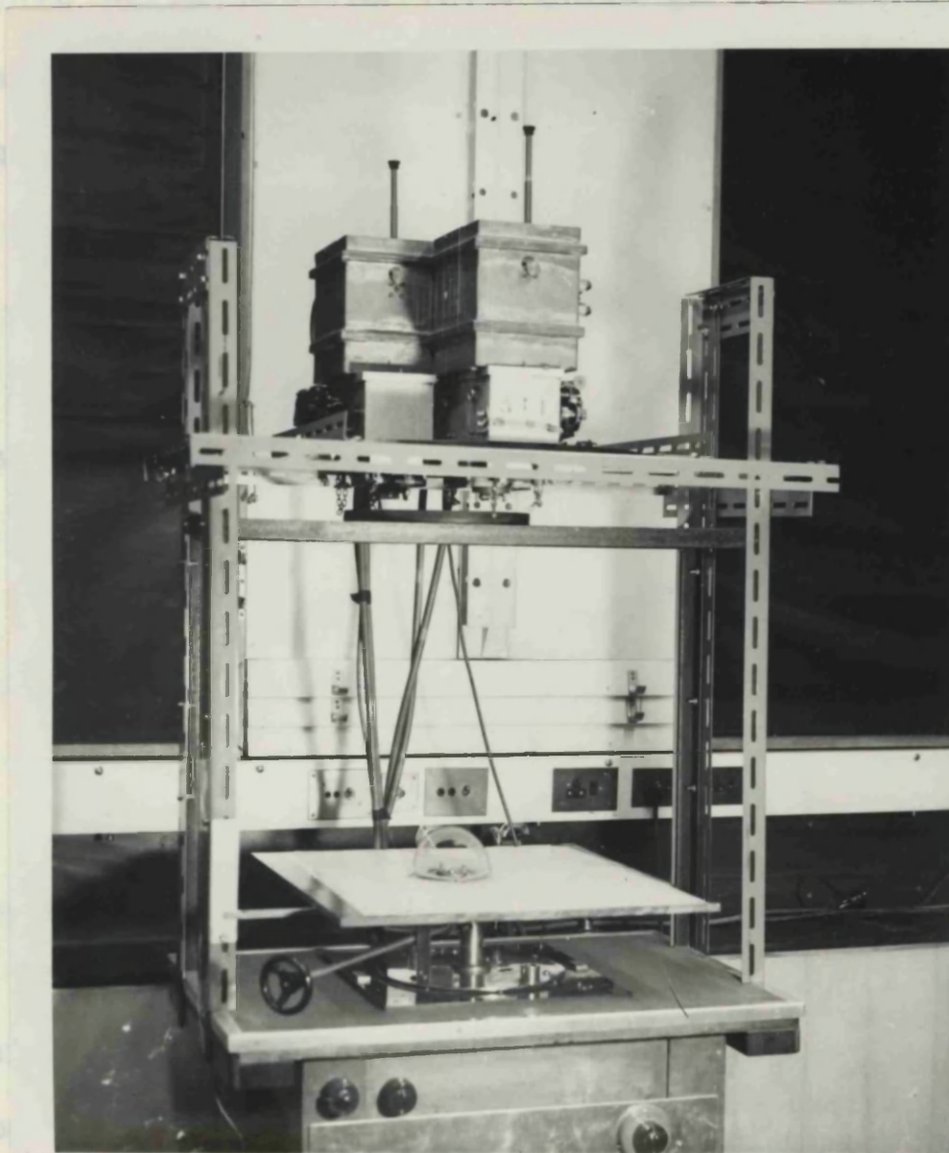


Figure 15.

The reprojection stand with the track simulator on the moveable table.

In this procedure the top-plate of the chamber was inserted between the cameras and the table to cancel the effects of refraction introduced by the glass while the exposures were being made. Thereafter any point in the chamber could be located in the reprojection system with the use of a millimetre grid fixed to the top of the table and a vertical scale alongside.

In the analysis of each track one normally wishes to obtain the following properties:-

- (1) the positions of the origin and end point of the track, should the latter lie within the sensitive volume of the chamber.
- (2) the angle between this track and a standard direction (i.e., the axis of the beam).
- (3) the length of the track.

When using the microscope technique the co-ordinates of a point on the track were measured with respect to the reference grid on the base of the chamber (Chapter II), and all the angles were measured with respect to the central grid wire. As mentioned earlier, this direction was chosen to be parallel and vertically below the axis of the beam.

The measurements were carried out as follows:-

- (a) Using the vernier scales associated with the microscope stage movements, the co-ordinates of the origin

and end-point of each track were measured relative to the nearest reference point on the central grid wire (for the T_1 film), and this process was then repeated for the second film. This yielded (x_1, y_1) and (x_2, y_2) . If these were then added to the co-ordinates of the chosen reference point, one obtained the co-ordinates of these points in the camera frame of reference.

(b) The angles between the track and the central grid wire were measured with the goniometer head on the microscope for both films. This gave γ_1 and γ_2 .

(c) The lengths of the track, as recorded on both films, were measured with the eye-piece scale of the microscope to yield L_1 and L_2 .

The co-ordinates (x, y, z) of the point could be calculated from

$$Z = C (|x_1 - x_2| + |y_1 - y_2|)$$

$$Y = my_1 (1 - z/h) + Y_{\text{ref.}}$$

$$X = mx_1 (1 - z/h) + X_{\text{ref.}}$$

where

C = a constant dependent on the dimensions of the camera system.

h = the vertical height of the lenses above the plane of the grid.

m = the magnification of the recording system.

The value of m was obtained from the ratio of "the distance between two specified reference points on the central grid wire as measured on the film with a microscope" to "the distance between the same two points measured in the chamber".

The calculations which derived the co-ordinates from the measurements on the film were based on the following conditions:-

- (1) The image of a track on any film was a horizontal projection of that track.
- (2) The height of a point above the grid was proportional to the displacement, from the grid, of its projection from a fixed point, which was not vertically above it. Consequently the height of a point was defined by the measurements of the displacements from two fixed points.

Although it was possible to calculate the angles of a track from the measurements made on the films, the necessary calculations were exceedingly laborious and a track simulator (Figure 16) was introduced into the reprojection system to facilitate the analysis. This track simulator was a mechanical device consisting of a needle, six inches in length, mounted in a ball and socket at the centre of a 360° protractor. Light was shone down through the cameras on to this device when situated on the reprojection table. The simulator was positioned in such a

radius that the co-ordinates of the center of the ball in the camera frame of reference were those of the origin of the event, if it lay lower than the end point. The

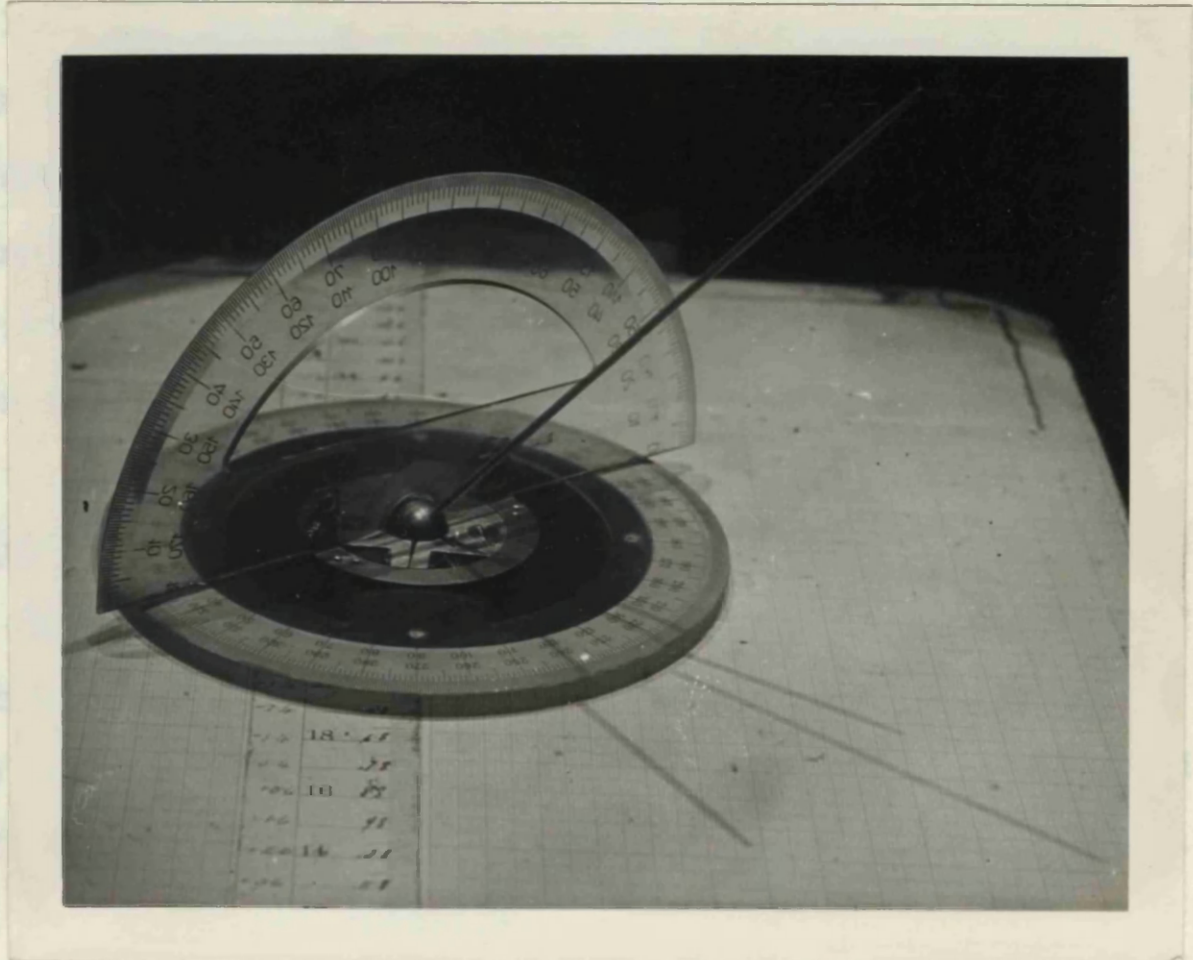


Figure 16.

The track simulator.

The technique was modified if the track direction was downwards. The simulator was moved to occupy the position of the bottom of the track, i.e., the end-point. As a result of this, the angle cast by the needle were now $\theta_1 + 180^\circ$ and $\theta_2 + 180^\circ$. The angle read off the vertical protractor was now negative. The angle in the vertical plane was designated by the symbol α while that in the horizontal plane by θ .

If θ was $> 180^\circ$ the values used in the angular

manner that the co-ordinates of the centre of the ball in the camera frame of reference were those of the origin of the event, if it lay lower than the end point. The 0° - 180° and 90° - 270° lines on the protractor were aligned with the X and Y axes respectively. The needle was then rotated until the shadows that it cast on the horizontal plane made angles with respect to the X-axis equal to the corresponding angles measured on the films. The needle then had the same orientation in the reprojection system as the track possessed in the chamber system. The required angles were then read off the protractor scales if allowance was made for the thickness of the needle by taking the mean of the readings obtained with the protractor on either side of the needle. The angle read off the vertical protractor was taken as positive, i.e., the track pointed upwards.

The technique was modified if the track direction was downwards. The simulator was moved to occupy the position of the bottom of the track, i.e., the end-point. As a result of this, the angles to be cast by the needle were now $\psi_1 + 180^{\circ}$ and $\psi_2 + 180^{\circ}$. The angle read off the vertical protractor was now negative. The angle in the vertical plane was designated by the symbol α while that in the horizontal plane by θ .

If θ was $> 180^{\circ}$ the values used in the angular

distributions were $360^\circ - \theta$. This was based on the reasonable assumption that the distribution between $\theta = 0^\circ$ and $\theta = -180^\circ$ was equivalent to that between $\theta = 0^\circ$ and $\theta = +180^\circ$.

Although the lengths of the tracks could be calculated from the co-ordinates, i.e.,

$\sqrt{\Delta x^2 + \Delta y^2 + \Delta z^2}$ it was considered more accurate to measure them on the films. These were the values L_1 and L_2 mentioned earlier. The track simulator was used to convert these values into true track lengths in the following manner.

When the simulator was positioned to determine the angles, only one lens was left uncovered and the simulator moved, without altering the orientation of the needle, until the end of the shadow coincided with the point defined by the co-ordinates of the end-point of the track, if α was positive. The length of the shadow was then measured L_1^S . The process was repeated with the second camera to give L_2^S . An analogous procedure was employed where α was negative.

The length of the track was obtained from

$$l_{\text{track}} = l_{\text{film}} \frac{l_{\text{needle}}}{l_{\text{shadow}}} M \left(1 - \frac{z_L}{h} \right)$$

where

z_L = the z co-ordinate of the lowest point on the track.

M = the magnification associated with the eye-piece scale. This was determined by a procedure analogous to that adopted earlier in finding the value of m .

In addition to the ease with which the process could be carried out, it was more reliable, since each step could be verified, e.g., if the co-ordinate measurements were in error it was not possible to obtain agreement between the 'shadow' angles and those measured on the films. Similarly, where three cameras were used, agreement could not be obtained if in fact one of the angles had been incorrectly measured.

There was one restriction to the applicability of this system. The mechanical design of the simulator prevented a measurement in the vertical plane of angles of less than 10° . However, the significant angle to be obtained was in fact γ (the angle between the track and the axis of the beam) and this is obtained from

$$\cos \gamma = \cos \theta \cos \alpha$$

and consequently where α was less than 10° the value of the cosine was close to unity and the error introduced in γ was small. The effect on the length measurements was also small. The error introduced into the measurements by assuming that $\cos \alpha = 0.995$ for all tracks with $\alpha < 10^\circ$ was less than 1%.

The accuracy of the microscope measurements was estimated from a ten-fold analysis of a track, selected at random, using the microscope technique only. The results obtained from this survey showed that

- (1) for the measurement of X and Y co-ordinates (40 measurements) the standard deviation was approximately 0.05 cm.
- (2) for measurements of Z co-ordinates (20 measurements) the standard deviation was 0.125 cm.
- (3) measurement of the length using the eye-piece scale had a standard deviation of 0.025 cm. in actual track length. This figure could be larger if the track quality were poor.
- (4) the standard deviation in the measurement of angles, using the goniometer, was of the order of one degree. It was believed that, using the track simulator, the error in θ would be about the same, i.e., 1° , while that in α would be slightly larger - about three degrees.

As can be seen from the above results, the accuracy of the determination of the lengths of the tracks from the co-ordinate measurements depended largely on the accuracy of the determination of the Z co-ordinates. It was for this reason that the ranges of the charged particles

measured in the experiments reported in Chapters IV and V were taken from the track simulator readings rather than from the co-ordinates. It was believed that the error in this process amounted to less than 0.1 cm.

The reprojection system was checked by comparing the lengths as measured by this method with those obtained from the co-ordinates of the end-points of the tracks (this also checked the accuracy of the orientation of the track simulator) for a large number of events. A typical example of this process is illustrated in Chapter V.

In an attempt to estimate the extent of subjective errors, a large number of events were analysed by two independent workers and the results indicated that these errors were of the order of or less than those discussed above.

CHAPTER IV.

PHOTOPROTONS FROM NEON.

4.1. Introduction.

The photodisintegration of neon was studied primarily to investigate the multiple emission of nuclear fragments such as α -particles and protons (Appendix II). However, a considerable number of photoprotons were recorded and it was decided that these were worthy of detailed analysis. This was made difficult by the fact that all but three of the photoprotons did not stop in the sensitive volume of the chamber and as a result the energies of the protons could not be determined from their ranges.

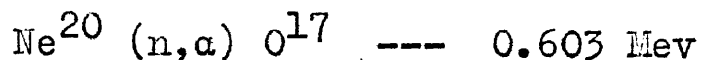
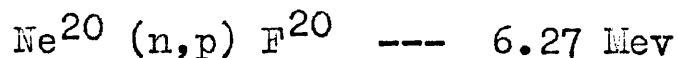
4.2. Specific experimental conditions.

A conventional volume-defined cloud chamber was filled with 'spectrally pure' neon, saturated with water vapour, to a pressure of 1.2 atmospheres and positioned in the beam of the 23 Mev synchrotron. A beam of peak energy 23 ± 0.5 Mev was passed through the centre of the chamber, care being taken to ensure that the beam did not strike the chamber base or the top plate. The tracks were recorded by three cameras on 5G91 recording film and the tracks were subjected to the analysis procedure described in Chapter III. The total irradiation dose was determined to be 0.1 r and a total of 900 exposures was made.

4.3. Experimental Results.

The thresholds for the (n,p) and (n,α) reactions

which were liable to be confused with the (γ ,p) and (γ , α) reactions are given below:-



The introduction of 4 inches of paraffin wax, behind the collimator, served to moderate the fast neutrons. The effectiveness of this precaution was demonstrated by the fact that very few events were recorded with origins outside the known dimensions of the beam.

As neon was mono-atomic, its stopping power was low, and in all but three of the 303 recorded (γ ,p) events the photoproton left the sensitive volume. It was decided that it was feasible to measure the F^{19} recoil tracks and from these obtain the proton energies although the accuracy of such a procedure was poor. The recoiling F^{19} nuclei rarely travelled more than 4 mm. and it was estimated that the error in the calculated energy of any individual event was of the order of 1 Mev.

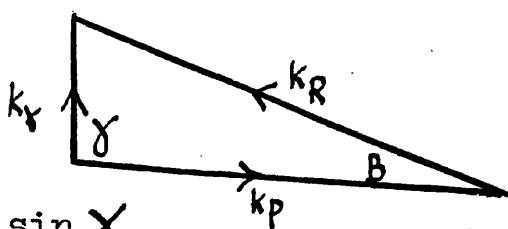
Measurements were made of the lengths of the tracks of the recoiling F^{19} nuclei and the angles between the photoproton tracks and the beam direction. The energies of the recoils were determined from a range-energy curve for F^{19} nuclei in neon as derived by D.R.O. Morrison (67). This relationship was extrapolated to low energies and the validity of this extrapolation was determined by comparing

the energies of the F^{19} recoiling nuclei calculated from the energy of the proton and also from the length of the recoil track in the three events where the protons stopped in the sensitive volume.

It was assumed that in each case the F^{19} residual nucleus was left in its ground state and then the energy of the absorbed photon (E_γ) could be obtained from

$$E_\gamma = E_p + E_R - Q$$

where E_R was the energy of the F^{19} nucleus. In the momenta (k) were obtained from the corresponding energies (E), the following momentum diagram could be used:-



where $\sin B = \frac{k_\gamma \sin \gamma}{k_R}$ and $k_p = \frac{\sin(B + \gamma) k_R}{\sin \gamma}$

The value of k_γ was then obtained by a method of successive approximations. In practice it was found to be more convenient to prepare a series of curves of photon energy versus recoil range for a sufficiently large number of values of the angle (γ) to allow reasonably accurate interpolation. The above procedure was adopted, as it was inconvenient to measure the angle (B) to any degree of accuracy.

Before the shape of the cross-section could be

determined, allowance had to be made for the varying number of photons in each energy interval of the bremsstrahlung beam. It was assumed that the spectrum tabulated by Katz and Cameron (68) was applicable to these results. The resulting histogram is shown in Figure 17. The shape of this curve bears no resemblance to the familiar 'giant resonance' form which is illustrated in Figure 18 where the cross-section for the $\text{Ne}^{20} (\gamma, n)$ reaction, measured by Ferguson et al. (69), is presented. Because of the dissimilarity in shape of the cross-sections for the (γ, p) and (γ, n) reactions, careful checks were made of the accuracy and the consistency of the measurements and calculations and it was concluded that there were no grounds to conclude that an appreciable error arose in them.

In drawing the angular distribution, 30° intervals were chosen to provide reasonable statistics although the experimental accuracy ($\sim 3^\circ$) would have justified a finer subdivision. The distribution was corrected for varying solid angle for equal angular intervals by dividing the number of events in any interval by the mean value of the sine of the angle in that interval. The experimental distribution was consistent with isotropy and the straight line shown in Figure 19 is the weighted mean of the experimental points. No difference was recorded in a comparison of the angular distributions of the events due to

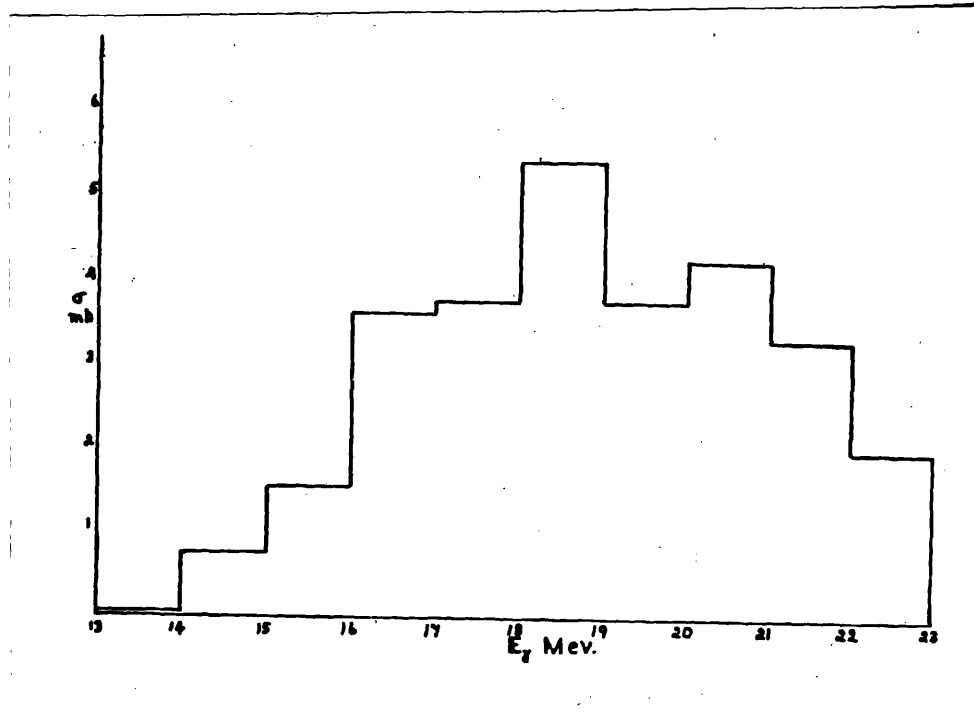


Figure 17.

Cross-section for the $\text{Ne}^{20}(\gamma, p)\text{F}^{19}$ reaction on the assumption that all the F^{19} nuclei were left in their ground states.

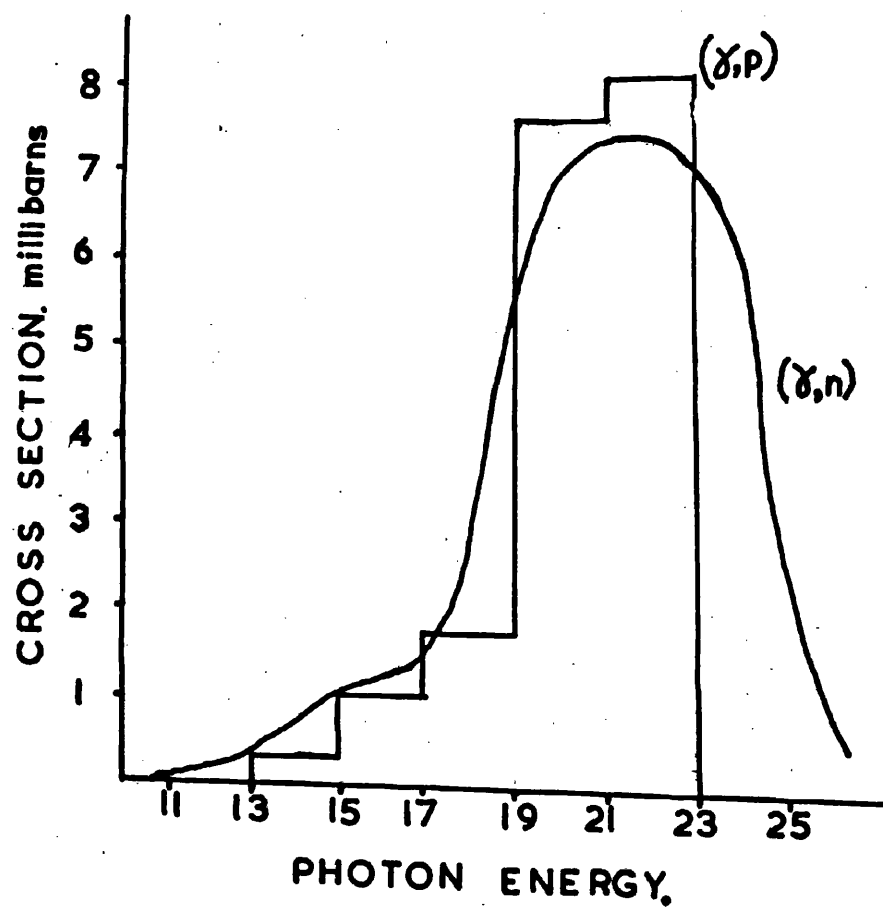


Figure 18.

The corrected cross-section for the $\text{Ne}^{20}(\gamma, p)\text{F}^{19}$ reaction. The smooth curve is the cross-section for the $\text{Ne}^{20}(\gamma, n)\text{Ne}^{19}$ reaction determined by Ferguson et al. (69).

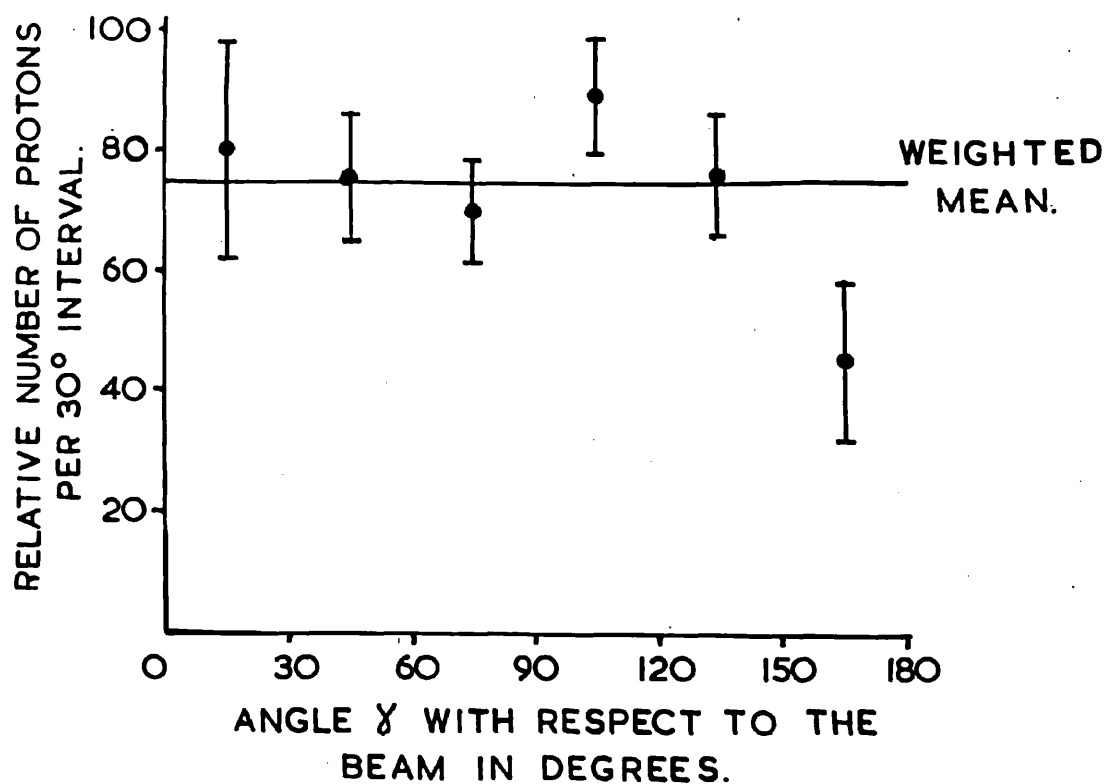


Figure 19.

The angular distribution of the
protons from the $\text{Ne}^{20}(\gamma, p)\text{F}^{19}$
reaction.

photons of energies greater than or less than 18 Mev.

The choice of 18 Mev was purely arbitrary but there was no indication that a division at any other energy would in fact show any significant difference.

4.4. Discussion of the results.

There were grounds for suspecting the original assumption that the residual F^{19} nucleus was left in its ground state. The work of Arthur et al. (68), on the $F^{19}(p,p')$ reaction, has considerable bearing on this point. With protons of 8 Mev it was shown that the F^{19} nucleus could be left in any one of eleven excited states contained in an energy interval of about 4.5 Mev, extending upwards from the ground state. If it is considered that photon absorption in the 'giant resonance' region resulted in the formation of a compound nucleus and that the same compound nucleus was formed in the inelastic proton scattering process then the results of the above workers are directly applicable here, since an 8 Mev proton would correspond to an excitation energy of about 21 Mev in Ne^{20} . It therefore seemed reasonable to suppose that the F^{19} nucleus could be left in any one of these excited states following a (γ, p) reaction in neon.

It was therefore assumed that one-third of the transitions which followed photon absorption in the energy range 19 Mev to 23 Mev left the F^{19} nucleus in its ground

state, one-third in the energy levels between 0 and 2 Mev and one-third in the levels between 2 and 4.5 Mev. The energy of the photon which produced the reaction was then

$$E_{\gamma} = (E_{\gamma}) + E^{*}$$

where (E_{γ}) was the value calculated previously and E^{*} was the excitation energy of the residual F^{19} nucleus.

The cross-section curve was then reconstructed as shown in Figure 18. It can be seen that there is close agreement between the two curves and the degree of agreement is illustrated in the following table:-

<u>Reaction</u>	<u>Integrated cross-section</u> (Mev-barns x 10^{-3})	<u>Energy at maximum</u> (Mev)	<u>Peak cross-section</u> (millibarns)
(γ, p)	39	22	8
(γ, n)	43	21.5	7.3

The predominant mode of decay of the compound nucleus would be by s-wave p or n emission and this would yield an isotropic angular distribution. The 'independent particle' model of Wilkinson (38) would have predicted an angular distribution of the form $a + b \sin^2 \theta$. The statistics in the experimental angular distribution would not allow the detection of a distribution of this form with $a > b$, if it were present.

Hence it was concluded that the experimental results were consistent with photon absorption which

proceeded with the normal 'giant resonance' form of the cross-section and produced a compound nucleus which decayed by s-wave proton emission to both the ground state and the excited states of F^{19} .

CHAPTER V.

LOW ENERGY PHOTOPROTONS

FROM OXYGEN.

5.1. The published data on the $O^{16} (\gamma, p) N^{15}$ reaction.

Because of the continuous energy spectrum of the photons in a bremsstrahlung beam, it is necessary to investigate the contributions made by photons below the 'giant resonance' before a correct estimate can be made of the photon absorption mechanism in the resonance itself. In an investigation of the $O^{16} (\gamma, p) N^{15}$ reaction, Spicer (71) irradiated oxygen with bremsstrahlung of peak energy 18.7 Mev. This energy was chosen in order that his emulsions would not detect protons which resulted from transitions to the excited states of N^{15} , the first of which was 5.3 Mev above the ground state. He obtained a peak in the proton energy distribution at a proton energy of approximately 2.6 Mev which corresponded to a peak in the cross-section at a photon energy of about 14.7 Mev and of magnitude ~ 4.6 millibarns. Johansson & Forkman (72) chose to work with a peak bremsstrahlung energy of 20.5 Mev and under these conditions protons of energy greater than about 3 Mev resulted from transitions to the ground state of N^{15} , while those of energy below 3 Mev originated in transitions to either the ground state or the first excited states of N^{15} . He concluded that the peak reported by Spicer was three times greater than his own measurement, which in itself was an upper limit, but did not profess to know the reason for the discrepancy. A comparison of the

angular distributions for the protons of energy approximately 2.5 Mev brought out yet another discrepancy. The angular distribution measured by Spicer had the form $(1 + \cos^2 \theta)$ while that measured by Johansson and Forkman was claimed to be isotropic with some sign of a $\sin^2 \theta$ component. One might regard Johansson and Forkman's isotropic angular distribution as a superposition of the $(1 + \cos^2 \theta)$ angular distribution as measured by Spicer and a $(1 + \sin^2 \theta)$ contribution from the transitions to the excited states of N^{15} . This interpretation, however, will only tend to increase the discrepancy between the two sets of results with regard to the magnitude of the cross-section. The proton energy spectra measured by Spicer and Johansson and Forkman are presented in Figure 20.

Further criticism of Spicer's results stems from the work of Wilkinson and Bloom (73) on the inverse reaction $N^{15} (p, \gamma) O^{16}$, who concluded that Spicer's results were in some way misinterpreted. These workers found little or no sign of the peak corresponding to a photon energy of 14.7 Mev and concluded that the low energy protons recorded in the (γ, p) experiments were in fact due to transitions to the excited states of N^{15} and not to the ground state. This might imply that the energy calibration of the Illinois betatron was at fault.

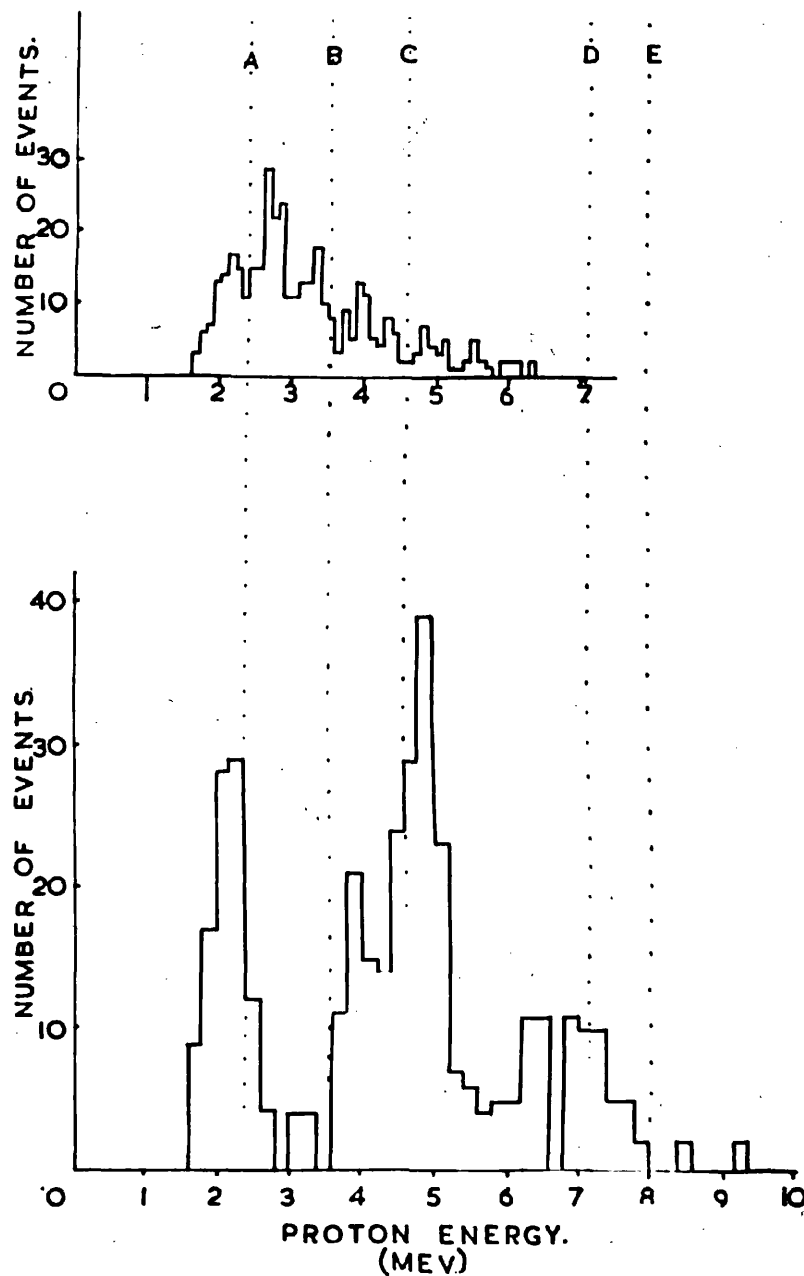


Figure 20.

Energy distributions of the photo-protons from the $^{16}\text{O}(\gamma, p)^{15}\text{N}$ reaction measured by Spicer (upper curve) at 18.7 Mev and Johansson & Forkman (lower curve) at 20.5 Mev.

Spicer concluded that the peak in the cross-section at a photon energy of 14.7 Mev was due to E2 and M1 absorption, but this conclusion must be regarded as suspect as long as his results remain in disagreement with those of other workers.

However, it seems probable that there are minor peaks in the proton energy spectrum which, if interpreted as resulting from transitions to the ground state, correspond to resonances in the cross-section at photon energies of about 14.7 Mev and 17.6 Mev.

Bearing these results in mind, now consider the reaction in the energy region including the 'giant resonance'. Here it is possible to compare the results of Johansson and Forkman, Cohen et al. (74), Milone et al. (75) and Livesey (76). In the proton energy spectrum measured by Cohen et al., six peaks were detected and the comparison with the results of other workers will be made with special reference to these. Several workers display cross-section curves (Figure 21) but as these involve the sometimes doubtful use of the bremsstrahlung spectrum in the transformation to a cross-section from the proton energy spectrum, it is felt that the proton spectrum is a more reliable quantity for study.

The proton energy spectrum measured by Cohen et al. is shown in the accompanying diagram (Figure 22) and the

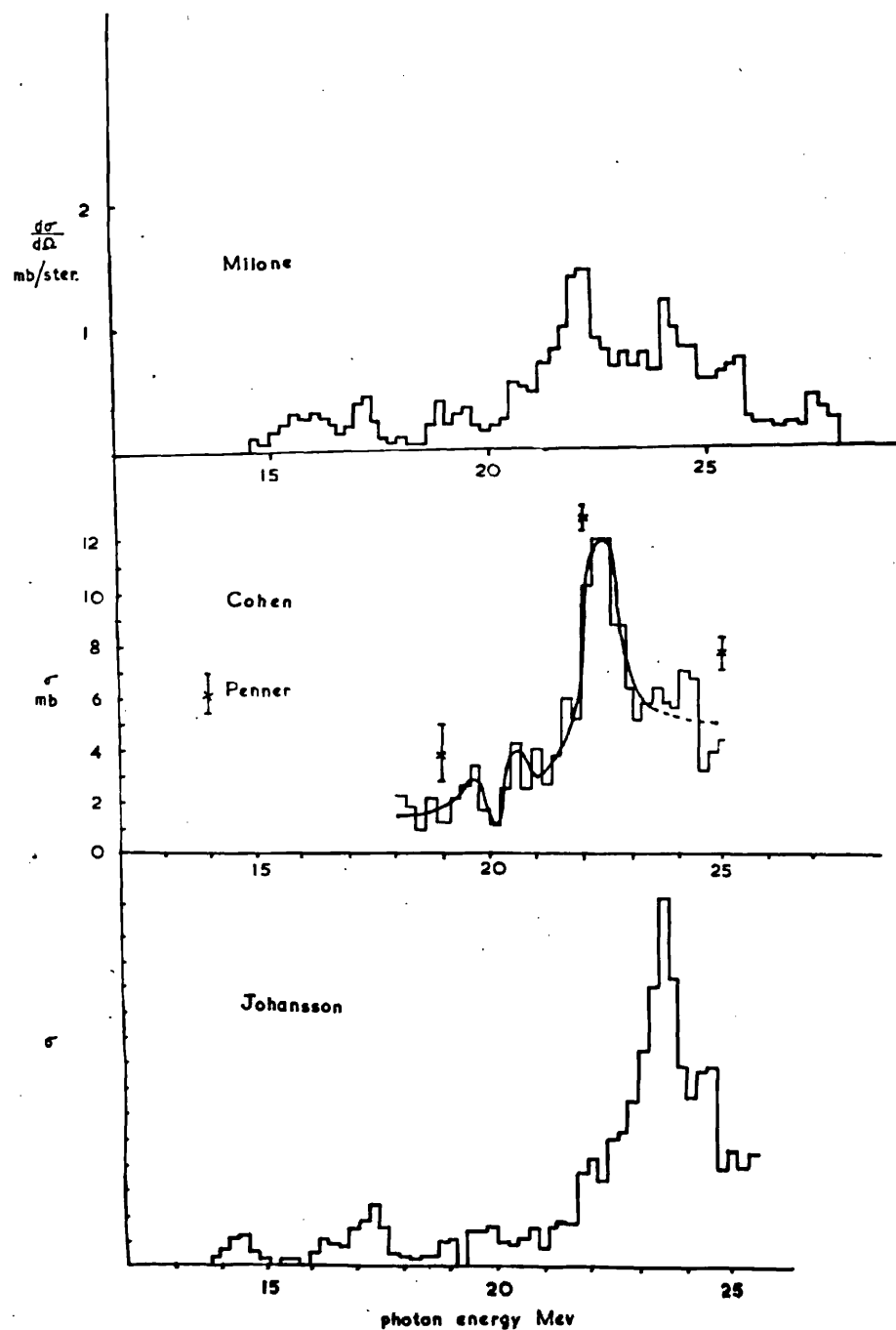


Figure 21.

Cross-sections for the $O^{16}(\gamma, p)N^{15}$ reaction.

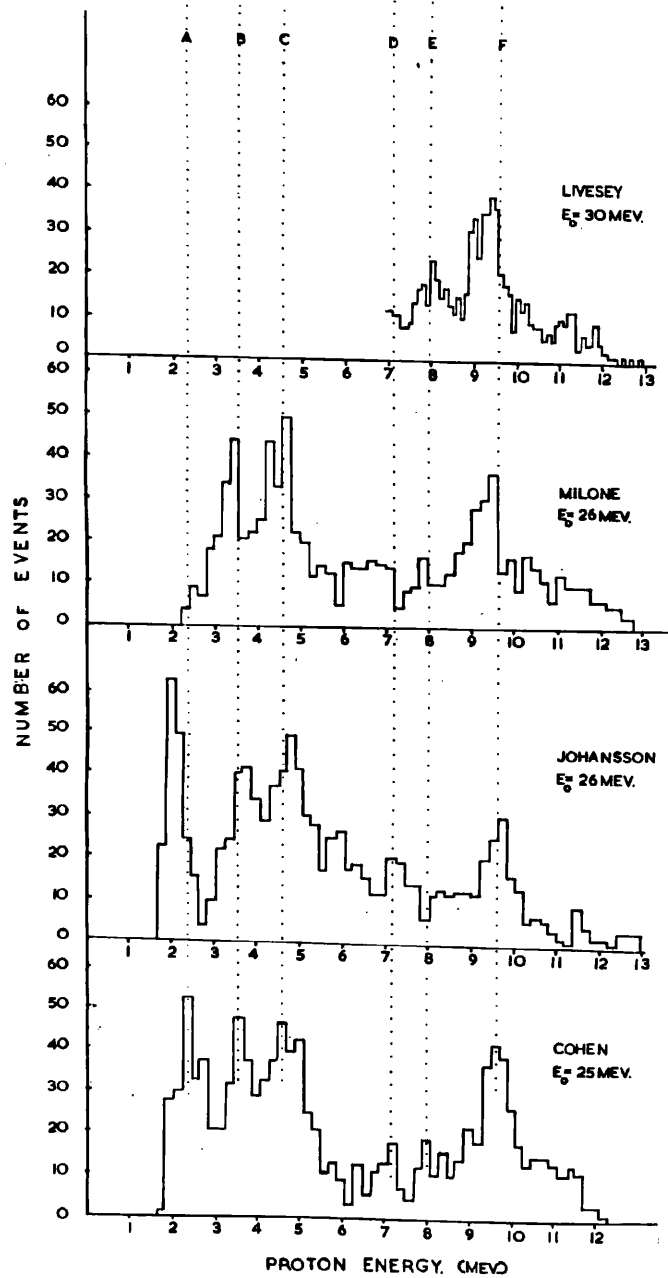


Figure 22.

Energy distributions of the protons from the $^{16}\text{O}(\gamma, p)^{15}\text{N}$ reaction determined by other workers.

peaks are labelled with the letters A to F. Each will be considered in turn.

GROUP A.

This peak occurs at a proton energy of between 2 and 3 Mev. Spicer's measurement appears to be at a slightly higher energy than those of Cohen et al. and Johansson and Forkman, but it is probable that they all correspond to the same proton group. The spectra measured with bremsstrahlung beams of peak energies 25 or 26 Mev will contain ground state contributions as pointed out by Spicer but they will also contain protons resulting from transitions to the excited states. This is well seen in the figure depicting the difference between the spectra measured at 23 and 26 Mev. (Figure 23). This group is not detected by the Italian workers.

GROUP B.

This group is composed of protons with energies between 3.5 and 4 Mev. It is not present in Spicer's distribution but it might be present to a small extent in that of Johansson and Forkman (Figure 20) if one allows an error of about 0.2 Mev in the absolute values of their energy scale. It is an appreciable part of the total proton yield as measured by Johansson and Forkman, Milone et al. and Cohen et al. at peak energies of 26, 26 and

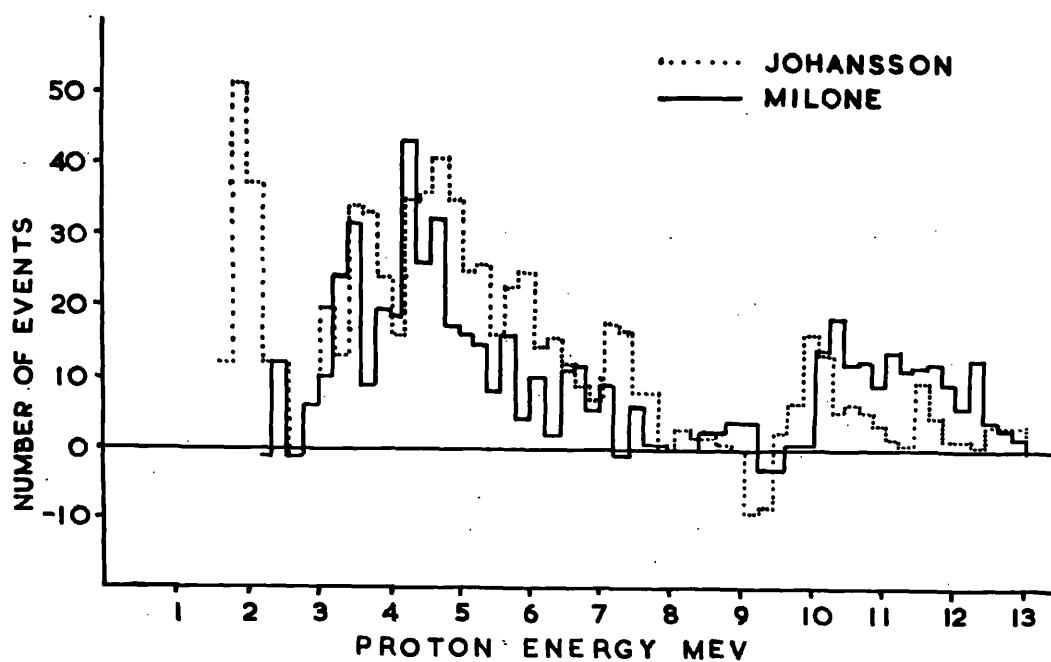


Figure 23.

The difference between the energy distributions of the photoprotons from oxygen measured at $E_0 = 26$ Mev and $E_0 = 23$ Mev.

25 Mev respectively. The work of Svantesson (77) on the decay photons from the residual nuclei formed by the photodisintegration of O^{16} indicated a high probability for those transitions to the 6.3 Mev state of N^{15} . If one now assigns this group of protons to transitions to the 6.3 Mev state of O^{16} this would infer the absorption of photons of energy about 22.2 Mev, which is the energy at which the 'giant resonance' occurs and the above explanation would therefore seem reasonable. Confirmation of the correlation of this group with transitions involving the excited states of N^{15} is obtained in the (26 Mev - 23 Mev) difference spectrum shown in Figure 23.

GROUP C.

This corresponds to a proton group of energy between 4.5 and 5 Mev. It is a major fraction of the Johansson & Forkman distribution measured at 20.5 Mev and represents those protons emitted in transitions, to the ground state, which follow the absorption of photons of energy around 17.5 Mev. The (23 Mev - 20.5 Mev) difference spectrum (Figure 24) as measured by Johansson & Forkman shows no sign of a contribution to this group, but the (26 Mev - 23 Mev) difference spectrum shows an appreciable yield. This latter contribution results from the absorption of photons of energy between 23 Mev and 26 Mev, followed by the emission of

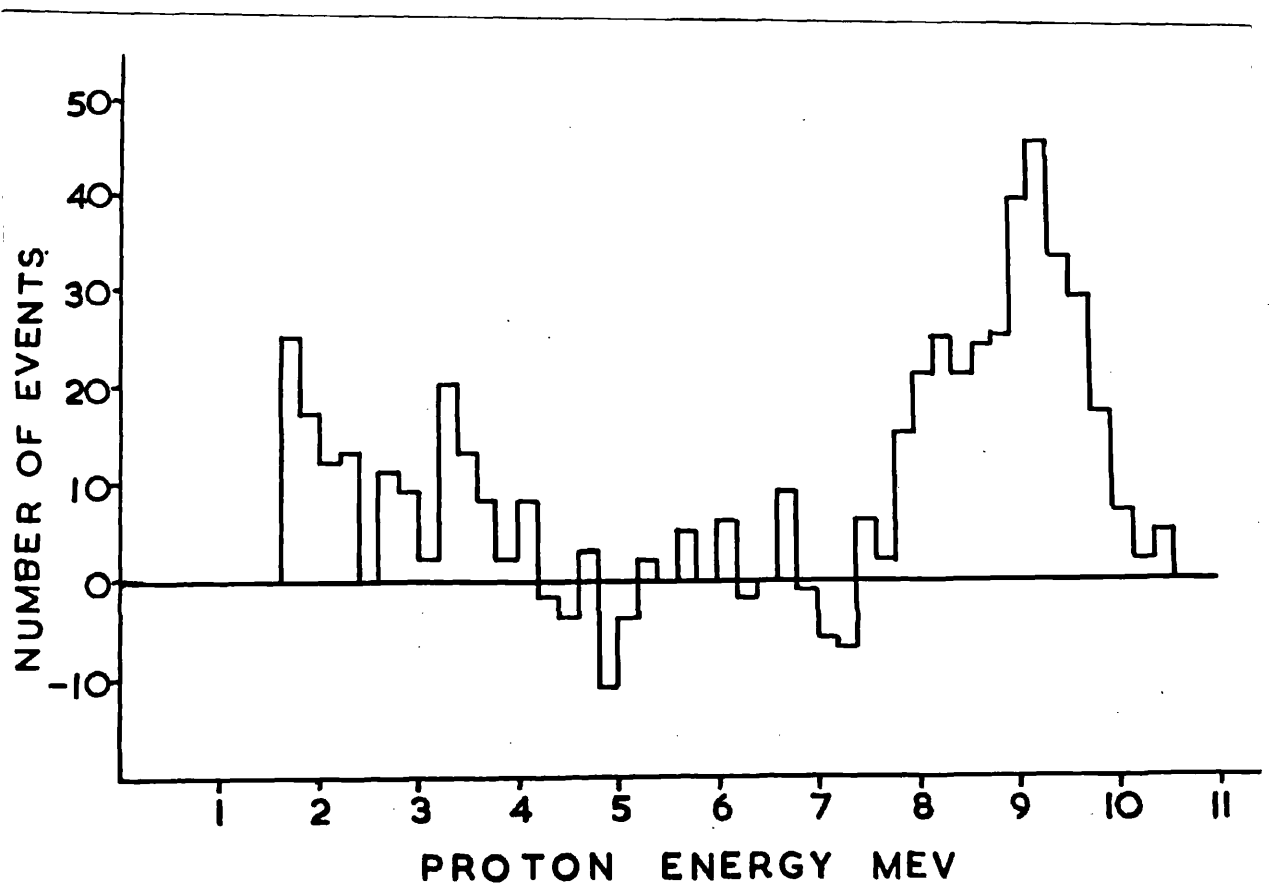


Figure 24.

The difference between the energy distributions of the photoprotons from oxygen measured at $E_0 = 23$ Mev and $E_0 = 20.5$ Mev (72).

protons in transitions to the 6.3 Mev and 7.3 Mev levels of N^{15} . Milone et al. estimated that the transitions to these levels were in the ratio 2:3 respectively.

GROUPS D AND E.

The groups designated by Cohen et al. as D and E are small. This is reflected in the comparison with the results of other workers. Group D is seen by Cohen et al., Johansson and Forkman and possibly also by Milone et al. Group E, on the other hand, is recorded by Cohen et al., Milone et al. and Livesey, but not by Johansson and Forkman. Since groups D and E are composed of protons of energies approximately 7 Mev and 8 Mev respectively, they correspond to photon absorption in the energy range approximately 19 Mev to 20 Mev, which is then followed by transitions to the ground state of N^{15} . At this stage it is of interest to examine the difference spectra. The (23 Mev - 20.5 Mev) spectrum measured by Johansson and Forkman shows no 7 Mev group but displays an 8 Mev group. The (26 Mev - 23 Mev) spectra of Milone et al. and Johansson and Forkman both display a lack of the 8 Mev group, but Johansson and Forkman record a 7 Mev group while Milone et al. apparently do not. The two difference spectra can be brought into qualitative agreement if one assumes a small error in the energy scale of one set of results.

GROUP F.

This is a proton group of energy 9 Mev to 10 Mev. It corresponds to transitions to the ground state of N^{15} and in fact constitutes the 'giant resonance'. It is seen by all groups of workers.

It should also be noted that there exists a considerable 'tail' in the cross-section at energies greater than that of the 'giant resonance'. This is seen in the cross-section derived by Penner (78) (Figure 21) and is also partially revealed in the cross-sections obtained by Cohen et al., Johansson and Forkman and Milone et al. The latter in fact stated that fine structure existed in the cross-section in this region and claimed two peaks which corresponded to proton energies of approximately 11 Mev and 12.8 Mev respectively. The former was confirmed by Livesey.

5.2. Introduction to the present investigation.

This experiment was performed in order to obtain information concerning the mode of photon absorption in oxygen, below the 'giant resonance'. Determinations were made of the energy and angular distributions of the protons which were emitted in the $O^{16} (\gamma, p) N^{15}$ reaction.

Particular care was taken to ensure that attention was confined to the protons which were emitted in transitions

to the ground state of N^{15} . This was achieved by reducing the peak energy of the bremsstrahlung beam to 18 Mev. This choice of peak energy was based on the following facts: (i) the reaction $O^{16} (\gamma, p) N^{15}$ had a threshold of 12.1 Mev, and (ii) the first excited state of N^{15} lay 5.3 Mev above its ground state. Although the choice of a lower peak energy would perhaps have been preferable, one had to contend with the rapid reduction in photon flux which accompanied a decrease in peak energy. Consequently it was decided to run at the highest peak energy consistent with the exclusion of transitions which involved the excited states of N^{15} .

5.3. Specific experimental conditions.

The cloud chamber was operated at a working pressure of 1.23 atmospheres of oxygen at a temperature of $15^{\circ} C$ and an expansion ratio of 1.31. The oxygen was of medical purity and no account was taken of the presence of the isotopes O^{17} and O^{18} . It was aligned in such a manner that the beam passed symmetrically through the sensitive volume. The dimensions and the relative positions of the chamber and the collimator with respect to the synchrotron target are illustrated in Figure 25. The expansion ratio and the delays between the expansion, beam pulse and lamp flash were adjusted to obtain optimum track quality. Satisfactory track quality was obtained with a delay of

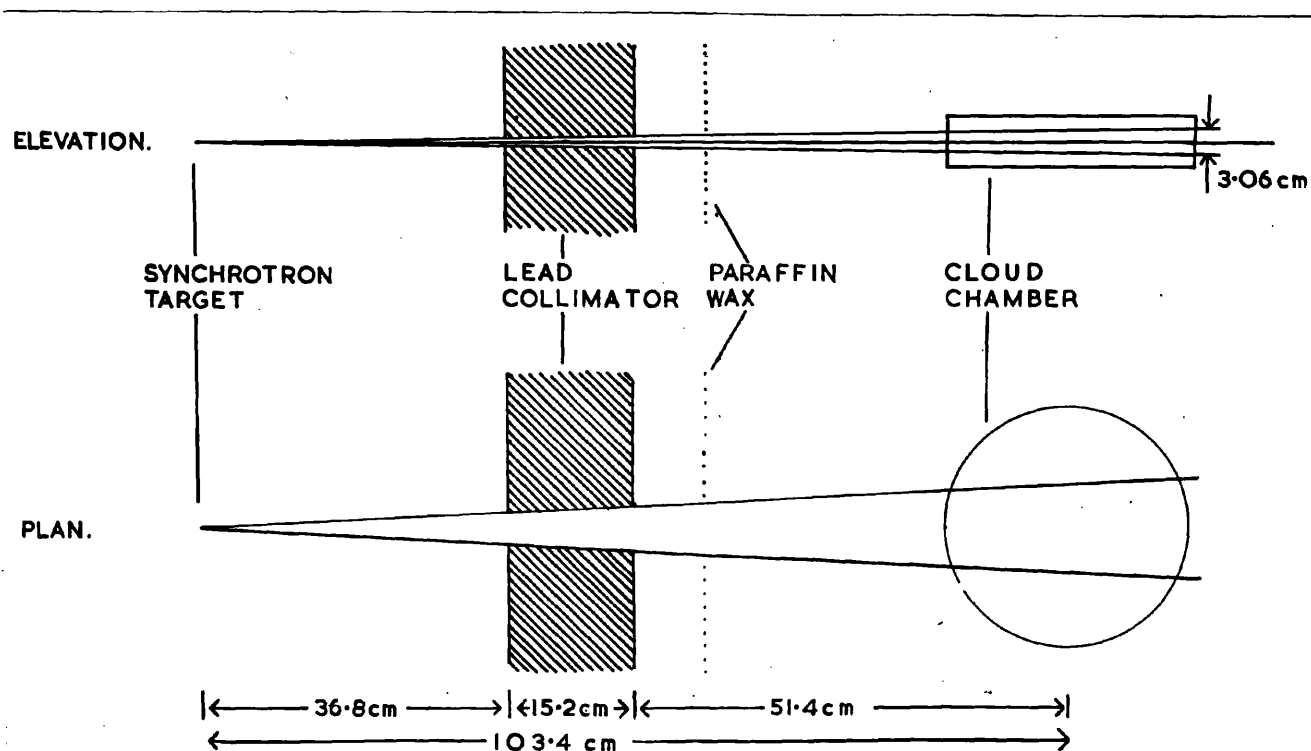


Figure 25.

Relative positions of synchrotron,
collimator and cloud chamber.

35 milliseconds between the fast expansion and the beam pulse and a further delay of 75 milliseconds between the beam pulse and the lamp flash.

For this experiment two cameras were employed, because the yield of events per frame was so low that the use of a third camera was considered to be wasteful of film.

Before the chamber was assembled, the co-ordinates of the points of reference (i.e., intersections of the grid wires) were measured in order to convert the microscope measurements into the chamber frame of reference.

At the start, this experiment was only considered as a preliminary investigation and a more detailed study, involving irradiations at various peak energies, was to be carried out after these results had been analysed. Unfortunately difficulties encountered with the synchrotron resulted in the abandonment of this proposed programme. A crude calibration of the beam intensity was obtained, in the manner described in Chapter II, during the initial series of irradiations and because of the above difficulties a detailed calibration was not obtained. This calibration provided a rough scale for the cross-section curve derived from the measured proton spectrum.

5.4. The classification of the events.

After development, the films were replaced in the cameras and light shone through them in order to cast images

on a reprojection table. These images were examined individually to locate, number and classify the recorded tracks. The results of this survey were grouped into the general classifications:-

- 'flags' - single tracks accompanied by a recoil.
- 'singles' - single tracks with no visible recoil and including events from the walls of the chamber.
- 'stars' - events with more than one track.

The efficiency of this process was determined from a comparison of the results obtained when each film was examined by two independent workers. The efficiency was estimated to be 95%.

The experimental distribution, classified in terms of the above scheme, was derived from a total of 1281 frames and is given below.

<u>Type of event</u>	<u>Number of events recorded</u>
'flags'	456
'singles'	219
'stars'	5

The large number of 'singles' demands further explanation. Of the 219 events, 58 originated in the chamber walls. The remainder were events whose origins lay outside the illuminated region of the chamber and whose

recoils were consequently not recorded, or normal (γ, p) events whose recoils had been obscured by the general background, or events where the track quality prevented accurate classification. Those whose origins lay outside the beam might have originated from (γ, p) or (n, p) reactions in the chamber base or the top plate, but this source was not considered to be the major contributor to the yield of 'singles'.

Of the 'flags', 22 were classified as (γ, α) events, 376 as (γ, p) events which could be fully analysed and a further 58 were classified as (γ, p) events which were later rejected from the distributions as a result of doubt concerning the positions of their origins with respect to the photon beam. Only those events whose origins lay within the geometrical confines of the beam as defined by the lead collimator and a fixed point source were accepted. Adjustments to the gun and target positions during the irradiations and the finite size of the source probably gave a greater spread of the beam than that calculated, but it was felt that all possible sources of doubt should be removed and consequently all the events which originated outside the calculated beam geometry were rejected. Confirmation of the beam position as it passed through the chamber was obtained from the distribution of the Z_0 -co-ordinates of the analysed tracks (see Figure 26).

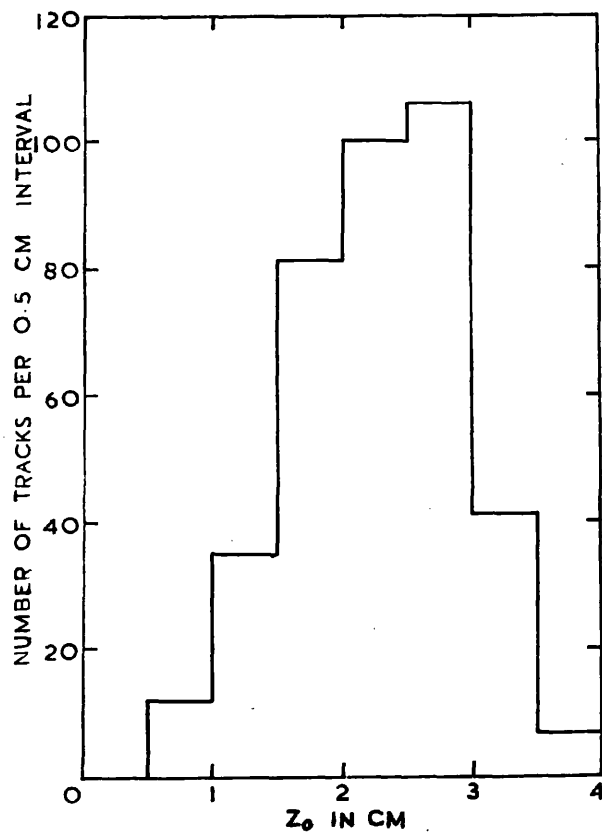


Figure 26.

The distribution of the Z co-ordinates of the origins of the measured (γ, p) events.

If one assumed that all the events which occurred outwith the beam were to be considered as a background, then their energy distribution had to be determined before a correction could be applied to the photoproton energy spectrum. The energy distribution, based on 38 analysed events, is shown in Figure 27. As the beam occupied a quarter of the total volume of the chamber, this correction was consequently reduced.

5.5. The experimental energy distributions.

The tracks were then fully analysed and of the 376 (γ ,p) events, 98 left the sensitive region. As a result, the number of events in the energy distribution was reduced to 285. The ranges of these protons were calculated from the co-ordinates of the origins and end-points of the tracks and also from the lengths of the tracks as measured on both films. As the working gas was wet oxygen at 1.23 atmospheres pressure, these ranges were reduced to equivalent ranges in dry oxygen at S.T.P.

Before these ranges could be converted into energies a suitable range-energy relationship had to be found. The majority of the events analysed had ranges less than 5 cm. and the range-energy curve quoted by Aron, Hoffman and Williams (79) could not be read to the required degree of accuracy. Consequently use was made of the relationship for low energy protons in air, quoted by

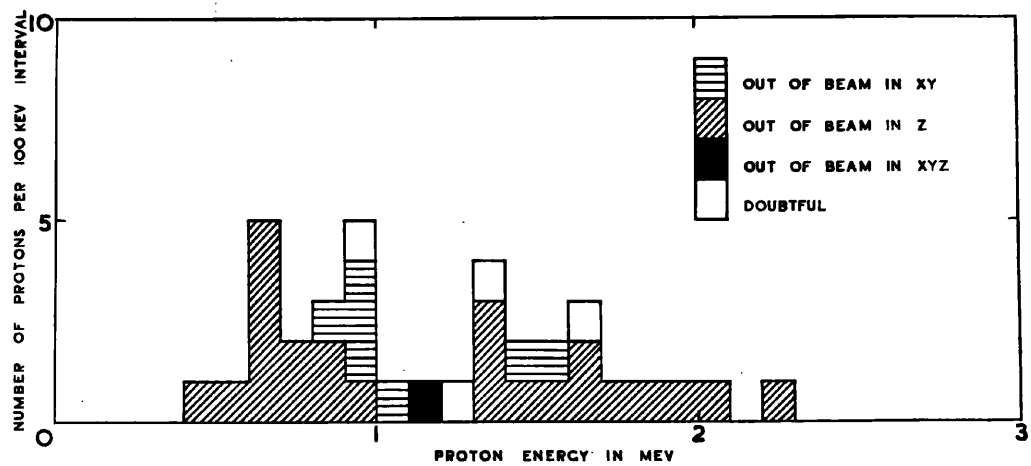


Figure 27.

Energy distribution of the events
whose origins lay outside the beam.

Bethe and Ashkin (80) and the equivalent relationship tabulated by Jesse and Sadauskis (81). This curve was normalised to that of Aron, Hoffman and Williams for protons in oxygen at an energy of 1 Mev to produce a reasonably accurate curve for low energy protons in oxygen.

The energy distribution shown in Figure 28 was compiled only from protons which stopped in the chamber. As a result, it is biased in favour of protons of low energy, since they have shorter ranges and are therefore more likely to stop in the sensitive region. This was corrected by dividing the measured distribution by the probability of stopping in the chamber as a function of energy, to yield the true proton energy distribution (free from any limitations imposed by the apparatus). This distribution is shown in Figure 29.

Since the choice of peak photon energy in the experiment excluded any transitions to the excited states of N^{15} , one can state

$$E_{\gamma} = E_p + E_{N^{15}} - Q$$

and this can be approximated by

$$E_{\gamma} = \frac{16}{15} E_p - Q$$

Using this expression, the proton energy distribution was converted into the corresponding photon energy distribution. Finally, allowance had to be made for the shape of the bremsstrahlung spectrum and this was done by dividing the

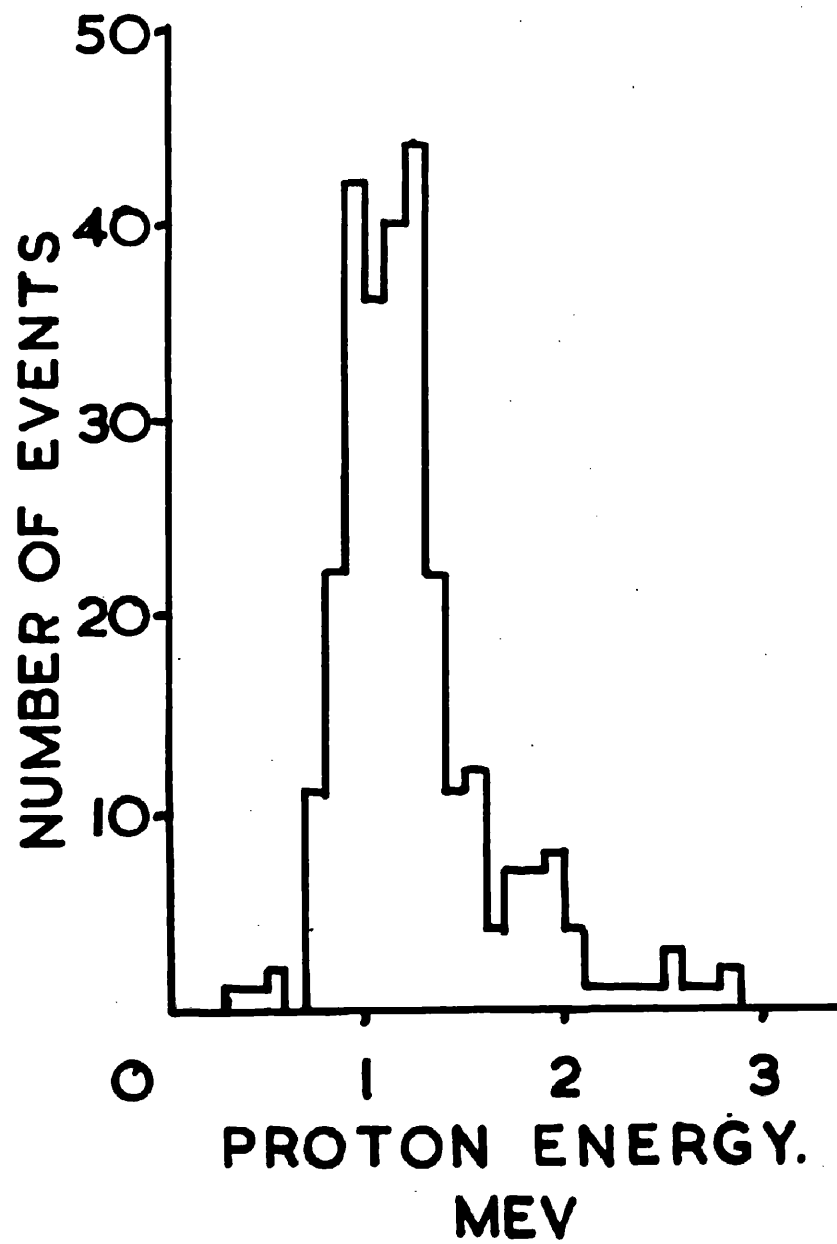


Figure 28.

Measured energy distribution of
the photoprotons from oxygen.

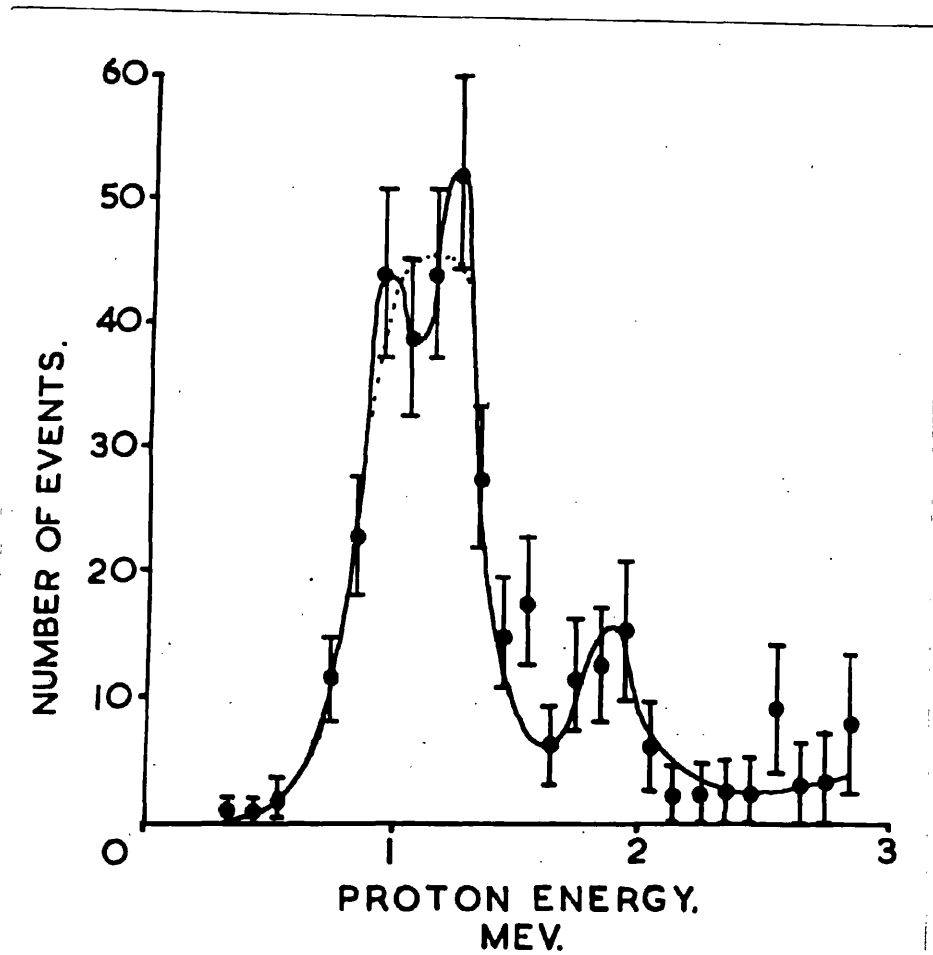


Figure 29.

Energy distribution of the photo-protons from oxygen, corrected for the probability of stopping.

photon energy distribution by the tabulated spectrum quoted by Katz and Cameron (68) to yield the relative cross-section curve shown in Figure 30.

Before proceeding to a discussion of the results, it is worthwhile to note the difference between the energies of the protons derived from the co-ordinates and also from the track lengths. As can be seen in Figure 31, 77% of the events had an error of less than 0.1 Mev.

The summed dose of radiation received by the chamber gas was estimated to be 0.2 r.

5.6. Discussion of the results on the energy distributions.

Although this is the first experiment carried out on the $O^{16} (\gamma, p) N^{15}$ reaction in this energy region, several workers have studied the inverse reaction $N^{15} (p, \gamma) O^{16}$ (82,83) and concluded that in O^{16} the only level below 14 Mev which was involved was that at 13.09 Mev. This level had a width of 150 kev and a peak cross-section of 1 millibarn. One might therefore deduce that in a study of the reaction $O^{16} (\gamma, p) N^{15}$ one would expect to detect a single proton group corresponding to photon absorption into this level. This proton group would have an energy of 0.91 Mev. The experimental results showed a proton group of mean energy 1.1 Mev with a width at half-height of about 0.5 Mev. In the photon energy distribution this corresponded to a peak at 13.3 Mev and a half-width

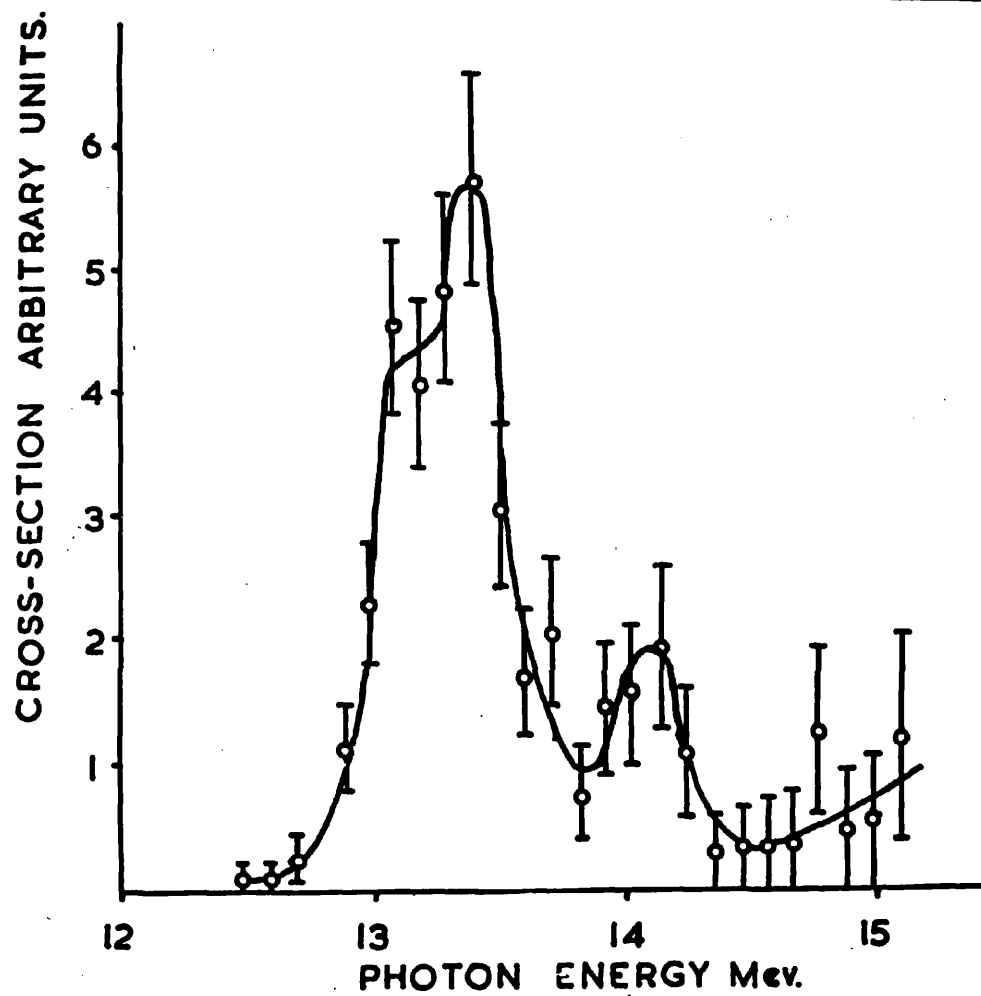


Figure 30.

The cross-section of the $^{16}\text{O}(\gamma, p)^{15}\text{N}$ reaction.

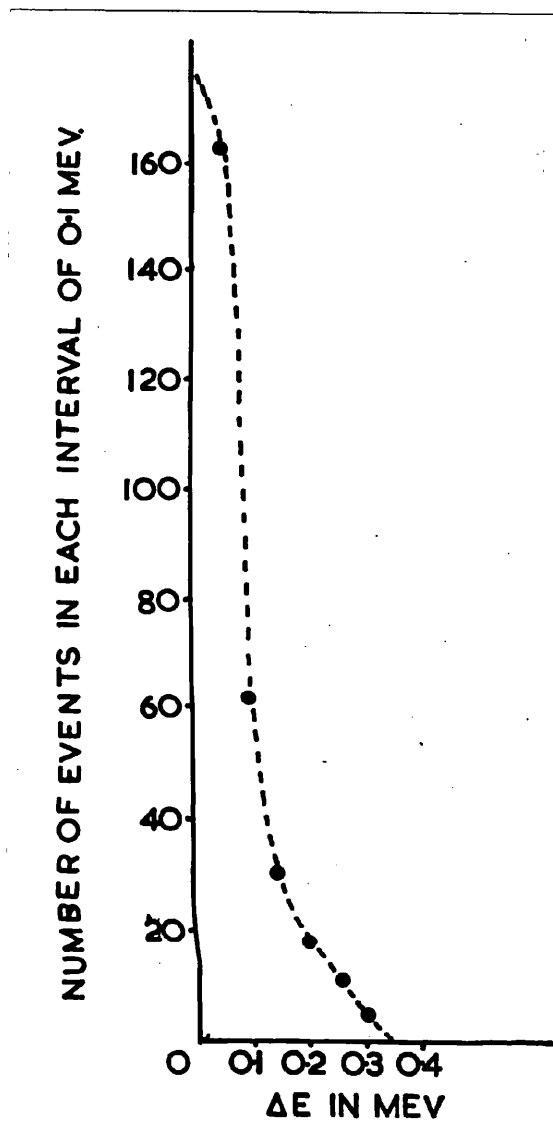


Figure 31.

The difference between the proton energies calculated from track lengths and also from co-ordinates.

of 0.5 Mev. When the peak cross-section, corresponding to the 46 events at 13.1 Mev, was calculated using the spectrum tabulated by Katz and Cameron (68), a value of about 3 millibarns was obtained. By applying the principle of detailed balancing to the inverse (p, γ) reaction, an expected peak cross-section of approximately 10 millibarns was calculated for the (γ, p) reaction. This discrepancy could be partially accounted for if all the events which were excluded from the energy distribution were attributed to the (γ, p) reaction. However, it was known that many of these events involved particles with energies in excess of those considered here, and further, that a considerable number of them originated in reactions other than the (γ, p) , i.e., protons from the walls, etc. The difference between the measured and calculated widths would still remain unresolved. Alternatively, these discrepancies could be accounted for if the majority of the events in the photon distribution, which had been attributed to photons of energy between 13.1 and 13.4 Mev, resulted from absorption into the 13.09 Mev level. It would require a considerable error to account for this discrepancy which, if it existed, was not detected. It is felt confident that the source of this unknown error did not lie in the measurements, range-energy relationship or the range straggling. However, if in fact the peak energy of the

beam did not remain stable at 18 Mev but in fact drifted widely, some of the recorded protons could have resulted from transitions to the first excited state of N^{15} . This would require a photon energy of approximately 18.7 Mev and in order to obtain a yield comparable to that from the 13.09 Mev level in O^{16} to the ground state of N^{15} , the peak energy of the beam would have had to be in excess of this figure. Carbon in the form of polythene was irradiated but no appreciable activity was recorded and it was therefore concluded that the drift in the peak energy of the synchrotron output could not account for the shape of the proton energy distribution.

On the other hand, the experimental distribution would be consistent with contributions from several levels. In fact, if two levels at 13.09 Mev and 13.39 Mev were assumed to have widths of 250 kev and cross-sections as shown in the cross-section curve, then the curve could be reproduced from 13.0 Mev to 13.6 Mev.

The 13.09 Mev level is well established from the inverse reaction and Hornyack and Sherr (84) who studied the reaction $O^{16}(p,p')O^{16}$ tentatively suggested a level at 13.39 Mev. It would not seem unreasonable to assign the same spin and parity to both these levels. In fact, Zimmerman (85) has studied the properties of the low-lying states of N^{16} and since N^{16} , O^{16} and F^{16} form an isobaric

triplet, one can infer the spins and parities of the O^{16} levels corresponding to the excited states of N^{16} where the N^{16} ground state corresponds to the first $T=1$ state of O^{16} at 12.95 Mev. This suggestion would lead to a 0^- or 1^- assignment to both levels.

This explanation of the experimental distributions is in disagreement with the predictions of the principle of detailed balancing as applied to the inverse reaction. As a result, neither explanation can be forwarded without criticism. A further investigation has since been carried out by Menzies (86) with the Cambridge synchrotron in order to check the results reported here. His preliminary results confirmed that the peak was approximately 0.5 Mev wide and he estimated that the peak cross-section was approximately 3 millibarns.

The remainder of the (γ, p) cross-section curve could either be regarded as the 'tail' of the low energy resonance or resonances but it is more likely that it was due to small contributions from levels at about 14.1 Mev and 14.7 Mev. The latter state has been detected by Spicer and Johansson & Forkman (71,72) when they studied the $O^{16}(\gamma, p)$ reaction. They disagree, however, as to the magnitude of the cross-section by a factor of three. Wilkinson and Bloom (73) estimated from their own results on the inverse reaction that Spicer's value for the cross-

section was in error by a factor of 30. As a result, one can only suggest that such a level exists with a cross-section less than that quoted by Spicer. Here the protons which were emitted in transitions to the ground state of N^{15} following the absorption of 14.7 Mev photons had a very low probability of stopping in the chamber (0.25) and consequently only three such events were recorded.

A level has been suggested by Stoll (87) at 14.2 Mev after studying the $O^{16} (\gamma, \alpha)$ reaction. From the present results one would estimate that this level would have a cross-section of approximately one-third of that of the 13.09 Mev level, on the hypothesis of several participating levels.

The 22 (γ, α) events were not analysed as there were so few of them, but the ratio of the α -particle yield to that of the protons was of the order of one in twenty.

The 'stars' were all four-pronged and were probably $O^{16} (\gamma, 4\alpha)$ events and these also were not analysed. The lengths of the α -particle tracks were short and this indicated that the photons responsible were of low energy.

5.7. The experimental angular distribution.

The angle between the photoproton track and the beam direction was determined for the (γ, p) events which were accepted for the energy distribution. The same angle

was also measured for all the (γ ,p) events in which the proton left the sensitive volume of the chamber. The results were grouped into 20° bins and a correction applied to account for the variation of solid angle for equal angular intervals. This was done by dividing the number of events in each angular interval by the mean value of the sine of the angle in that interval.

No significant difference was found between the distributions corresponding to 'stopping' protons and 'leaving' protons. The angular distribution compiled from both sets of photoprotons is shown in Figure 32 where the errors are purely statistical. The accuracy of measurement of the angle was of the order of 3° but the results were grouped into 20° intervals to provide reasonable statistics.

The experimental distribution is isotropic. The state at 13.09 Mev is considered to be 1^- (73) and one would expect s-wave proton emission to the N^{15} ground state to follow E1 absorption into this level, thus yielding an isotropic angular distribution. The hypothesis that absorption proceeded into two levels would still be consistent with the angular distribution, as it was assumed that both levels had the same spins and parities.

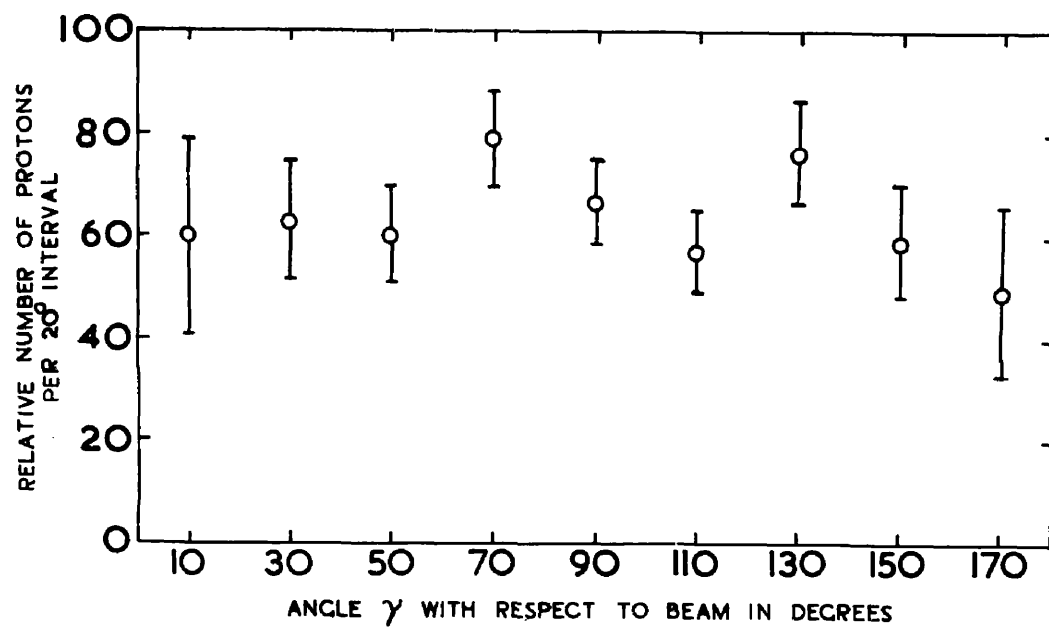


Figure 32.

Angular distribution of the photo-protons from oxygen.

CHAPTER VI.

THE EMISSION OF He^3 AND He^4
PARTICLES FROM OXYGEN AND ARGON.

6.1. Introduction.

It should be pointed out at the beginning of this chapter that the results presented in it are the first measurements of the yields of He^3 particles from photo-nuclear reactions. The author has been unable to find any reference to previous work on this topic.

In the past, several groups of workers have detected activities which they correlated with the photo-production of nuclei of the form $(Z-2, N-1)$ from target nuclei of the type (Z, N) . As has been mentioned earlier in Chapter I, these workers encountered three difficulties in the interpretation of their results:

(1) The target must be monoisotopic if unambiguous yield values are to be ascribed to the individual reactions.

(2) The yield values are quoted relative to some standard, for example, the yield of neutrons from the $\text{N}^{14} (\gamma, n) \text{N}^{13}$ reaction whose cross-section is not well established up to energies in the region of 300 Mev.

(3) The yield finally ascribed to the reaction $(N, Z)(\gamma, ?)(N-1, Z-2)$ was composed of the partial yields due to the $(\gamma, 2pn)$ reaction together with that from the (γ, He^3) reaction and there was no way of estimating their relative contributions to the total.

6.2. Equipment and Procedure.

The equipment (88) was originally built to study

the reaction $\text{He}^4 (\gamma, \pi^0) \text{He}^4$ by detecting the recoiling He^4 nuclei. It was necessary to distinguish between the He^4 particles which arose from the above reaction and the He^3 particles produced by the $\text{He}^4 (\gamma, n) \text{He}^3$ reaction.

Use was made of the standard technique commonly used in high energy nuclear physics for distinguishing between particles of different mass by the simultaneous measurement of the specific ionisation and the total energy of the particle (i.e., $\frac{dE}{dx}$ and E). The method had been previously used to separate mesons from electrons and protons (89,90), and also to distinguish between protons and deuterons (91). These methods employed scintillation detectors but were unsuitable for this study, since an extremely thin scintillator would be required for the $\frac{dE}{dx}$ measurement, (e.g., a 15 Mev α -particle would lose about 5 Mev in passing through 0.003 inches of plastic scintillator). Further, the non-linear variation of light output with energy loss in scintillating crystals reduced the effective separation between the two types of densely ionising particles. Use was therefore made of gas counters where the specific ionisation of doubly-charged particles was so high that they still could be detected in a relatively high background flux of electrons and photons without 'pile-up' seriously affecting the resolution.

The target chamber was a tube 4 feet long and

3 inches in diameter with 0.005 inches 'Melinex' windows at either end. The chamber was positioned in such a manner that the beam passed along the axis of the target tube whose 'entry' window was as near as possible to the 'exit' port of the collimator vacuum system. The target was filled to a pressure of $1\frac{1}{2}$ atmospheres with the gas under investigation and the He^3 and He^4 particles were detected in two gridded ionisation chambers mounted at 90° to the axis of the beam (see Figure 33). They had a common H.T. electrode and the collector plates were separate, thus measuring $\frac{dE}{dx}$ and E of the particle. The E chamber was flared out to include a reasonable solid angle of acceptance. The earthed guard ring and the wire conductors, held at suitable potentials, maintained the required field distribution near the edges of the chamber. The earthed strip inserted between the collector plates served to reduce the capacity between them (2.2 pf). Collimated polonium sources were mounted in both chambers. The chamber was filled with a mixture of 90% and 10% methane to a pressure of $1\frac{1}{2}$ atmospheres. The target was separated from the chambers by a 'Melinex' window 0.0005 inches thick supported on a wire grid.

The mass and energy of the particle were determined from the energy losses E_1 and E_2 as measured by the heights of the coincidence pulses obtained from the collectors when

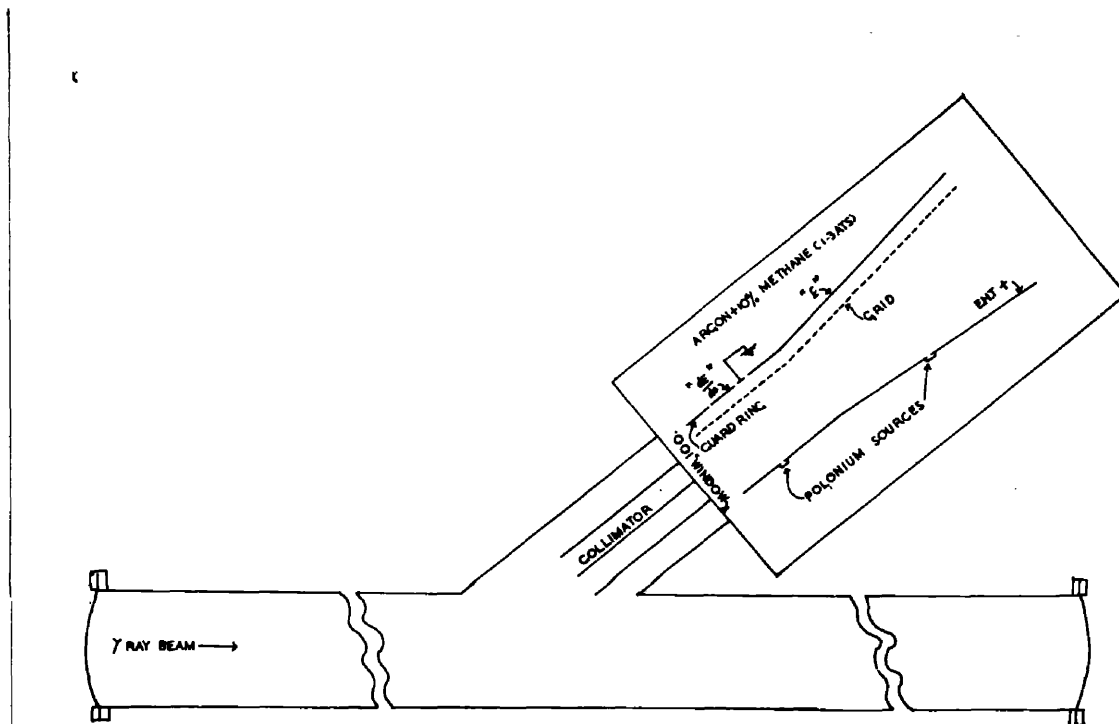


Figure 33.

The target tube and the ionisation chambers.
 Note in these experiments the chambers were
 mounted at 90° with respect to the beam
 direction.

a particle traversed both chambers. This information was displayed on a C.R.O. by a spot whose co-ordinates were proportional to E_1 and E_2 respectively. A block diagram of the electronics is shown in Figure 34. With the aid of two shorted delay lines, it was possible to eliminate the 'pile-up' of electron pulses which occurred within the beam duration (500 μ s) and obtain square pulses of 3 μ s duration.

The energy losses E_1 and E_2 varied between the limits 1.3 Mev to 3 Mev and 2 Mev to 18 Mev respectively. The statistical fluctuation in E_1 under typical conditions was about 25 kev.

The spots on the C.R.O. were photographed and each exposure lasted two hours. The number of spots per frame varied between 7 and 20. The E_1 and E_2 axes for each exposure were plotted using the pulses from the polonium sources and coincidences were obtained by joining the inputs to the coincidence unit and earthing the input to each amplifier in turn. This also yielded the calibration of the E_1 and E_2 deflections in terms of energy loss, and, in fact, the procedure was repeated with the calibration spots spread out in a direction at right angles to the required deflection in order to locate accurately the region of maximum density. For any set of runs the calibration deflections were in sufficient

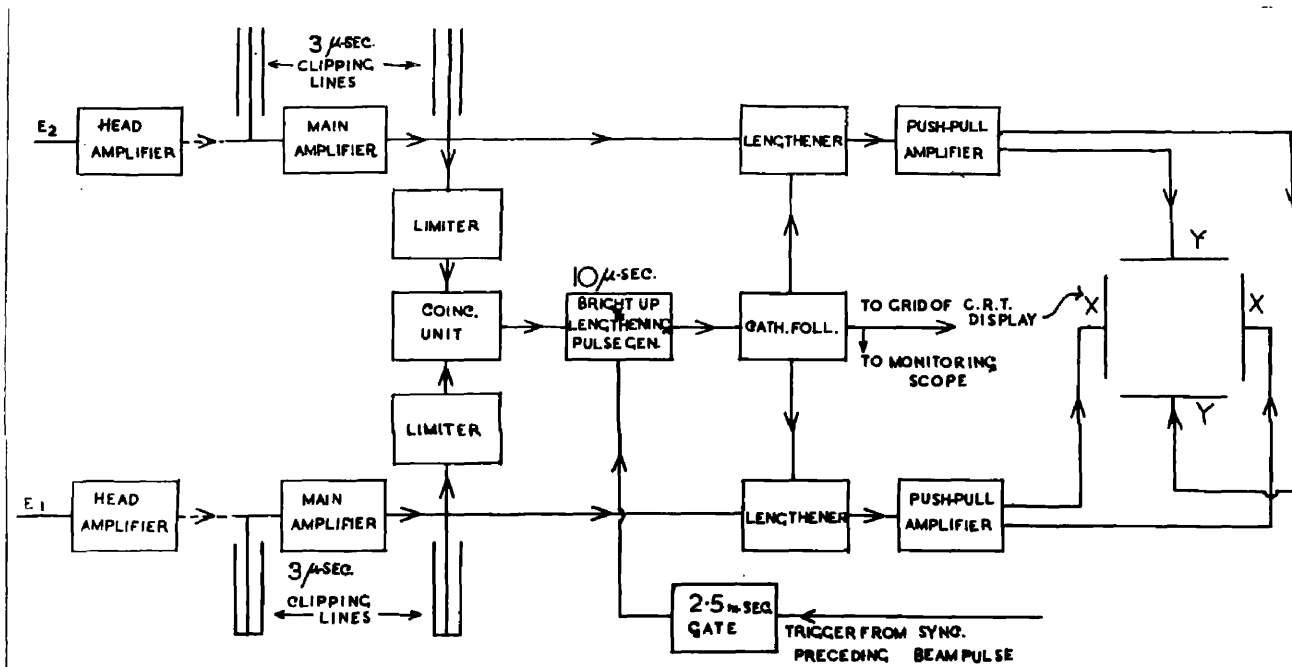


Figure 34.

Block diagram of the electronics used.

agreement that their mean value could be used throughout.

The data was analysed as follows:- From the theoretical range-energy relationships (79,92) for nuclei in argon, the calibration deflections, the geometry of the chamber and the gas pressure, it was possible to calculate the curves along which He^3 and He^4 particles would be expected to lie. The space between the curves and on either side of them was sub-divided into channels in such a way that each curve lay along the centre of a channel. The number of points in each channel was counted and a histogram obtained. A limit was imposed on the region of counting in order to eliminate those particles which passed completely through both chambers.

6.3. Results.

The results presented in Figure 35 were obtained by Palit and Bellamy (93) who irradiated a helium target with 325 Mev bremsstrahlung and detected the emitted He^3 and He^4 particles. The upper curve (a) displays the yield of He^3 particles, at 90° with respect to the beam direction, from the reaction $\text{He}^4 (\gamma, n) \text{He}^3$. At this angle the kinematics of the $\text{He}^4 (\gamma, \pi^0) \text{He}^4$ reaction rule out the emission of He^4 particles. The yields of He^3 and He^4 particles at 40° with respect to the beam direction from both the above reactions are illustrated in

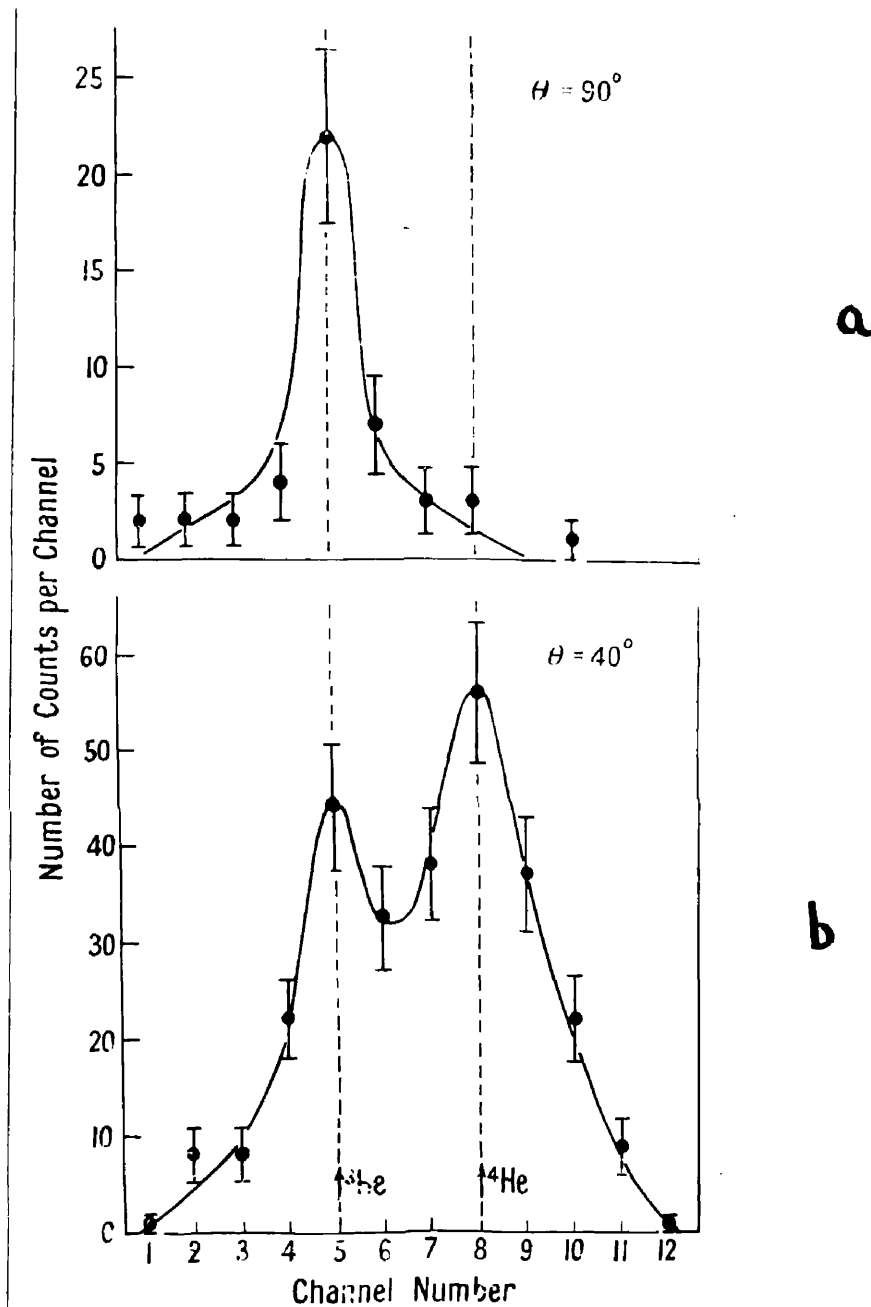


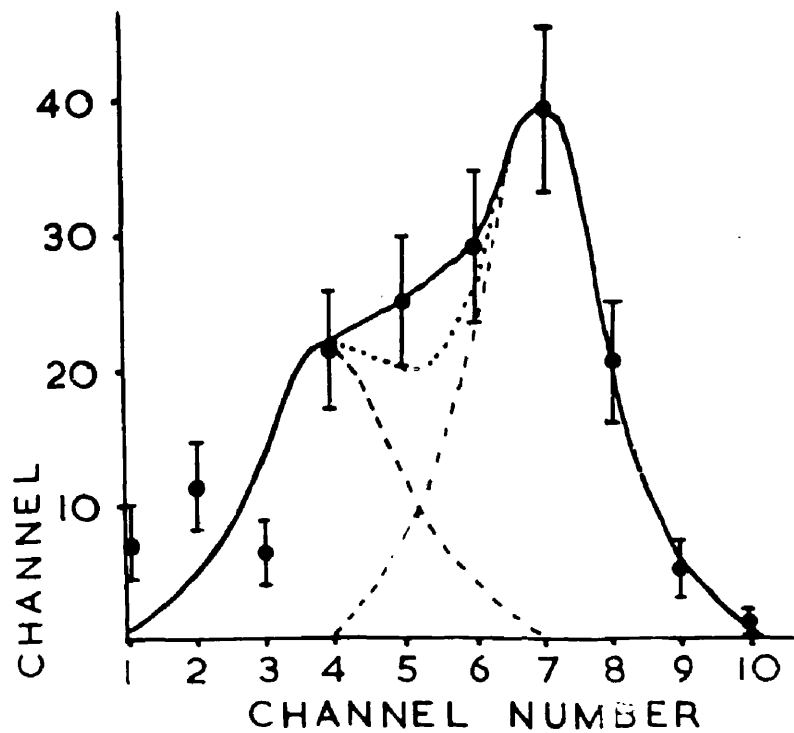
Figure 35.

Mass distribution of the He^3 and He^4 particles reported by Palit & Bellamy (93)

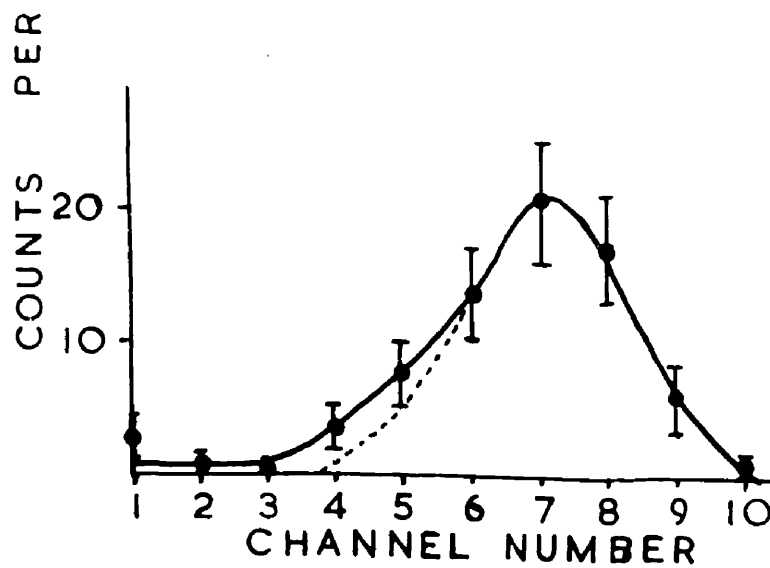
- a. Measured at 90° with respect to the beam direction.
- b. Measured at 40° with respect to the beam direction.

the lower curve (b). From Figure 35(a) one can see that the intrinsic resolution of the device was quite good and that the peak occurred in the proper channel.

The results of the present experiments are illustrated in Figure 36. Here the mass distribution (a) shows the yields of He^3 and He^4 particles of mean energy ~ 20 Mev, which were obtained from an oxygen target irradiated with 325 Mev bremsstrahlung when the detector was positioned at 90° with respect to the axis of the beam. As can be seen, the two groups are not completely resolved, but on the assumption that the distributions were of the form represented by the two symmetrical dotted curves, the ratio of the yields of He^4 and He^3 particles was 75:47. By counting the number of points on either side of the middle channel, this ratio was confirmed within experimental error. Figure 36(b) shows a similar distribution obtained with an argon target and here there is no sign of a peak in the He^3 channel. The curve, however, is not symmetrical and, if one assumes that the degree of divergence from symmetry represents an upper limit for the production of He^3 particles, then the ratio in this case is $159: < 30$. This ratio was again confirmed within experimental error by dividing the distribution at the middle channel. Since the energy range was small, an energy distribution would not in fact be very illuminating, but it appears that the number of particles



a



b

Figure 36.

Mass distributions of the He^3 and He^4 particles measured at 90°

- a. from an oxygen target.
- b. from an argon target.

decreased with increasing particle energy, particularly in the case of the He^4 particles. A drift in the gain of one of the amplifiers appeared during the runs and this, although not seriously affecting the energy measurements, seemed to have slightly reduced the resolution to an extent that the He^3 and He^4 particles were not resolved. However, on the basis of the previous results, the contributions due to both types of particles were separated as described above.

6.4. Discussion.

There is no theory with which these results can be directly compared and in the Discussion they are compared with data obtained in investigations in similar or related fields.

The two targets were assumed to be composed of entirely O^{16} and A^{40} respectively, since the gases were of industrial purity and the percentage abundances of the other isotopes of oxygen and argon were negligible. It should be pointed out that it was not possible to study the (γ, He^4) reactions in oxygen and argon by the activation technique referred to in the Introduction to this Chapter, as both the daughter nuclei were stable. Similarly the C^{13} nuclei, which resulted from the emission of He^3 particles from O^{16} , were also stable and therefore undetectable by this method.

In order to obtain an order of magnitude for the ratios to be expected for the He^4 to He^3 yields it was assumed that the particles were emitted in the decay of a compound nucleus as envisaged in Blatt and Weisskopf (94). In these calculations it was assumed that (a) the cross-sections for the formation of the compound nucleus O^{16*} by He^3 and He^4 particles incident on C^{12*} and C^{13*} respectively were approximately equal and (b) that the ratio of the capture cross-section for the photon in oxygen to the sum over all decay channels of the compound nucleus, was a slowly varying function of energy. The level densities were calculated from the following formula which was derived by Lang and LeCouteur (95):-

$$D_0 = 0.11 A^2 (U + t)^2 \exp - \left[2 \left(\frac{AU}{11} \right)^{\frac{1}{2}} + \frac{3}{32} (11U)^{2/3} \right]$$

$$\text{where } t = \left(\frac{10.5 U}{A} \right)^{\frac{1}{2}} - \frac{7.9}{A}$$

As a first approximation, the level densities corresponding to states with spin zero were used. Account was also taken of the work of Brown and Muirhead (96) who found that, for nuclei of the same mass and excitation energy, the average level densities for odd-even and even-even nuclei were given by

$$\frac{\omega_{o-e}}{5} \approx \frac{\omega_{e-e}}{1}$$

The above procedure was repeated for argon. The results

obtained from both sets of calculations are summarised in the following table.

<u>Energy of the absorbed photon</u>	<u>70</u>	<u>120</u>	<u>170</u>	Mev
He ⁴ to He ³ yield ratio for O ¹⁶	4.4	1.5	0.8	
He ⁴ to He ³ yield ratio for A ⁴⁰	33.4	5.1	1.5	

If one were to take these results at their face value it would appear that the particles resulted from photon absorption in the energy region around 120 Mev. However, the threshold for the emission of 20 Mev α -particles lay below 30 Mev, i.e., in the region of the 'giant resonance' in the photon absorption cross-section, and therefore one would expect that a large fraction of the measured yield resulted from photon absorption below 50 Mev, where the cross-section was much greater than at higher energies. That 20 Mev α -particles were emitted from nuclei when irradiated with low energy photons was demonstrated by Millar (97) who worked at a peak photon energy of 70 Mev. His energy distributions were in agreement with those calculated on a statistical theory.

It is very difficult to envisage any other process apart from the evaporation mechanism by which the He⁴ particles could have been emitted.

The differential yield rose by a factor of 2 when the atomic number was increased from eight to eighteen.

As it is now considered that the α -particles resulted from photon absorption at energies not too different from that corresponding to the peak of the 'giant resonance', it is interesting to compare the present results with the published data on α -particle yields obtained with photon beams of low peak energy. The yields from a wide range of nuclei have been investigated by Toms and McElhinney (57) at a peak energy of 21.5 Mev and by Erdos, Scherrer and Stoll (58) who worked with a peak energy of 32 Mev. Their results were illustrated in Chapter I (Figure 9). This data indicated that the total yield increased as the atomic number of the target nucleus was increased up to $Z = 29$ or 30 and thereafter decreased at greater values of Z . The atomic numbers of oxygen and argon would correspond to the rising portion of this curve and a ratio of 1:2 for the differential yields of α -particles from these two nuclei would therefore not be inconsistent with the trend implied by the results shown in Figure 9.

He^3 particles with energies of the order of 20 Mev would not be emitted until the energy of the absorbed photon exceeded approximately 40 Mev. Apart from threshold considerations one would anticipate that, on a statistical theory, the energy dependences of the emitted He^3 and He^4 particles would be similar. Therefore it is suggested that the He^3 particles were emitted after the absorption of

photons with energies slightly greater than those proposed for the (γ , He⁴) reaction. On the other hand, from the theoretical calculations it was known that the ratio of the yields of He⁴ to He³ particles increased rapidly as the excitation energy was decreased. At low energies on a statistical theory, therefore, one would have expected to detect very many more He⁴ particles than He³ particles. The particle yields obtained from the argon target were in agreement with this conclusion since, although there was a large He⁴ yield, there was little or no sign of a significant yield of He³ particles. In contrast to the argon results there was a large yield from oxygen. One was then led to predict that another mechanism was responsible for the emission of these He³ particles, and in particular to consider a direct interaction between the incident photon and a quasi- α -particle sub-unit within the oxygen nucleus. This interaction would bear a close resemblance to the photodisintegration of a free helium nucleus.

The same experimental procedure had been used previously by Palit and Bellamy (93) and their value of the differential yield of He³ particles from helium at 90° is quoted overleaf, together with the results from the present experiments.

<u>Target Nucleus</u>	<u>Differential yield at 90°</u> <u>10⁻³⁰ cm²/sterad/Mev/Q.</u>
He ⁴	0.55
O ¹⁶	0.47
A ⁴⁰	<0.30

All that can be said at the moment is that from the above table it would appear that the probability of such a direct process was very much higher for oxygen than for argon.

The energies of the photons responsible for the photodisintegration of free helium nuclei with the subsequent emission of He³ particles of mean energy ~ 20 Mev were calculated from the reaction kinematics to be of the order of 120 Mev. Consequently the energies of the photons which produced the O¹⁶ (γ , He³) C¹³ reactions would be of the same order of magnitude.

It seemed reasonable to assume that there would be a rough similarity in the dependence on the mass number of the yields of H³ and He³ particles for either an interaction between the incident γ -ray and an α -particle sub-unit within the nucleus or a mechanism involving the statistical decay of the compound nucleus, neglecting Coulomb barrier effects. To date no high energy measurements have been made on the yields of (γ , t)

reactions. At low photon energies, Heinrich and Waffler (98) have shown that there was a sharp decrease in the total yields of tritons when the mass number of the target nucleus was increased. This decrease occurred between aluminium and copper and was in fact a factor of approximately 5. They found that their results could be fitted by the statistical theory except for the heavy nuclei. One might therefore have anticipated a decrease in the differential yields of He^3 particles when the oxygen target was replaced by one of argon.

The conclusions which can be drawn from the above speculative discussion are summarised below.

- (i) The α -particles were probably emitted in an evaporation process which followed the absorption of photons of energies only slightly greater than those corresponding to the 'giant resonance'.
- (ii) The increase in the differential yields of α -particles as a function of the mass number was consistent with the published data on total yields obtained at low energies.
- (iii) The He^3 particles could have been evaporated from complex nuclei formed by the absorption of intermediate energy quanta and the trend of the dependence on the mass number of the He^3 yields would be consistent with such a mechanism.

- (iv) Although the ratio of the yields of He^4 to He^3 particles for argon was in agreement with (iii), this was not the case for oxygen where, on a statistical process, a greater ratio would have been expected.
- (v) Consequently a fraction of the yield of He^3 particles from O^{16} may be due to a direct interaction between the incident γ -ray of energy approximately 120 Mev and an α -particle sub-unit within this complex nucleus.

Throughout this Discussion no consideration has been given to the yields of He^4 and He^3 particles from meson-induced events on the grounds that the cross-sections for such reactions would be much less than those of the low energy photodisintegration reactions.

It is intended to investigate the emission processes for nitrogen in order to obtain more data which, it is hoped, will help to clarify the relative importances of these two mechanisms in oxygen. Further, the irradiation of other nuclei of higher atomic number will help to ascertain the variation of the He^4 and He^3 particle yields over a wider range of atomic numbers.

Although it would appear obvious that to clarify this problem the experiments should have been repeated at

a peak photon energy considerably lower than 320 Mev, this was not possible, as the intensity of the photon beam decreased sharply as the peak energy was reduced. Since the counting rate in the experiments reported here was already very small (in the order of 5 counts per hour), an experiment under these conditions would be impracticable.

Continuation of these investigations is dependent on the availability of 'machine time', which is very limited because of the intensive experimental programme at present in existence.

APPENDIX I.

The determination of some of the
parameters of the photon and electron
beams of the 340 Mev synchrotron.

The peak electron energy of the Glasgow high energy synchrotron was 340 Mev. The γ -ray beam was produced by allowing the electron beam to strike a tungsten rod target placed perpendicularly to the median plane of the magnet. A bremsstrahlung spectrum was produced with the photons being emitted in a narrow cone in the forward direction with respect to the electron beam. The photon beam passed out through the ceramic wall of the vacuum chamber, between two 'C' sections of the magnet and into the beam room.

The machine was synchronized to the 50 cycles/sec. A.C. mains and a beam pulse was produced on each eleventh mains cycle, i.e., approximately 4.5 bursts of photons per second. A detailed description of this machine was given by W. McFarlane et al. (99).

Before any attempt was made to collimate the photon beam, its dimensions and intensity were first determined. A 'Victoreen' thimble, surrounded by 1/8th of an inch of lead, was used in the determinations of the dimensions of the photon beam. The quantity of lead, namely 1/8th of an inch, was chosen to conform with similar measurements made previously on other electron synchrotrons with peak energies of about 300 Mev. The thimble was moved through the beam in both the horizontal and vertical planes independently, with the direction of

motion always at right angles to the axis of the beam. The 'Victoreen' was mounted on the carriage of a travelling microscope, fitted with the usual vernier scales in two mutually perpendicular directions. The thimble was 6 metres from the synchrotron target and was irradiated for periods varying between $\frac{1}{4}$ of a minute and one minute. The satisfactory periods of irradiation chosen for each series of measurements (i.e., a single traverse in one plane) varied according to the standard levels of intensity of the synchrotron beam obtainable on the days during which these measurements were made. The output intensity was kept constant throughout each of these traverses and was monitored with an ionisation chamber. The dose recorded by the thimble was then normalised to this particular value of the beam intensity. The ionisation chamber mentioned above was a copy of the chamber designed and calibrated at Cornell University.

On each occasion the thimble was first moved in a horizontal direction until a maximum in the beam intensity was located. When this had been achieved, the thimble was placed at this position (M) of maximum intensity and a series of readings were then taken with the thimble situated at various points vertically above and below M.

Figure 37 illustrates typical data obtained in

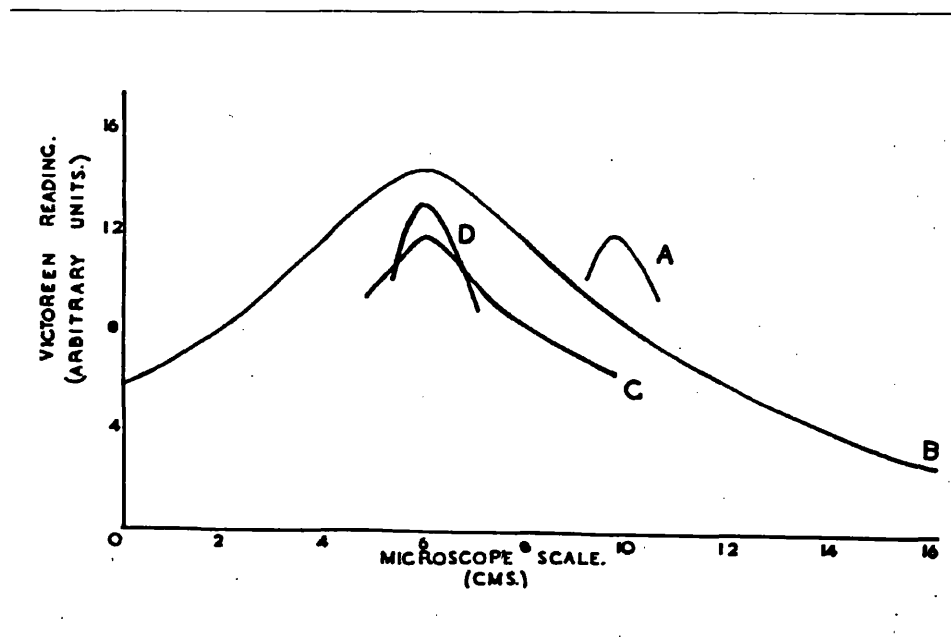


Figure 37.

Intensity distributions of the output
from the 340 Mev synchrotron.

A & D: collimated beam.

B & C: uncollimated beam.

this manner. Curves B and C correspond to measurements on an uncollimated beam while A and D refer to measurements with the collimator in position. It should be noted that the maximum of curve A for a horizontal traverse was considerably displaced with respect to the others. This was an example of incorrect collimation.

The now accepted standard intensity distribution in the horizontal plane through the centre of the beam is shown in Figure 38. The width at half-maximum was approximately 10^{-2} radians. Although the tungsten target was cylindrical and 0.060 inches in diameter, Hughes (100) has calculated that the measured intensity distribution was consistent with a rectangular target 0.020 inches thick. At 6 metres from the target the uncollimated photon beam was approximately 5.5 cm. in diameter with the low intensity 'shoulders' extending considerably beyond this. When the collimator had been correctly positioned, the distribution was well represented by the dotted curve shown in Figure 38. Under such circumstances the beam was approximately 3.5 cm. in diameter at 6 metres with very little intensity outwith this region. This is well illustrated in Figure 39, where the relative intensities of the collimated beam and the low intensity 'halo' are recorded by the degree of blackening on an X-ray film. This film was exposed at 1.85 metres from the target.

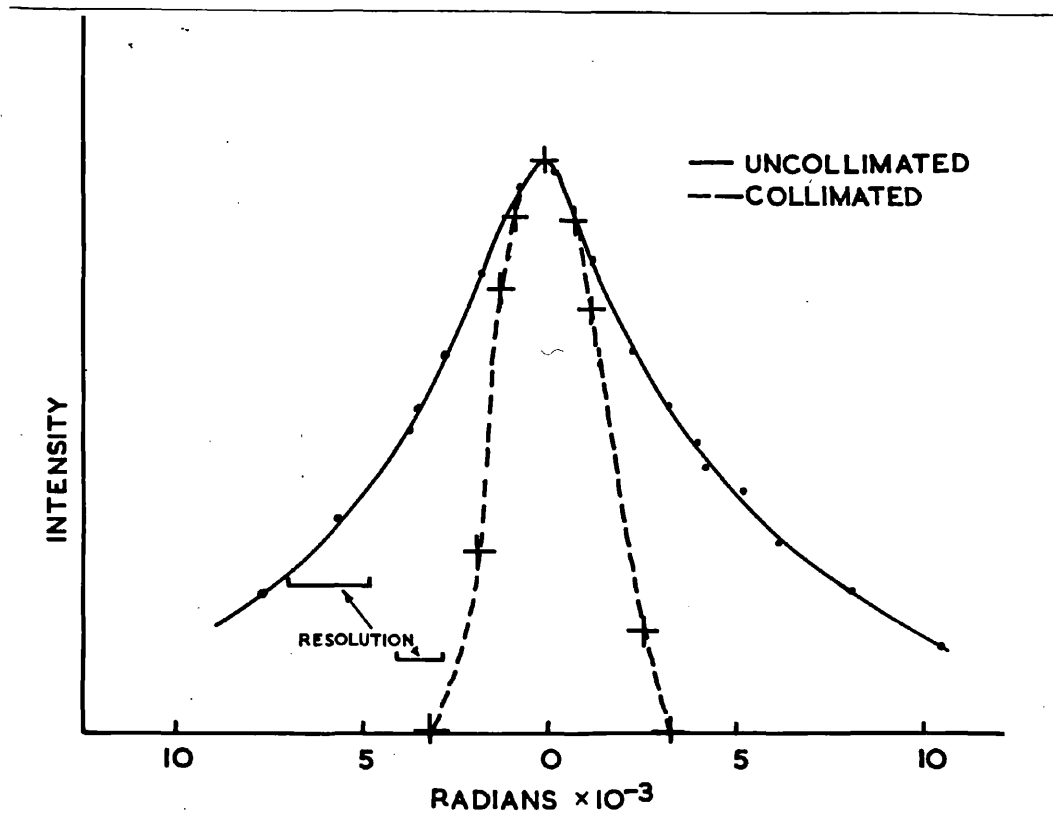
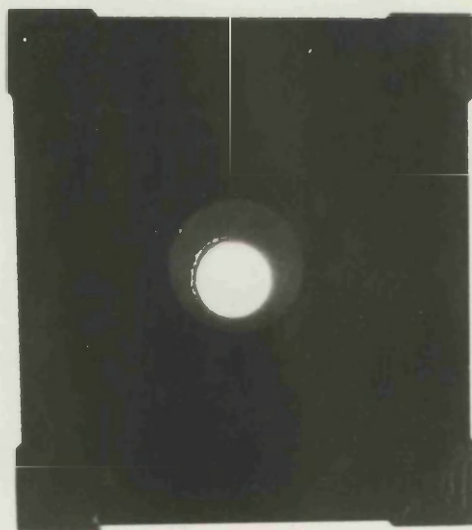


Figure 38.

Standard intensity distribution of the collimated and uncollimated beams of the 340 Mev synchrotron.

During the early measurements it was concluded that the beam did not travel horizontally through the beam pipe. It was estimated that this discrepancy arose



This exposure was made at the end of the 3" pipe nearest the synchrotron target. The very intense spot was the photon beam while the less intense circle was due to stray radiation passing along the $\frac{3}{4}$ " diameter pipe leading from the flared section. At this point the beam was $\frac{7}{16}$ " in diameter. Since the beam was not passing along the axis of the pipe the latter was adjusted until this was achieved.

Figure 39.

During the early measurements it was concluded that the beam did not travel horizontally through the beam room. It was estimated that this discrepancy arose in the positioning of the magnet. This was confirmed by measuring the deviation from the horizontal plane of the magnet base plate, which, on the manufacturers' specifications, could be taken as a plane surface. It was found that the magnet dipped 0.003 radians below the horizontal plane in the direction of the emergent beam. This slight discrepancy had considerable effect during the alignment of equipment in the beam room, especially if the components were long or widely separated.

The collimator consisted of a lead cylinder 4 inches in diameter and 9 inches in length with a $\frac{1}{4}$ -inch hole drilled along its axis. The surface of the latter was coated with a layer of paint to counteract the porosity of the lead because it was later to be evacuated. The end facing the synchrotron target was sealed with a thin glass window. At the other end the collimator was coupled to the beam tube through which the beam passed into the beam room. The orientation of the cylinder could be altered by four motor-driven worm screws, one for both the horizontal and vertical movements at each end of the cylinder and these could be controlled remotely. The collimator lay within the yoke of the synchrotron magnet where there was a varying magnetic field and when correctly

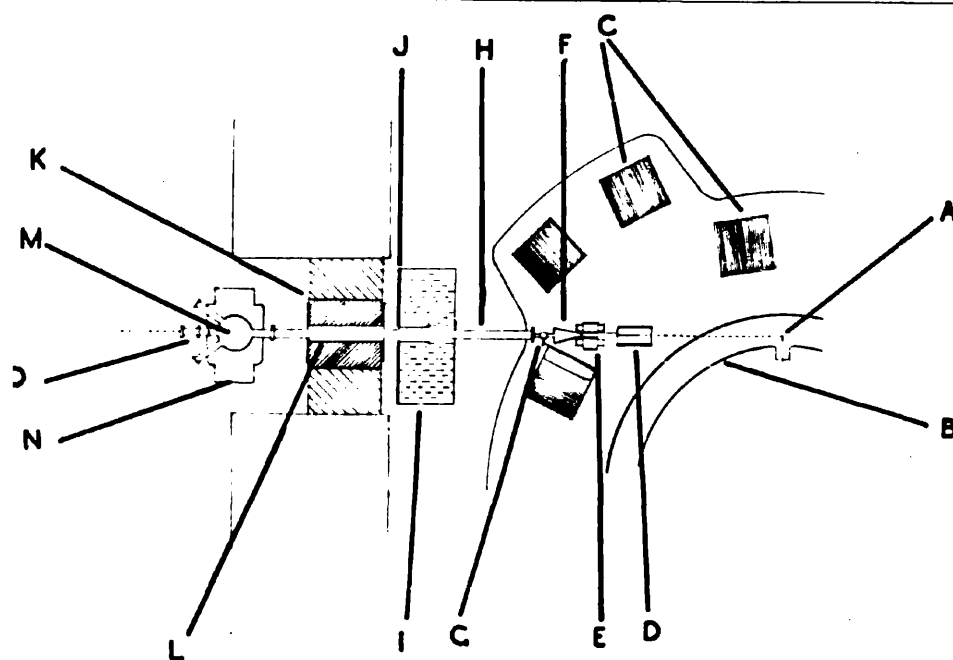
aligned it was bolted to the supporting platform. This prevented the cylinder from moving due to the vibration of the machine. In this position eddy-current heating was found to be negligible. The collimator was locked in position with the glass window 50 cm. from the point at which the photon beam emerged from the vacuum chamber.

After traversing the collimator, the beam passed between the poles of a D.C. magnet which provided a field of 5,500 gauss. The secondary electrons produced by the γ -rays striking the collimator window, etc., were thus deflected out of the beam. To accommodate these deflected electrons, the beam tube was flared out to a cross-sectional area of 4 square inches at a distance of 12 inches from the magnet. The photon beam passed out from the flared section through an aperture situated symmetrically at the end of this section and entered into an iron pipe $\frac{3}{4}$ -inch in diameter. Electrons of energy up to approximately 100 Mev were sufficiently deflected to prevent them passing through to the beam room.

The whole collimator assembly up to this point was rigidly bolted to the synchrotron magnet frame and, as the machine was mounted on springs, flexible bellows were introduced to couple the iron pipe to the next section which consisted of a pipe 5 feet long and 3 inches in diameter. This tube projected through the shielding wall

into the beam room where it was coupled to a vacuum box 12 inches in diameter and 2 inches deep with three exit arms approximately 2 inches in diameter. One was in the straight-through position while the other two were located symmetrically at either side. The cylinder sat between the poles of a D.C. magnet capable of producing a peak field of 10,000 gauss which acted as a pair-spectrometer. The ports were sealed with thin windows of aluminium or 'Melinex' foil 0.002 inches thick. The beam tube and collimator were evacuated by a 4-inch diffusion pump. The whole assembly is illustrated in Figure 40.

An optical telescope was set up at the far end of the beam room and focussed on the point at which the beam emerged from the vacuum chamber. The collimator and each section of the beam tube were then installed in such a manner that they did not obscure the view of the above point. The collimator was then orientated in such a way that the central hole was symmetrically disposed with respect to the beam direction. The position of the collimator was adjusted by remote control until the intensity of the transmitted beam was a maximum and a circular beam profile was recorded on the X-ray film exposed behind the collimator. An X-ray film was exposed at the end of each section and its position adjusted until the beam passed symmetrically through the whole system.



- A. The synchrotron target.
- B. The donut.
- C. Magnet 'C' sections.
- D. The collimator - the lead cylinder.
- E. The 'scrubber magnet'.
- F. The flared section.
- G. The supporting clamp.
- H. The 3" brass pipe.
- I. The water tank.
- J. The sheet of cadmium.
- K. The wall of barytes bricks with enclosed lead shielding.
- L. The 6" steel pipe.
- M. The vacuum box.
- N. The pair spectrometer magnet.
- O. The 'T' piece.

Figure 40.

The complete collimator assembly.

Finally the intensity distribution at the centre of the beam was measured with a small ionisation chamber to confirm that the axial intensity was unaltered by the inclusion of the collimator.

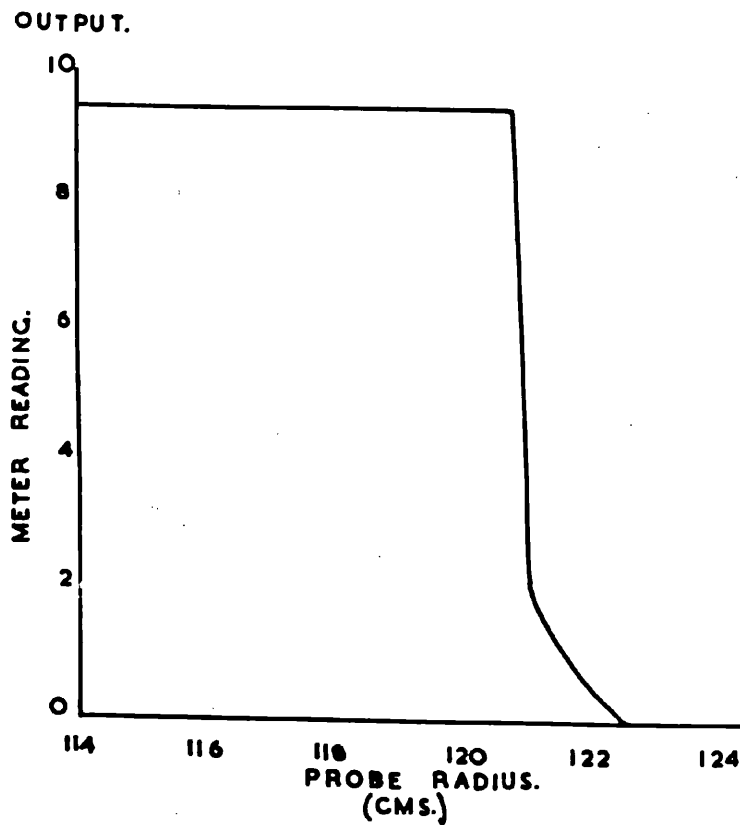
The wall between the synchrotron chamber and the beam room shielded the latter and any recording equipment installed there from the stray radiation of the machine. The beam passed through an aperture in a large water tank backed by a cadmium sheet 0.022 inches thick on the side remote from the machine in order to reduce the neutron background which resulted from photonuclear reactions within the machine room. The wall consisted of a double wall of barytes bricks each 9 inches thick. A steel tube was inserted through a gap in the wall and the space between this tube and the bricks was filled with lead blocks packed as tightly as possible. The remaining spaces were then filled with lead shot and this was kept in position by steel plates held against both walls by tie bars which ran through the wall. The 3-inch tube was passed through the steel tube and the annular separation between these was also filled with lead shot. Finally, a lead collimator 4 inches long and $1\frac{1}{2}$ inches internal diameter was inserted in the beam tube immediately before the pair spectrometer to complete the shielding.

Determinations were then made of the behaviour

of the synchrotron output as a function of the radial positions of the gun and probe.

The gun position was fixed and the location of the probe phosphor was varied radially. At each radial position of the probe the output of the machine was recorded by the Cornell ionisation chamber. As can be seen in Figure 41, the output dropped sharply when the probe was at a radius of 120.8 cm. During this series of measurements the gun and target were at radii of 119.4 cm. and 121.6 cm. respectively. At first sight these figures were somewhat surprising, as it was expected that the synchrotron output would only drop once the probe was at a greater radius than the target. However, it was estimated that there could be an error of up to 1 cm. in the radial measurements, because the axis of the vacuum chamber was slightly displaced with respect to that of the magnet and all radial positions were estimated from measurements of the penetration of the electrodes into the vacuum chamber. The reduction in the intensity of the collimated beam was caused by the probe 'robbing' the synchrotron beam as it spiralled in. As a result, the probe produced a photon beam which emerged from the vacuum chamber in a direction considerably displaced from that of the axis of the collimator.

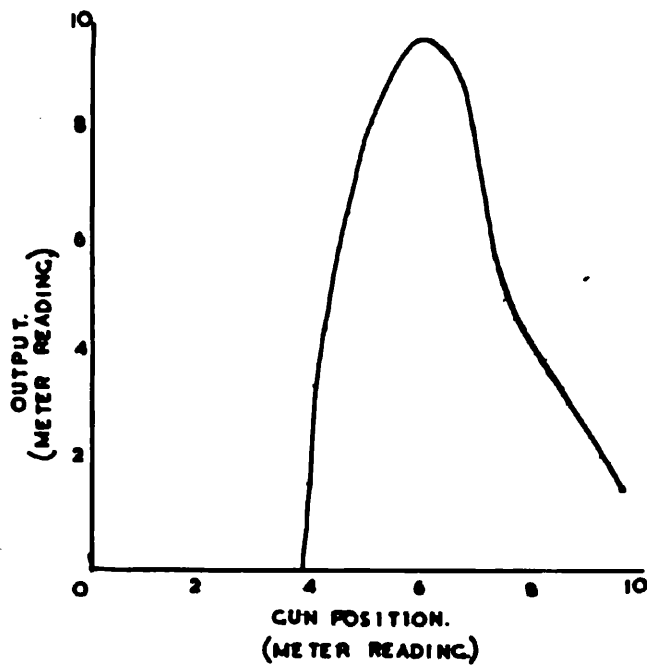
When the variation of the photon beam intensity



This figure shows the variation in intensity of the photon beam from the 340 MeV synchrotron caused by varying the radial position of the scintillator probe. The intensity dropped sharply when the probe was at a radius of 120.8 cm. The gun and target radii were 119.4 cm. and 121.6 cm. respectively.

Figure 41.

was measured as a function of the radius of the gun, the probe was retracted clear of the accelerating region - in fact, to a radius of 116.5 cm. The target was then at a radius of 121.6 cm. Figure 42 illustrates the measured behaviour. The beam intensity rose as the radius increased and reached a maximum at a radius of 120.4 cm. Thereafter the output decreased sharply. As before, the values of the radial positions were somewhat suspect but the increase represented the approach of the gun to the region of acceptance for acceleration, while the sharp cut-off resulted from two effects which could not be separated. The first was similar to that quoted above for the probe measurements, i.e., the synchrotron beam was 'robbed' by the gun once it was at a radius greater than that of the target. The second was due to the fact that, once the gun protruded into the region where electrons were captured for acceleration, the effective area for capture was decreased and consequently the betatron and hence synchrotron beam intensities were diminished.



The output from the 340 MeV Synchrotron dropped sharply when the gun filament was at a radius of 120.4 cm. While this was being tested, the probe and target were at radii of 116.5 cm. and 121.6 cm. respectively. The scale indicating the filament position was that of the remote control meter. A value of 7 on this scale corresponded to a radius of 119 cm. Each scale division represented 0.45 cm.

Figure 42.

APPENDIX II.

Photonuclear reactions in neon.

The following results are included in this thesis in order to present, together with the results reported in Chapter IV, a complete picture of the photodisintegration of neon.

As was mentioned in the Introduction to Chapter IV, a part of the interest in this experiment centred around reactions in which more than one particle was emitted, i.e., the $(\gamma, \alpha\alpha)$ and $(\gamma, \alpha p)$ reactions. The experimental results are presented in the following table:-

<u>Reaction</u>	<u>Threshold</u>	<u>No. of events</u>	<u>Integrated cross-section. Mev-mb.</u>
(γ, p)	12.87	303	39
(γ, α)	4.75	30	-
$(\gamma, \alpha p)$ or $(\gamma, p\alpha)$	16.86	40	7
$(\gamma, \alpha\alpha)$	11.9	20	2
(γ, pn)	23.1	none	-
(γ, d)	20.9	none	-

The energy of the incident photon was calculated from the sum of the kinetic energies of the reaction products and the reaction threshold for each event. Care had to be exercised in the interpretation of the results, because no account could be taken of the possibility that the residual nucleus was left in an excited state. A momentum balance was then carried out

on the measurable events to ensure that the character of the events which had been assigned after visual examination was in fact correct. Thereafter the character of the unmeasurable events was accepted to be that determined visually. The accepted events had a momentum unbalance of less than 30 Mev/c and in all cases the first assignments were confirmed.

Briefly the conclusions reached from these results are presented below. In all the reactions it was assumed that a compound nucleus state was formed following the absorption of the photon.

The (γ, α) reaction.

On the basis of the assumption that the residual nucleus was left in its ground state, the majority of the events of this type resulted from absorption in the photon energy region about 8 Mev. The results of Erdman and Barnes (101) indicated that in neon, following the absorption of 17.6 Mev quanta, the residual oxygen nucleus was more likely to be left in an excited state between 6 and 7 Mev above the ground state than in the ground state itself. Consequently, a number of events which had previously been correlated with photon energies around 8 Mev were then regarded as having originated from photon absorption between 15 and 16 Mev. The events which left the residual oxygen nucleus in states

below 13 Mev (i.e., states with isotopic spin $T = 0$) resulted from that portion of the M1 and E2 absorption with $\Delta T = 0$ or from E1 absorption ($\Delta T = 1$) with the inclusion of some impurity in the isotopic spin states. Those which left O^{16} in states higher than 13 Mev would most probably result in the excited nucleus decaying by the emission of another particle. The yield of events produced by the 23 Mev bremsstrahlung beam was 7×10^3 /mole/r.

The (γ, α) reaction.

This reaction was assumed to proceed by an α -particle cascade through the excited states of O^{16*} to the residual nucleus Cl^{12} . The latter was in its ground state in the majority of cases. As it was not possible to determine which α -particle was emitted first, two values of O^{16*} were obtained, only one of which was significant. However, for almost all the events one value at least was consistent with the known levels of O^{16} . Since most of these events corresponded to photon energies in excess of 18 Mev (i.e., the energy interval associated with the 'giant resonance'), it was reasonable to assume that the events resulted from E1 absorption with the subsequent violation of the isotopic spin selection rules. These, if they were absolute, would prohibit the reaction until the residual Cl^{12} nucleus was left in a $T = 1$ state,

the first of which lay about 15 Mev above the ground state. This state was energetically inaccessible in this experiment.

The (γ , α p) or (γ , α n) reaction.

As above, it was not possible to determine whether the α -particle was emitted before the proton or vice versa. The calculated energy distributions for the excited states of the two alternative intermediate nuclei (O^{16*} and F^{19*}) both appeared probable. It was therefore assumed arbitrarily that both decay channels were equally likely and that they contributed equally to the yield of $1 \pm 0.2 \times 10^4/\text{mole/r}$. With no exceptions the photon energies were estimated to be greater than 20 Mev and again (for the same reason as in the (γ , $\alpha\alpha$) reaction) it seemed reasonable to assume that this reaction proceeded after E1 absorption in Ne^{20} .

Lastly, it was concluded that the photon absorption cross-section was small below 15 Mev and that above this energy it increased rapidly. If it was assumed that the (γ ,n) reaction yielded as many events as had been classified as essentially (γ ,p) in form, then one-seventh of the total yield could be attributed to reactions of a basic (γ , α) character.

REFERENCES

1. Chadwick, J. and Goldhaber, M. Nature, 134, 237 (1934).
2. Szilard, L. and Chalmers, T.A. Nature, 134, 494 (1934).
3. Bothe, W. and Gentner, W. Naturwiss, 25, 90, 126, 191, 284 (1937).
4. Kerst, D.W. Phys. Rev., 60, 47 (1941).
5. Bishop, G.R. and Wilson, R. Hand. der Physik., 42, 309 (1957).
6. Katz, L. and Cameron, A.G.W. Can. J. Phys., 29, 518 (1951).
7. Weil, J.W. and McDaniel, B.D. Phys. Rev., 92, 391 (1953).
8. Goldemberg, J. Phys. Rev., 93, 1426L (1954).
9. Koch, H.W., McElhinney, J. and Cunningham, J.A. Phys. Rev., 81, 318 (1951).
10. Marshall, L. Phys. Rev., 83, 345 (1951).
11. Titterton, E.W. Prog. in Nuclear Phys., 4, 1 (1955).
12. Wright, I.F., Morrison, D.R.O., Reid, J.M. and Atkinson, J.R. Proc. Phys. Soc., 69A, 77 (1956).
13. Balfour, D. Private communication.
14. Ferrero, F., Gonella, L., Malvano, R., Tribuno, G. and Hanson, A.O. Nuovo Cimento (Ser.10), 5, 242 (1957).
15. Massachusetts Institute of Technology. Progress Report. Feb. 1956, and 1956-57, p.108.
16. Montalbetti, R., Katz, L. and Goldemberg, J. Phys. Rev., 91, 659 (1953).
17. Schuhl, C. and Basile, R. Physica, 22, 1144A (1956).
18. Nathans, R. and Halpern, J. Phys. Rev., 92, 207L (1953).

19. Yergin, P.F. and Fabricand, B.P. Phys. Rev.,
104, 1334 (1956).
20. Goldemberg, J. and Lopes, J.L. Phys. Rev.,
99, 1053L (1955).
21. Hartley, W.H., Stephens, W.E. and Winhold, E.J.
Phys. Rev., 104, 178 (1956).
22. Levinger, J.S. and Bethe, H.A. Phys. Rev., 78,
115 (1950).
23. Gell-Mann, M., Goldberger, M.L. and Thirring, W.E.
Phys. Rev., 95, 1612 (1954).
24. Feenberg, E. Phys. Rev., 49, 328 (1936).
25. Siegert, A.J.F. Phys. Rev., 52, 787 (1937).
26. Christian, R.S. and Hart, E.W. Phys. Rev., 77,
441 (1950).
27. Baldwin, G.C. and Elder, F.R. Phys. Rev., 78,
76L (1950).
28. Price, G.A. and Kerst, D.W. Phys. Rev., 77,
806 (1950).
29. Terwilliger, K.M., Jones, L.W. and Jarmie, W.N.
Phys. Rev., 82, 820 (1951).
30. Halpern, J., and Mann, A.K. Phys. Rev., 82, 733
(1951).
31. Jones, L.W. and Terwilliger, K.M. Phys. Rev., 91,
699 (1953).
32. Goldhaber, M. and Teller, E. Phys. Rev., 74,
1046 (1948).
33. Mann, A.K., Stephens, W.E. and Wilkinson, D.H.
Phys. Rev., 97, 1184L (1955).
34. Milone, C. and Ricamo, R. Nuovo Cimento (Ser.10),
5, 1338L (1957).
35. Diven, B.C. and Almy, G.M. Phys. Rev., 80, 407
(1950).
36. Weisskopf, V.F. and Ewing, D.H. Phys. Rev., 57,
472 (1940).

37. Byerly, P.R. Jr., and Stephens, W.E. Phys. Rev., 83, 54 (1951).
38. Wilkinson, D.H. Physica, 22, 1039 (1956).
39. Katz, L., Haslam, R.N.H., Horsley, R.J., Cameron, A.G.W. and Montalbetti, R. Phys. Rev., 95, 464 (1954).
40. Penfold, A.S. and Spicer, B.M. Phys. Rev., 100, 1377 (1955).
41. Cohen, L.D., Mann, A.K., Patton, B.J., Reibel, K., Stephens, W.E. and Winhold, E.J. Phys. Rev., 104, 108 (1956).
42. Toms, M.E. and Stephens, W.E. Phys. Rev., 92, 362 (1953).
43. Ferrero, F., Hanson, A.O., Malvano, R. and Tribuno, C. Nuovo Cimento, 4, 418 (1956).
44. Hirzel, O. and Wäffler, H. Helv. Phys. Acta, 20, 373 (1947).
45. Dawson, W.K. Can. J. Phys., 34, 1480 (1956).
46. Halpern, J., Mann, A.K. and Rothman, M. Phys. Rev., 87, 164L (1952).
47. Fabricand, B.P., Allison, B.A. and Halpern, J. Phys. Rev., 103, 1755 (1956).
48. Mann, A.K., Halpern, J. and Rothman, M. Phys. Rev., 87, 146 (1952).
49. Price, G.A. Phys. Rev., 93, 1279 (1954).
50. Leikin, E.M., Osokina, R.M. and Ratner, B.S. Nuovo Cimento, 3, Suppl.1, 105 (1956).
51. Goward, F.K. and Wilkins, J.J.

(a,b)	Proc. Phys. Soc.,	<u>A63</u> ,	662,1171(1950)
(c,d)	" "	<u>A64</u> ,	312,94(1951).
(e)	" "	<u>A65</u> ,	671 (1952).
(f)	Proc. Roy. Soc.	<u>A217</u> ,	357 (1953).
52. Livesey, D.L. and Smith, C.L.

(a)	Proc. Phys. Soc.	<u>A65</u> ,	758 (1952).
(b)	" "	<u>A66</u> ,	689 (1953).

53. Dawson, W.K. and Livesey, D.L. Can. J. Phys.,
34, 241 (1956).
54. Millar, C.H. and Cameron, A.G.W. Can. J. Phys.,
31, 723 (1953).
55. Hsiao, O. and Telegdi, V.L. Phys. Rev., 90,
494 (1953).
56. Gell-Mann, M. and Telegdi, V.L. Phys. Rev., 91,
169 (1953).
57. Toms, M.E. and McElhinney, J. NRL Quarterly for
Nuclear Science & Technology.
January 1958.
58. Erdős, P., Scherrer, P. and Stoll, P. Helv.
Phys. Acta, 30, 639 (1957).
59. Kikuchi, S. Phys. Rev., 83, 1255L (1951).
60. Debs, R.J., Eisinger, J.T., Fairhall, A.W.,
Halpern, I. and Richter, H.G.
Phys. Rev., 97, 1325 (1955).
61. Sugihara, T.T. and Halpern, I. Phys. Rev., 101,
1768 (1956).
62. Holtzman, R.B. and Sugarman, N. Phys. Rev., 87,
633 (1952).
63. Levinger, J.S. Phys. Rev., 84, 43 (1951).
64. Barton, M.Q. and Smith, J.H. Phys. Rev., 95,
573L (1954).
65. Wattenberg, A., Odian, A.C., Stein, P.C., Wilson, H.
and Weinstein, R.M. Phys. Rev.,
104, 1710 (1956).
66. Wright, I.F. Private communication.
67. Morrison, D.R.O. Private communication.
68. Katz, L. and Cameron, A.G.W. Can. J. Phys., 29,
518 (1951).
69. Ferguson, G.A., Halpern, J., Nathans, R. and
Yergin, P.F. Phys. Rev., 95,
776 (1954).

70. Arthur, J.S., Allen, A.J., Bender, R.S. Hausman, H.J. and McDole, C.J. Phys. Rev., 88, 1291 (1952).
71. Spicer, B.M. Phys. Rev., 99, 33 (1955).
72. Johansson, S.A.E. and Forkman, B. Private communication and later Arkiv. Fys., 12, 359 (1957).
73. Wilkinson, D.H. and Bloom, S.D. Phys. Rev., 105, 683 (1957).
74. Cohen, L.D., Mann, A.K., Patton, B.J., Reibel, K., Stephens, W.E. and Winhold, E.J. Phys. Rev., 104, 108 (1956).
75. Milone, C., Ricamo, R. and Rinziivillo, R. Nuovo Cimento, 5, 532 (1957).
76. Livesey, D.L. Can. J. Phys., 34, 1022 (1956).
77. Svantesson, N.L. Nuclear Phys., 3, 273 (1957).
78. Penner, S. Private communication from National Bureau of Standards, Washington, D.C.
79. Aron, W.A., Hoffman, B.G., Williams, F.C. AECU-663 (1949).
80. Bethe, H.A. and Ashkin, J. Exptl. Nuclear Phys., Vol. I, p. 166 (Wiley) (1953).
81. Jesse, W.P. and Sadauskis, J. Phys. Rev., 78, 1 (1950).
82. Schardt, A., Fowler, W.A., Lauritsen, C.C. Phys. Rev., 86, 527 (1952).
83. Kraus, A. Phys. Rev., 94, 975 (1954).
84. Hornyack, W.F. and Sher, R. Phys. Rev., 100, 1409 (1955).
85. Zimmerman, W. Jr., Phys. Rev., 104, 387 (1956).
86. Menzies, D.C. Private communication.
87. Stoll, P. Helv. Phys. Acta, 27, 395 (1954).

88. McWhirter, R.W.P., Palit, P. and Bellamy, E.H.
Nuclear Instr., 3, 80 (1958).
89. Yamagata, T., Barton, M.Q., Hanson, A.O. and
Smith, J.H. Phys. Rev., 95, 574 (1954).
90. Tollestrup, A.V., Keck, J.C. and Worlock, R.M.
Phys. Rev., 99, 220 (1955).
91. Wolfe, B., Silverman, A. and de Wire, J.W.
Rev. Sci. Inst., 26, 504 (1955).
92. Rich, M. and Madey, R. UCRL-2301 (1954).
93. Palit, P. and Bellamy, E.H. Proc. Phys. Soc.,
A72, 880 (1958).
94. Blatt, J.M. and Weisskopf, F. "Theoretical
Nuclear Physics". Wiley (1952).
95. Lang, J.M.B. and LeCouteur, K.J. Proc. Phys. Soc.,
A67, 586 (1954).
96. Brown, G. and Muirhead, H. Phil. Mag., 2, 473
(1957).
97. Millar, C.H. Can. J. Phys., 31, 262 (1953).
98. Heinrich, F. and Wäffler, H. Helv. Phys. Acta,
29, 232 (1956).
99. McFarlane, W., Barden, S.E. and Oldroyd, D.L.
Nature, 176, 666 (1955).
100. Hughes, I.S. Private communication.
101. Erdman, K.L. and Barnes, C.A. Proc. Roy. Soc.
(Can.) 47, 131 (1953).